A Reproduced Copy

NASA CONTRACTOR REPORT 166609

Study to Eliminate Ground Resonance Using Active Controls

F. K. Straub

CONTRACT NAS2-11261
October 1984

NASA

NASA CONTRACTOR REPORT 166609

Study to Eliminate Ground Resonance Using Active Controls

F. K. Straub
Hughes Helicopters, Inc.
Culver City, CA

Prepared for
Ames Research Center
under Contract NAS2-11261

National Aeronautics and
Space Administration

Ames Research Center
Moffett Field, California 94035

TABLE OF CONTENTS

PREFACE

This report was prepared by Hughes Helicopters, Inc., under NASA Contract NAS2-11261 funded by the National Aeronautics and Space Administration. The Hughes Helicopters' project engineer was Dr. F. K. Straub. Technical program direction was provided by Dr. W. Warmbrod of NASA Ames Research Center (Moffett Field, California).

SUMMARY

Helicopter ground resonance conditions typically require incorporation of augmented blade inplane damping and tailoring of rotor and fuselage frequencies. The present study investigates the effectiveness of active control blade feathering in increasing rotor/body damping and possibly eliminating ground resonance instabilities.

An analytical model representing rotor flapping and lead-lag degrees of freedom and body pitch, roll, longitudinal and lateral motion is developed. The equations of motion are linearized and transformed into constant coefficient form. Blade feathering appears as a forcing term in each of the degrees of freedom. A thorough correlation with experimental model hingeless rotor data is conducted to validate the model and the computer program.

Active control blade feathering is implemented as state variable feedback through a conventional swashplate. The influence of various feedback states, feedback gain, and weighting between the cyclic controls (feedback phase) is studied through stability and response analyses. Results show that blade cyclic inplane motion, roll rate and roll acceleration feedback can add considerable damping to the system and eliminate ground resonance instabilities.

The feedback phase is seen to be a powerful parameter. If chosen properly it maximizes augmentation of the regressing lag mode inherent damping. For roll acceleration feedback the feedback phase has considerable effect on the roll mode frequency. This could be used for active control of frequency placement and would indirectly improve system stability.

Rotor configuration parameters, namely blade root hinge offset, flapping stiffness, and precone have considerable influence on the control effectiveness. Results show that active control is particularly powerful for hingeless and bearingless rotor systems.

INTRODUCTION

Aeromechanical rotor/fuselage instability, specifically ground resonance instability, can occur for articulated, hingeless, and bearingless rotors. Typically a range of various payload configurations are encountered for a particular helicopter. This makes it very difficult to avoid ground resonance by tailoring the body and inplane rotor mode frequencies to avoid coalescence for all operating conditions. Thus, the designer in many cases has to resort to mechanical lead-lag dampers for articulated rotor systems. This means increased cost, complexity, maintenance, weight and hub drag. Hingeless rotor systems have not seen extensive uses in the helicopter industry, in part, because of poor inherent aeroelastic stability characteristics. Consequently a means to increase aeromechanical stability in a reliable manner could significantly improve the utilization of all rotor hub design configurations.

The purpose of the present study is to evaluate the potential use of active blade pitch control to increase rotor/body system damping. Such an application could possibly eliminate the need for mechanical lead-lag dampers to augment rotor system damping. Stabilizing effects can arise both from the coupling between blade flap and body degrees of freedom, as well as Coriolis coupling between blade flap and lag motion.

The concept of active control blade feathering has been successfully demonstrated for vibration reduction and the technology is now available for advanced applications. Showing analytically the feasibility of using active control to eliminate ground resonance would represent a further step towards an advanced, fully integrated, multimode control system.

Section 2 starts with a literature review of the two ingredients of the present study: helicopter aeromechanical stability and application of active control blade feathering. This is followed by a summary of the objectives of the present work. Next, in Section 3 the assumptions on which the mathematical model of the rotor/fuselage is based are described and an outline of the derivation of the equations of motion and solution procedure is given. The complete equations of motion are listed in the Appendix. To validate the governing equations of motion a correlation study was performed. In Section 4 results of the present analysis are compared with experimental data and existing analyses.

The implementation of the active control system and various control methods are described in Section 5. All numerical results, described in Section 6, are based on state variable feedback control. These active control simulations are intended to show the effect of various feedback variables on system stability and provide a systematic approach in choosing the feedback parameters. The effect of key rotor

parameters is also investigated as is the rotor response behavior. The report closes with a summary of the major findings and conclusions.

BACKGROUND

Possibly the most fundamental instability associated with rotorcraft is ground resonance. This description strictly is incorrect since the phenomenon is in fact not a resonance but a true instability. A more appropriate name is mechanical instability which has seen more use in recent years. This is an appropriate description because the phenomenon can occur in a vacuum.

Ground resonance, as a mechanical instability in articulated rotors, is well understood. The classical works of Coleman and Feingold, Reference 1, and Deutsch, Reference 2, identified the rotorcraft parameters and their relationships in defining this mechanical instability. Their works showed that the phenomenon is fundamentally simple but that the relationships required for stability among the parameters are very complex. They also showed that mechanical instability is possible only when the natural frequency of the rotor blade lagging (or inplane) motions is less than the speed of rotation of the rotor.

In simple terms, mechanical instability can occur if: 1) The lag frequency of the rotor blades is less than the rotor speed (soft inplane), 2) The lag frequency minus the rotor speed, i.e., the regressive lag mode frequency, approaches or coalesces with the frequency of an airframe mode, and 3) Certain relationships among the blade lag damping and

airframe modal damping, and the effective rotor mass and airframe modal masses are satisfied.

Coleman's equations have been used extensively to define stability boundaries for articulated rotors and determine the blade and fixed system damping values required to prevent ground resonance. For example see Reference 3.

Hingeless rotor systems of the soft inplane type have added another aspect to the mechanical stability problem. Their inherently low blade structural damping and lack of mechanical blade dampers can result in severe mechanical instability problems on the ground (as an exception, the Lynx rotor has mechanical dampers). Bearingless rotors, in many cases, incorporate elastomeric snubbers which can be designed to add damping to the blade structural damping for inplane blade motion. In addition, the elastic flapping of hingeless or bearingless rotors and the resulting large hub moments lead to greater aeroelastic coupling between the rotor and airframe both on the ground and in flight. Thus a hingeless rotor can experience both ground and air resonance, more appropriately described with the common term aeromechanical instability.

Evidence of the significance of the encountered problems are the numerous publications dealing with the aeromechanical stability of actual hingeless and bearingless rotor designs, References 4-10.

While hingeless rotor designs are attractive through their mechanical simplicity, analytical modeling is complicated due to strong aerodynamic, inertial, and structural coupling as well as inherently nonlinear blade deformations. Considerable research effort has been directed towards a better understanding of the hingeless rotorcraft aeromechanical stability problem and investigation of design parameters that would increase blade lead-lag damping. A small sample of this work, which is used in the present study, is cited in References 11-17. Both analytical, Reference 11, and experimental work, References 12 and 13, have been performed. Recently, increased emphasis has been placed on correlation between analytical and experimental results. In References 14-16, three different analyses of various sophistication are correlated with the experimental data reported in References 12 and 13. For this relatively simple hingeless rotor/body configuration, agreement is generally good. Furthermore, it seems that some of the discrepancies can be removed by improvements in the aerodynamic modeling, as shown in Reference 15. However, Reference 17 indicates that when attempting to model more realistic hingeless blade designs or bearingless rotors, existing analyses lack sufficient accuracy and consistency in their aeromechanical stability predictions. Thus, it is evident that considerably more research is needed to develop better analytical models and validate them against test data.

A modern rotorcraft must operate in a severe dynamic and

aerodynamic environment. This includes atmospheric turbulence, higher harmonic blade air loading and bending and shaft loads, stall flutter and other potential blade instabilities, impulse loading due to blade/fuselage interference, and advancing blade Mach number effects. The application of active control blade feathering makes it feasible to alleviate some or maybe all of these effects while improving rotorcraft vibration and handling characteristics and thus expanding the rotorcraft flight envelope. Some of the different approaches and possible uses for active control systems for rotors are described in References 18-20.

Most of the past studies in active control for rotorcraft have dealt with gust alleviation, e.g., References 21, 22, or vibration reduction. Reference 23 describes the first successful flight of higher harmonic active control for vibration reduction. It also contains an extensive review of previous work in this area. In these studies, both open loop and closed loop adaptive and gain scheduled controls have been used to minimize vibrations. Research in this area is still ongoing, e.g., References 24-26. However, the data reported in Reference 23 clearly shows that advances in onboard computers, sensor and actuator design, and modern control theory have made vibration reduction through active control a reality.

Application of active control to improve rotor stability has

received little attention in the past. Of particular interest therefore is Reference 27 in which the aeromechanical stability of hingeless rotor helicopters and the application of feedback control to augment system damping was studied The baseline rotor/fuselage configuration resembles an S-58 helicopter. However, the rotor is modelled having four hingeless blades with a flap and lead-lag frequency of 1.15 and 0.70 cycles per revolution, respectively, at a rotor tip speed of 650 ft/sec. Blade structural damping is assumed to be one-half percent of critical lead-lag damping. This configuration exhibits a slight aeromechanical instability on the ground, for thrust to weight ratios greater than 0.6, and in hover. The unstable mode is dominantly a fuselage roll mode. The use of active control was studied by implementing fuselage roll position and roll rate feedback into a set of swashplate actuators in order to generate longitudinal and lateral cyclic blade pitch commands. Feedback of fuselage pitching motion was not pursued since the unstable mode has only a relatively small pitch component. Numerical results of Reference 27 are presented by plotting damping values of the critical mode as obtained from eigenanalyses. The corresponding frequencies are not presented. These results show that feedback of roll position and roll rate can stabilize the unstable roll mode both on the ground and in hover. In Reference 28 blade lag rate feedback through individual-blade-control was used to augment the lead-lag mode damping of isolated rotor blades. Two blade mounted

accelerometers are used to sense blade lead-lag acceleration. This signal is then integrated and rate information is fed back to an actuator that controls the pitch angle of an individual blade. This control system is applied to an articulated model rotor blade. Data from a simplified analytical hover model show that feedback control can increase the lag damping ratio, while the flap damping ratio is slightly reduced. Experimental results confirm that feedback increases damping of the lag mode both in hover (83/4 = 8 deg) and even more so in forward flight (μ = 0.27). Reference 29 formulated the equations of motion for air resonance of hingeless rotor helicopters with active control of the collective, longitudinal and lateral cyclic blade pitch inputs. Here, the blade motions are represented by the fundamental elastic mode shapes. No numerical results are presented. In Reference 30 feedback control was used to improve the pitch-flap stability and response of single rotor blades in hover. The control system is assumed to have four independent actuators, permitting independent control of the flap and pitch displacements and velocities. The control system parameters are determined using classical and modern control theory techniques. Numerical results are presented for a nine-foot diameter model rotor system. For this rotor the flutter speed could be raised from 67 rad/sec to 150 rad/sec through application of feedback control. At the same time the dynamic response of the rotor at subcritical rotor speeds was lowered.

From a review of the literature it is clear that most of the previous applications of active control to rotors have dealt with response problems, such as gust alleviation or vibration reduction. While by no means simple problems, measurement of the quantities to be controlled, namely gust or vibration response, is well understood. Thus, control systems for these problems are generally designed to be adaptive. In addition, for vibration control the frequency of the oscillatory control inputs is fixed at multiples of the rotor speed. Thus, for preliminary investigations, the accelerations of the pilot's seat could be used in an open loop type of control to minimize vibrations in steady flight; Reference 23.

To directly evaluate the performance of an active control system or design an adaptive control system for stability augmentation is a considerably more difficult problem. Dynamic stability measurements, even off-line, are particularly problematic for helicopter aeromechanical stability where rotating and nonrotating systems are directly coupled, many degrees of freedom are involved, and the process and measurement noise levels can be very high; Reference 31 Potential use of real-time parameter identification techniques to determine rotor damping parameters or complete system dynamic stability has been studied; References 32 and 33. This issue will require additional work in the future if the concept of active control to increase rotorcraft aeromechanical stability is to

be fully utilized.

The purpose of the present study is to evaluate in depth the potential for using active blade pitch control to increase rotor/body system damping. The detailed objectives can be summarized as follows:

1) Investigate the influence of state variable feedback on system damping. Include body acceleration and rotor state feedback systems which have not been considered before. In addition, evaluate changes in the system frequencies and response.

2) Study the effects of feedback parameters; that is feedback gain and weighting between the time-dependent cyclic controls. Determine a systematic approach to choose these parameters for optimal stability augmentation.

3) Investigate the use of control scheduling with rotor speed to ensure stability during rotor run up.

4) Assess the influence of rotor design parameters on the performance of feedback control.

ANALYTICAL MODEL

Analytical prediction of coupled rotor/body aeromechanical stability is a difficult task because of the strong aerodynamic, inertial, and structural coupling and nonlinearities inherent in modern rotors. The modification of system damping through small changes in blade pitch settings requires a model that includes all the ingredients of an aeroelastic stability analysis. However, care must be taken to make the model simple enough to allow efficient simulation of various active control concepts in order to demonstrate the feasibility of this approach. At the same time, sufficient detail should be included to systematically study the effect of rotor/body parametric changes on the control laws.

MATH MODEL

A brief description of the mathematical model developed for this study and the system parameters modelled follows. The math model is similar to the models used in References 11 and 16. The helicopter body is represented as a rigid fuselage having pitch and roll rotations ($\theta y, \theta x$) about the center of mass and longitudinal and lateral translations (Rx, Ry) of the center of mass; see Figure 1. The fuselage physical properties required for modelling are its mass, pitch and roll inertias, and effective landing gear stiffnesses and damping in rotation and translation. The rotor hub is

located a distance h above the fuselage mass center. The blades are assumed to be rigid and rotate against spring and damper restraints about coincident flap and lead-lag hinges offset from the axis of rotation, see Figure 2. The orientation of the hinges can be different from the aerodynamic pitch angle, thus allowing modeling of variable structural flap-lag coupling and pitch input inboard or outboard of the hinges. Blade precone is included. This parameter was deemed to be important in this study since it directly contributes to the Coriolis forces which augment blade lag damping.

BASIC ASSUMPTIONS

The major assumptions on which this study is based are listed below.

1. The fuselage or rotor support is a rigid body with lateral, longitudinal, pitch and roll degrees of freedom. Vertical motion and yaw rotation are not included (Figure 1).

2. The unperturbed rotor shaft is vertical (direction of gravity) The fuselage center of mass is located on the rotor shaft but offset below the hub center by a distance h.

3. The rotor operates in a hovering state with low disk

loading. The rotor speed is constant.

4. The rotor consists of three or more rigid blades.

5. The blade root hinge is offset from the rotor shaft. The feathering axis is preconed.

6. Each blade has rigid body flap and lead-lag degrees of freedom. These motions are restrained by a set of springs and viscous dampers.

7. The blade cross-section reference points coincide with the feathering axis. Built-in twist is zero.

8. The induced inflow is uniform along the blade.

9. The aerodynamic forces are based on two dimensional quasi-steady theory. Apparent mass, compressibility and stall are neglected.

10. The pitch control input is composed of two parts: the time independent collective pitch, identical for all blades; and the time-varying "active" pitch.

11. For the results presented here the blade active control is applied through a conventional swashplate.

ORDERING SCHEME

In deriving the equations of motion for this model a large number of small terms appear. Many of these can be neglected systematically by appropriately using an ordering scheme. This is based on the magnitude of blade slopes, which are typically in the range of $0.1 < \varepsilon < 0.2$. The various parameters in the equations are assigned orders of magnitude. Fuselage motions are assumed to be of order $O(\varepsilon^{1.5})$. The active control blade pitch angle is assumed to be of order $O(\varepsilon^{1.5})$, based on experience with the HHC actuator control inputs, Reference 23. In applying the ordering scheme it is then assumed that terms of order $O(\varepsilon^2)$ are negligible in comparison with unity. In addition, all terms that contain products of the fuselage degrees of freedom are neglected.

EQUATIONS OF MOTION

The system equations of motion are derived using the Newtonian approach. First the blade distributed inertia and aerodynamic loads, using quasi-steady aerodynamics are derived. The N flap and N lag blade equations ($N \geq 3$) are obtained by integrating the distributed blade loads over the length of the blade and enforcing moment equilibrium at the root hinge. For a detailed description of this procedure see Reference 34. The four fuselage equations are derived from dynamic equilibrium at the center of mass, including the rotor loads at the hub, fuselage inertia and gravity loads, and fuselage constraint loads due to landing gear springs and dampers.

The resulting governing system of 4+(2*N) equations is coupled, nonlinear and has periodic coefficients.

The active control pitch input appears as aerodynamic forcing expression in all equations. The values in the blade lag and fuselage translation equations are one order of magnitude smaller than in the flap equations and in the fuselage pitch and roll equations. From these equations it therefore seems that two primary mechanisms exist to stabilize ground resonance. First, the fuselage pitch and roll motion can be controlled through the pitch and roll moments arising from flapping. The magnitude of each is directly related to the blade root hinge offset and flap spring stiffness. The second mechanism is lead-lag damping augmentation through Coriolis coupling with blade flap motion. This requires presence of either steady coning deflection or precone.

As discussed in References 15 and 28, unsteady aerodynamic effects (dynamic inflow) can at times have a considerable effect on the blade flap motion. Since flapping plays an important role in stabilizing ground resonance perhaps the conclusions of the present study would be changed to some degree. In particular for high flap stiffness rotors unsteady aerodynamics should be included in a more refined model.

SOLUTION METHOD

The nonlinear equations of motion can be solved directly in the time domain. However, for parametric stability studies a frequency domain solution is much more desirable. The equations are therefore linearized to allow an eigenanalysis capability. The steady-state, nonlinear equilibrium position is obtained assuming that the fuselage degrees of freedom and the active blade pitch are zero. In the case of hover, the blade equilibrium position is independent of time and can be obtained iteratively using the Newton-Raphson technique. The linearized perturbation equations are then written as

$$[M(q_o,\psi)]\,\ddot{\underset{\sim}{q}} + [C(q_o,\psi)]\,\dot{\underset{\sim}{q}} + [K(q_o,\psi)]\,\underset{\sim}{q} + \underset{\sim}{f}\,(\theta_A, q_o, \psi) = 0$$

The complete set of equations is given in Appendix B.

The linear, periodic coefficient perturbation equations can be solved using Floquet theory; Reference 35. In the present study, the equations are converted into a constant coefficient system using the multiblade or Fourier coordinate transformation; Reference 26. This is possible under the assumptions that all blades are identical and that the active pitch input is generated through a conventional swashplate with three "active" actuators in the fixed system. With the rotor being in a hover condition only the first cyclic blade motions in flap and lead-lag couple with the fuselage motions. The collective and reactionless blade equations are

not needed. The problem size is thus reduced to 2 flap, 2 lead-lag and 4 fuselage equations.

$$[M(q_o)]\ddot{\underset{\sim}{q}} + [C(q_o)]\dot{\underset{\sim}{q}} + [K(q_o)]\underset{\sim}{q} + [C^{\sigma}(q_o)]\underset{\sim}{u} = 0$$

$$\underset{\sim}{q}^T = [\zeta_c, \beta_c, \zeta_s, \beta_s, \theta_x, \theta_y, R_x, R_y],$$

$$\underset{\sim}{u}^T = [\theta_{Ac}, \theta_{As}]$$

Stability of the ground resonance problem in the fixed system is then evaluated by transforming the equations into first order form and performing an eigenvalue analysis. This form of the governing equations is also used to compute the time history response and frequency response of the system.

$$\dot{\underset{\sim}{x}} = [A]\underset{\sim}{x} + [B]\underset{\sim}{u},$$

$$\underset{\sim}{x}^T = [\underset{\sim}{q}^T, \dot{\underset{\sim}{q}}^T]$$

CORRELATION WITH GROUND RESONANCE DATA

In order to validate the governing equations of motion, a correlation study was performed for some of the rotor/body configurations reported in References 37, 12 and 13. No active controls are utilized for these results.

An excellent and extensive body of experimental and analytical data regarding the state of the art in aeroelastic stability analysis was presented at the ITR Methodology Assessment Workshop held at NASA Ames (May 1983); Reference 17. From the correlation studies presented, it is clear that in certain cases considerable differences exist between analytical predictions and experimental results. However, the simple analytical model used for the present investigation should be expected to predict the frequency crossovers and damping trends adequately for the rotor/body systems modelled here. It is not the purpose of the current study to improve upon the state of the art of aeroelastic stability predictions.

Results of a classical ground resonance model were used for initial correlation. The model chosen from Reference 37 consisted of blade lead-lag and fuselage longitudinal and lateral degrees of freedom but no aerodynamics. All blade dampers are working, i.e., the rotor is isotropic. The parameters of this model, herein termed configuration A, are listed in Table 1. As seen in Figure 3, the results of the

present analysis (solid symbols) show very good agreement with those of Reference 37.

The experimental data in References 12 and 13 used here was obtained to investigate rotor/body stability of a hingeless model rotor. The gimbal body support has pitch and roll degrees of freedom. The blade root attachment consists of orthogonal flap and lag flexures at radial station 0.105R, without kinematic couplings. Collective pitch is introduced outboard of the flexures. In Reference 12 tantulum rods are used instead of blades. The parameters for this model, herein termed configuration B, are listed in Table 2. For the two B configurations, note that the pitch mode is essentially locked out, for case B1, while for case B2 both pitch and roll motions are present. The model blade used in Reference 13 has a cambered airfoil with zero lift at -1.5 degree angle of attack. Thus, even at zero collective pitch the rotor develops a small amount of thrust. Two cases from Reference 13 are considered: configuration 1 (as identified in Reference 13) with a soft flap flexure of about one-fourth the stiffness of the lag flexure, see Table 3, and identified in this study as configuration C; and configuration 4 with equal (matched) flap and lag flexure stiffnesses, see Table 3, and identified in this study as configuration D. System parameters in Reference 13 were chosen so that the systems experience a slight aeromechanical instability at the coalescence of the regressing lag and the body roll mode.

Experimental results reported in References 12 and 13 were included in the ITR Methodology Assessment Study. HHI's analytical results obtained under the ITR contract have been reported in References 14 and 17. To correlate with these results the present model includes blade lead-lag as well as flap and fuselage pitch and roll degrees of freedom.

Figures 4 and 5 show correlation with experimental data from Reference 12 where tantalum rods were used instead of blades. This essentially represents an "in vacuum" condition. Parameters for this model, configuration B, are listed in Table 2. System modal frequencies predicted by the current analysis (solid symbols) compare well with the experimental data and the E-727 analysis, Reference 14, both for the body roll only configuration B1, Figure 4, as well as for the body roll and pitch configuration B2, Figure 5 Damping data is not shown since the experiments only simulated a vacuum, i.e., aerodynamic drag forces are still present, whereas the present analysis cannot simulate this condition. Predicted damping levels for total vacuum are lower than the measured values. However, damping trends at frequency crossovers are very well predicted.

Figures 6 through 11 show correlation of the present analysis with experimental data from Reference 13 (configuration 1) and with the corresponding E-927 analyses from Reference 14. Parameters for this model, configuration C, are listed in Table 3. Frequencies and lead-lag damping levels for the

flat pitch case. Figures 6 and 7, show very good agreement. Corresponding roll and pitch damping values, Figures 8 and 9, are generally higher than experimental data but in the same range as E-927 predictions.

Lead-lag damping for nine degrees of collective pitch as a function of rotor speed is shown in Figure 10. Agreement of the present analysis (solid symbols) with experimental damping values is very good up to 650 rpm. This includes the crossover of the regressing lag mode with the body pitch mode. For higher rotor speeds, at crossover with the body roll mode, only general trends in damping are captured. This is certainly a shortcoming but it is felt that a better knowledge and/or adjustment of the body roll frequency and damping would improve results considerably. Furthermore, Figure 11 shows that the current analysis predicts damping trends as a function of collective pitch angle quite well for the regressing lag mode.

Figures 12 and 13 show correlation with experimental and analytical results from Reference 13 (configuration 4, matched stiffness case). Parameters for this model configuration D, are listed in Table 3. Correlation of the present analysis with the experiment is degraded when compared to that achieved in the soft flap flexure case. However, analytical results of the present study are in the same range as those shown in Reference 13. Results from Reference 15 show that dynamic inflow yields much better

correlation for this matched stiffness rotor.

It is concluded that the present model and computer code are sufficiently valid to investigate the effects of active controls on rotor/body aeromechanical stability.

CONTROL LAW DEVELOPMENT

Development of control laws and their evaluation for this study will be made with the objective to increase rotor/body system damping levels and eventually eliminate the need for blade dampers. Constraints on state and control variables have to be observed to avoid adversely affecting overall system performance. The selection trade-offs include active control system complexity, reliability, stability, and system interface requirements.

The basic mechanism for influencing lead-lag dynamics is provided through aerodynamic, Coriolis, and kinematic coupling with blade flapping and feathering inputs. For elastic blades, elastic flap-lag coupling would also play a major role. Fuselage dynamics are coupled with blade flapping through aerodynamic and gyroscopic forces.

In implementing the active control terms it is assumed that controls are applied through a conventional swashplate, i.e., control motions are generated by actuators in the fixed system. The active pitch input to the k'th blade can then be expressed as

$$\theta_{Ak} = \theta_{Ac(\psi)} \cos\psi_k + \theta_{As(\psi)} \sin\psi_k$$

where the control inputs θ_{Ac} and θ_{As} are yet to be determined functions of the nondimensional time parameter ψ.

From the above it is clear that the aeromechanical stability of a helicopter is a multi-input/multi-output control problem. In the present study three different control methods were implemented in the computer code: state variable feedback control, output feedback control, and open loop control. Figure 14a shows the block diagrams for state feedback and output feedback, each combined with open loop control. The system equations are

$$\dot{\underset{\sim}{x}} = [A]\underset{\sim}{x} + [B]\underset{\sim}{u} \;,\; \underset{\sim}{u}^T = [\theta_{Ac}, \theta_{Ac}]$$

$$\underset{\sim}{y} = [C]\underset{\sim}{x} \;,\; \text{where for}$$

state feedback: $\underset{\sim}{u} = [K]\underset{\sim}{x}$

output feedback: $\underset{\sim}{u} = [K]\underset{\sim}{y}$ $\quad \underset{\sim}{y} = \underset{\sim}{y}(\xi_1, \dot{\xi}_1, \psi)$

open loop control: $\underset{\sim}{u} = \underset{\sim}{v}$ $\quad \underset{\sim}{v} = \underset{\sim}{v}(\psi)$

Note, that with the output vector $\underset{\sim}{y}$ being a function of the lead-lag displacement and velocity of the first blade, the [C] matrix contains periodic coefficients. This implies that either a time history solution or Floquet theory must be used. In the latter case it might be more desirable to solve the periodic rotor/body equations in the first place rather than transforming the blade degrees of freedom and equations using Fourier coordinates. In the present study, time history integration (Hamming's Predictor-Corrector method) is

used to treat output feedback as well as open loop control.

The motivation for the present approach and some additional assumptions are as follows. State feedback is obviously a natural choice. Here it is assumed that all the states are known. However, only one state at a time is used for feedback. Combined feedback of two or more state variables was not considered. The above choice of the output vector $\underset{\sim}{y}$ is intended to help clarify the issue whether for the case of lead-lag feedback knowledge of the complete rotor state, i.e., ζ_c, ζ_s is necessary or whether it is sufficient to take measurements on one blade only. With respect to lead-lag damping identification, knowledge of one blade's response was sufficient (Reference 33). Open loop control is included here since it provides the capability to perform frequency response analyses. However, open loop control is not used to augment stability. No attempt was made at this stage to use multivariable optimal control techniques to maximize the damping augmentation since gaining a basic understanding of the problem was thought to be more important. For the same reasons and the aforementioned problems with dynamic stability measurements in rotorcraft adaptive control (combining identification and control) was not considered.

Returning now to the implementation of control inputs in more detail, define:

state feedback: $\underset{\sim}{u}^T = [K\cos\phi, K\sin\phi]\, d^n\zeta_i/d\psi^n \qquad n=0,1,2$

output feedback: $\underset{\sim}{u}^T = [K\cos\phi, K\sin\phi]\, y(\xi_1, \dot{\xi}_1, \psi)$

open loop control: $\underset{\sim}{u} = \begin{Bmatrix} K\cos\phi \cdot \cos(\bar{\omega}_A \psi + \phi_c) \\ K\sin\phi \cdot \cos(\bar{\omega}_A \psi + \phi_s) \end{Bmatrix}$

In the above expressions K is the control gain. The angle ϕ, herein termed "feedback phase" defines the relative weighting between the time dependent cyclic controls. In other words, ϕ defines the azimuthal position where the gain that individual blades experience has its maximum value. This point is 90 degrees from the axis of no feathering about which the swashplate oscillates; see Figure 14b. The quantity q_i is one of the system degrees of freedom, and y_j is a function of the lead-lag displacement and velocity of the first blade. The open loop control frequency is $\bar{\omega}_A$ and phasing of the cosine and sine input is denoted by ϕ_c and ϕ_s respectively. It should be pointed out that for simplicity state feedback is introduced into the second order equations, thus $\underset{\sim}{u}$ is proportional to q_i rather than x_i. State feedback can then be thought of as an addition to the system stiffness, damping, and/or mass matrix, for n = 0, 1, 2 respectively.

RESULTS

All the active control simulations in this study were performed for the rotor/body configuration C. This is a soft inplane hingeless rotor supported on a gimbal with pitch and roll degrees of freedom The baseline system parameters are listed in Table 3. When investigating the effects of rotor configuration the blade root hinge offset, precone, and flap stiffness were varied from their nominal values. Parameters for these cases, inasmuch as they differ from configuration C, are shown in Tables 5, 6, and 7 respectively. Nominal rotor speed for configuration C is 720 rpm. All cases are run with flat pitch, however, this rotor has a cambered airfoil which gives a small positive thrust at zero collective. The modal frequencies and damping for the baseline case without feedback are shown in Figures 6-9. Recall, that the regressing lag mode experiences an instability at the frequency crossover with the body roll mode, which occurs at 765 rpm.

All the results presented were obtained using state variable feedback control. First, the effect of individual feedback state variables on system stability is explored by varying feedback gain and phase systematically. These studies are performed at the point of minimum stability, i.e., at the coalescence rotor speed of 765 rpm. Plots of system damping and frequency versus feedback phase are used to select

candidate feedback states and define feedback phase angles for maximum damping augmentation. Next, these candidate feedback states are investigated in more depth by considering a range of rotor speeds to simulate rotor run up. Results show the sensitivity of the system dynamic behavior with respect to changes in feedback gain and phase. Following this, the effect of rotor configuration on active control damping augmentation is studied. To this end the blade root hinge offset, precone, and flap stiffness, which are key parameters in terms of control effectiveness, are varied to cover a range of values typical for articulated, hingeless, and bearingless rotors. Lastly, the rotor/body response behavior is considered. This provides a quantitative measure of the active blade feathering amplitudes required to achieve adequate stability margins. It also gives a better understanding of the rotor/body mode shapes.

STATE FEEDBACK STUDIES

For state feedback the active blade feathering angle is, for various analyses, set proportional to individual state variables, ζ_c, ζ_s, θ_x, θ_y, β_c, β_s, and their time derivatives.

Figures 15 through 28 show the effect of feedback on system damping, i.e., real part of the eigenvalue, and frequencies, i.e., imaginary part of the eigenvalue. Gain values of K=1, 2, and 3 and a complete range of feedback phase angles, $0<\phi<360.$, are considered. Also shown are the damping and frequency of the baseline system without active controls, i.e., K=0. The rotor speed in these figures is 765 rpm which corresponds to coalescence of the body roll mode and regressing lead-lag mode frequencies; Figure 6. From these plots feedback of the following states was found to be most suitable for stability augmentation: $\dot{\zeta}_c$, ζ_s, $\ddot{\zeta}_s$, $\dot{\theta}_x$ and $\ddot{\theta}_x$, see Figures 16, 18, 20, 22, and 23. Individual results are discussed in detail below.

Figure 15 shows the influence of cosine cyclic lead-lag position feedback (ζ_c) on system dynamics. The baseline (K=0) lead-lag regressing mode is unstable for this operating condition. Depending on the feedback phase, variations in feedback gain can increase damping and stabilize this mode ($250<\phi<30$ deg) or decrease damping and further destabilize it ($30<\phi<250$ deg). The opposite behavior is observed for the progressing lead-lag mode which is stable for K=0. It's

damping is decreased for feedback phase between 180 and 360 degrees and increased for feedback phase between 0 and 180 degrees. This makes the progressing lead-lag mode the least damped mode for feedback phase between 250 and 360 degrees and, depending on the gain value, can result in system instability. Therefore there exists only a small range of feedback phase angles, around ϕ=0, where the rotor/body system could be stabilized through active control. Feedback of ζ_c is therefore not considered to be a suitable choice. Similar findings can be made for $\ddot{\zeta}_c$ and $\dot{\zeta}_s$ feedback, see Figures 17 and 19.

Figure 16 shows the influence of cosine cyclic lead-lag rate feedback ($\dot{\zeta}_c$) on system dynamics. Again, depending on the feedback phase, the damping of the regressing and progressing lead-lag modes can be increased or decreased from the baseline values. This time, however, damping for both modes is increased over approximately the same range of feedback phase values. As a result the system can be stabilized for feedback phase between 0 and 110 degrees. The maximum increase in damping occurs at approximately 60 degrees feedback phase and is directly proportional to the feedback gain. Feedback of $\dot{\zeta}_c$ is thus considered to be a suitable candidate for stability augmentation. Similar findings can be made for feedback of ζ_s at ϕ=240 and feedback of $\ddot{\zeta}_s$ at ϕ=60 degrees, see Figures 18 and 20. Continuing the discussion of Figure 16, it is seen that $\dot{\zeta}_c$ feedback control changes the roll and regressing lag mode frequencies only to

a limited extend. Furthermore, at feedback phase angles of approximately 60 and 240 degrees these modal frequencies remain unchanged for all values of feedback gain. This clearly shows that the improved system stability at ϕ=60 degrees is a direct result of increasing the regressing lag mode inherent damping and not due to a change in coalescence rotor speed. Inspection of the roll mode and regressing lag mode damping indicates that the source of the increased lag damping is a reduction in roll mode damping. However, the roll mode is well damped in the baseline system and this exchange of damping is therefore beneficial for overall system stability.

The effect of roll attitude, rate, and acceleration feedback is shown in Figures 21, 22, and 23. Again, damping of the regressing and progressing lead-lag mode is increased or decreased depending on the feedback phase. In addition, roll attitude feedback (Figure 21) can lead to considerable instability of the roll mode and regressing flap mode at certain values of feedback phase. This behavior was also observed for roll rate and roll acceleration feedback for gains greater than those shown in Figures 22 and 23. Returning to Figure 21, roll attitude feedback could be used to stabilize the system for feedback phase between 45 and 120 degrees. However, the frequency plot shows that in this range the roll mode frequency is raised considerably. Any gains in system damping would thus largely be due to a shift of the coalescence rotor speed rather than an increase in

regressing lag mode inherent damping. Feedback of roll attitude is therefore not further considered. Feedback of roll rate (Figure 22) at a feedback phase between 90 and 120 degrees adds damping to the regressing lag mode while keeping the regressing lag and roll mode frequencies almost unchanged. However, the feedback gain would have to be increased to provide adequate system stability margins. Similar observations can be made for roll acceleration feedback (Figure 23) at a feedback phase between 240 and 270 degrees. Thus, both roll rate and acceleration seem to be suitable feedback states and will be studied in more depth.

Feedback of pitch attitude, Figure 24, is seen to have very little effect on damping of the regressing lead-lag mode. At the same time, damping of the pitch mode and regressing flap mode can be lowered to a point of considerable instability. Results from pitch rate and acceleration feedback, Figures 25 and 26, show no change in regressing lag mode damping and, for larger gains, can be expected to exhibit similar pitch mode instabilities as for feedback of pitch attitude. Pitch feedback is therefore not considered a suitable choice for eliminating the regressing lag/roll mode instability considered here.

The influence of flap feedback states on system damping is shown in Figures 27 and 28. While leading to large changes in damping of the regressing and progressing flap modes, the damping of the regressing lag mode is not improved and the

flap state variables are not considered for rotor/body damping augmentation.

Based on the above results feedback of $\dot{\zeta}_c$, ζ_s, $\ddot{\zeta}_s$, $\dot{\theta}_x$, and $\ddot{\theta}_x$ was further evaluated by considering rotor rpm sweeps and varying the gain K, while keeping the feedback phase ϕ at constant value; see Figures 29 through 33. The value of ϕ was chosen as discussed previously. The objective was to select a value of ϕ that would increase damping for the regressing and advancing lag mode but leave the frequencies of the regressing lag mode and roll mode unchanged. In selecting the gains K, an attempt was made to obtain approximately the same range of regressing lag mode damping values for all five feedback states. It is seen that in all five cases the system can be stabilized at all previously critical rotor speeds, although to a varying degree. This will be further quantified through response solutions. Feedback of the selected lead-lag states, Figures 29, 30, and 31, adds considerable damping to the regressing lag mode above 700 rpm and stabilizes the system. At the same time the frequencies and in particular the coalescence rotor speed of the regressing lag/roll mode are changed very little. However, at the crossover of the regressing lag mode with the body pitch mode (600 rpm) these feedback controls could destabilize the system, depending on the value of feedback gain. Feedback of roll rate and roll acceleration, Figures 32 and 33, also augment the damping of the regressing lag mode above 700 rpm and could be used to stabilize the system.

Roll feedback has no effect on the regressing lag mode damping at coalescence with the pitch mode. This is consistent with the previous observation that pitch feedback is not suitable to eliminate the coupled regressing lag/roll mode instability. It is further interesting to note that feedback of the body roll rate and in particular roll acceleration lead to considerable shifts in the frequency of the roll mode and therefore change the coalescence rotor speed. The stability gains seen in Figures 32 and 33 are thus attributable to a combination of increased inherent damping and frequency shifts. Whether such a change in roll frequency is desirable must be decided on a case to case basis.

The sensitivity of the system dynamic behavior with respect to the feedback phase is explored in Figures 34 through 37 for feedback of ζ_s, $\ddot{\zeta}_s$, $\dot{\theta}_x$, and $\ddot{\theta}_x$, respectively. In each case, three phase angles near the optimum value were chosen, while the gain was kept at a particular value representing approximately similar control effort in terms of active blade pitch angle amplitudes. These values were determined from response studies to be K=0.3, 3.0, 9.0, and 27.0 for ζ_s, $\ddot{\zeta}_s$, $\dot{\theta}_x$, and $\ddot{\theta}_x$ feedback, respectively. Note that for clarity only the regressing lag mode damping curves are shown in Figures 34 through 37. Other symbols show the damping of the progressing lag mode and other system modes. Again, feedback of ζ_s and $\ddot{\zeta}_s$ for the gain values shown in Figures 34 and 35 keeps the system frequencies unchanged. Damping results show

that feedback phase can be used to maximize the regressing lag mode damping at each rotor speed. This indicates that a phase schedule with rpm could be used. Feedback of the roll rate and roll acceleration, Figures 36 and 37, leads to roll mode frequency changes. However, the system is stable at the new coalescence rotor speed which means that inherent damping has been added to the regressing lag mode. Furthermore, while the feedback phase has little effect on system damping it is seen to be a powerful parameter for changing the roll mode frequency.

The results obtained so far are summarized in Figures 38 and 39. These figures show root locus plots for the candidate lead-lag and roll feedback state variables. In each case the regressing lag mode is the least damped mode and thus governs system stability. It is seen that feedback of the state variables $\dot{\zeta}_c$, ζ_s, $\ddot{\zeta}_s$, $\dot{\theta}_x$, and $\ddot{\theta}_x$ can be used to eliminate the inplane/roll instability of the baseline system. The feedback gain K can be increased to obtain a specified level of regressing lag mode damping at the coalescence rotor speed (Figures 38a,b and 39a,b). The feedback phase ϕ can be used to maximize the regressing lag mode damping augmentation at other rotor speeds (lead-lag feedback shown in Figures 38c and d) or change the roll mode frequency which indirectly changes the regressing lag mode damping (roll feedback shown in Figures 39c and d). These results also show that a different choice of feedback state variables and control parameters (K, ϕ) would be needed to eliminate an

inplane/pitch instability. Quantitative results are given in Table 4. For $\dot{\zeta}_c$, ζ_s, $\ddot{\zeta}_s$, and $\dot{\theta}_x$ feedback about 1 percent of critical damping is introduced for the regressing lag mode at a maximum active blade pitch angle, $\theta_{A_{max}}$, of one third degree per degree of cyclic lead-lag angle. For $\ddot{\theta}x$ about 1.5 percent of critical damping is introduced with the same control angle. (Figure 37 shows that the larger change in damping with $\ddot{\theta}x$ feedback is due to changes in the roll mode frequency.) The control angles shown in Table 4 are quite small in particular when considering the low frequency of the control motion. However, it will be important to engage the control system before the lead-lag motion can build up to large amplitudes.

The results shown so far are very promising. They indicate that several ways exist to augment rotor/body stability. The important aspect of control mechanization can thus be approached with considerable flexibility.

EFFECTS OF ROTOR CONFIGURATION

Very important rotor parameters in terms of control effectiveness are the blade root hinge offset, precone, and flap spring stiffness. These parameters were varied from their baseline values (configuration C, Table 3) to cover a range of values representative of articulated, hingeless, and bearingless rotors. At the same time the blade root spring stiffnesses, lead-lag damping and body roll stiffness were changed so that the modified rotor/body systems would closely approximate the baseline system at the coalescence rotor speed in terms of roll frequency and regressing lag mode frequency and damping. Use of these equivalent dynamic systems is intended to permit direct comparison of the stability results obtained with feedback control. Parameters for these systems, inasmuch as they are different from configuration C, are listed in Tables 5, 6, and 7.

Figure 40 shows the frequency and damping for the equivalent dynamic systems when the blade root hinge offset is varied from 10 to 5 and 2 percent. The regressing lag and body roll frequency remain unchanged at the coalescence rotor speed of 765 rpm. Also the damping curves match very closely between 720 and 850 rpm. The effects of precone and flap spring stiffness are investigated for the lowest value of hinge offset (e = .027). Precone has negligible effects on system frequencies. Figure 41 therefore only shows the damping for the equivalent dynamic systems when precone is changed from

0 to 2 and 4 degrees. It is seen that damping values are well matched throughout the unstable region. Figure 42 shows the system frequencies and damping when the flap stiffness is reduced to zero. Frequencies are well matched with the exception of the regressing flap mode. This mode changes its character from being regressing in the fixed system (rotating frequency greater than one) to being progressing (rotating frequency smaller than one) as the flap stiffness is reduced. As a result damping values match only at the coalescence rotor speed.

Investigation of active control is limited to feedback of the sine cyclic lead-lag position (ζ_s) and roll acceleration ($\ddot{\theta}_x$) state variables. For these two feedback states a brief study was conducted to determine approximately the optimal feedback phase angles and appropriate feedback gain levels. Tables 5, 6, and 7 list these feedback parameters and the resulting system damping values. Results for the various root hinge offsets (Table 5) and precone angles (Table 6) are obtained by keeping the active blade feathering angles constant ($\theta_{A_{max}}$ = 0.29 degrees for ζ_s feedback, approximately 0.4 degrees for $\ddot{\theta}_x$ feedback). It is seen that the system is stabilized for all the different configurations, both for ζ_s and $\ddot{\theta}_x$ feedback. Increases in hinge offset increase the damping levels even though the flapping frequency is reduced. Similarly, increases in precone angle increase the damping levels. When reducing the flap spring stiffness to zero (Table 7) larger active blade feathering angles (~2 degrees)

are required to obtain stability margins of approximately 0.5 percent critical damping. It should be pointed out, however, that typical articulated rotors have hinge offsets larger than the configurations in Table 7.

The above results, while being of a limited nature, show that the root hinge offset, flap spring stiffness, and precone have considerable influence on the control effectiveness. This had to be anticipated due to the action of hub moments and Coriolis coupling. It can be concluded that active control for rotor/body damping augmentation will be particularly powerful for hingeless and bearingless rotors which typically have a large virtual hinge offset and flap spring stiffness and in many cases also precone. Controlling the aeromechanical stability of typical articulated rotors will be a more difficult task. For these rotors it might be helpful to use collective blade pitch to introduce steady blade coning deflection. This should have similar beneficial effects on control effectiveness as precone.

ROTOR RESPONSE

Response results are intended to be of a qualitative nature, to give a better understanding of the rotor/body mode shapes or to give an indication of the required control input magnitudes.

Free Response from a set of initial conditions, forced response, and frequency response results are presented for configuration C. The free response results are computed using an appropriate eigenvector from the stability analysis, normalized to a maximum lead-lag amplitude of one degree, as an initial condition. Frequency response and forced response are computed by simulating a one degree blade pitch stick stir, either in the advancing or regressing direction. For frequency response the nondimensional excitation frequency $\bar{\omega}_A$ is varied from 0.1 to 0.7. Forced response is computed by starting with the system at rest (zero initial condition) and an excitation frequency $\bar{\omega}_A = .336$, corresponding to the frequency of the regressing lag mode at coalescence. The rotor speed is 765 rpm in all cases.

Figure 43 shows the response of the baseline system with no feedback controls applied. The progressing lag mode (high frequency) is seen to be stable. The regressing lag mode (low frequency) is slightly unstable, with critical damping of $\eta = -0.58$ percent. It's modal components consist largely of the cyclic lead-lag motions (ζ_c, ζ_s), the body roll degree

of freedom (θx), and lateral cyclic flapping (β_s). There is very little pitch and longitudinal flap motion. The inherent stability of the rotor/body system with sine cyclic lead-lag feedback control at K=1 and ϕ = 240 degrees is illustrated in Figure 44. The time history response of the regressing lag mode shows that with feedback this previously unstable mode (Figure 43b) is stabilized and both cyclic lead-lag degrees of freedom, ζ_c and ζ_s, reduce significantly in amplitude in only ten rotor revolutions. It is also seen that feedback control increases the participation of the flap and body pitch and roll motions in the regressing lag mode. This could be the source of the increased damping of this mode. The amplitude of active blade feathering in Figure 44 is 0.9 degrees initially and redures to less than 0.5 degrees over ten rotor revolutions.

Figures 45 and 46 show the response of configuration C to advancing and regressing stick stir excitation at the regressing lag mode frequency. No feedback controls are applied. The system is initially at rest. After ten rotor revolutions the excitation is stopped and the rotor/body system is allowed to move freely. This simulates a procedure typically used in helicopter ground resonance testing. It is seen that stick stir in either direction excites the unstable regressing lag mode and results in growing lead-lag motion amplitudes after the excitation is stopped. Note however, that the regressing stick stir (Figure 46) leads to much larger amplitudes than the advancing stick stir (Figure 45).

Examination of the regressing lag mode eigenvector shows that it's flapping contributions are sequenced in a regressing direction. This mode is therefore most readily excited with a regressing stick stir.

Frequency response analysis is used to compare the effect of increased blade lead-lag damping versus the application of feedback control. Figure 47 shows the influence of increasing the lead-lag damping from η_ζ = 0.52 percent to 2 percent and 8 percent critical. No feedback controls are applied. Figure 48 shows the influence of ζ_s feedback with increasing gain values, K = 0.3; 1.0, 3.0, and ϕ = 240 degrees. Damping is held at its nominal value of η_ζ = 0.52 percent. In both cases only the frequency response of the cosine cyclic lead-lag motion is shown. Comparing both magnitude and phase plots qualitiatively indicates that feedback control and additional blade damping have very similar effects in terms of system dynamics. This is an additional indication that active control can be used to augment rotor/body damping and reduce or even eliminate the need for lead-lag dampers.

CONCLUSIONS

The present study indicates that active control blade feathering through a conventional swashplate is a viable means to increase rotor/body damping levels and to eliminate ground resonance instabilities. The choice of control parameters depends on the rotor/body configuration under consideration and must take aspects of control mechanization into account. Based on the stability and response results presented here for state variable feedback control the following conclusions can be drawn.

Roll rate and acceleration and blade inplane motion ($\dot{\zeta}_c$, ζ_s, $\ddot{\zeta}_s$) feedback control can add considerable damping to the system. It eliminates the regressing lag/roll mode ground resonance instability of the hingeless model rotor under consideration. The feedback phase ϕ, i.e., weighting between the cyclic controls, is seen to be a powerful parameter. Depending on the value of ϕ the system can be completely stabilized or further destabilized. With the proper choice of feedback phase, damping of the regressing lag mode can be maximized without adversely affecting the damping of other system modes. The feedback gain K can then be adjusted to obtain a specified level of regressing lag mode damping at the coalescence rotor speed. For $\dot{\zeta}_c$, ζ_s, $\ddot{\zeta}_s$, and $\dot{\theta}x$ feedback about 1 percent and for $\ddot{\theta}x$ about 1.5 percent of critical damping is introduced for the regressing lag mode. This

damping augmentation is obtained with an active blade feathering amplitude of 1/3 degree per degree of blade cyclic lead-lag angle.

Inspection of the system eigenvalues indicates that the increased lag damping might be due to a reduction in damping of other system modes, notably roll or flapping. However, these modes are well damped and this exchange of damping is therefore beneficial for overall system stability. From the regressing lag mode response it is also seen that feedback control generally increases participation of longitudinal flapping and body pitch motions in this mode. This could be an additional source of the increased regressing lag mode damping.

Rotor rpm sweeps show that with the above feedback controls, selected at the coalescence rotor speed, the system is stabilized throughout the range of previously unstable operating conditions. For lead-lag feedback ($\dot{\zeta}_c$, ζ_s, $\ddot{\zeta}_s$) the system frequencies and in particular the coalescence rotor speed remain practically unchanged. Improvements in system stability are a direct result of increasing the regressing lag mode damping. Furthermore, scheduling the feedback phase with rotor speed can be used to maximize the damping augmentation. For roll feedback ($\dot{\theta}x$, $\ddot{\theta}x$) the feedback phase has a considerable effect on the roll mode frequency. Besides increasing the regressing lag mode damping, roll acceleration feedback in particular can be

designed to shift the coalescence rotor speed. This would indirectly improve system stability through active control of frequency placement. Lastly, it is seen that a different choice of feedback state variables and control parameters would be necessary to eliminate an inplane/pitch instability. For the present configuration the active controls should be applied only at rotor speeds above the crossover of the regressing lag mode with the body pitch mode.

Increasing the root hinge offset, flap spring stiffness, and precone improves the control effectiveness considerably. It can be concluded that active control for rotor/body damping augmentation will be particularly powerful for hingeless and bearingless rotors Controlling the aeromechanical stability of articulated rotors will be a more difficult task.

REFERENCES

1. Coleman, R P., "Theory of Self-Excited Mechanical Oscillations of Hinged Rotor Blades", NACA ARR No. 36, July 29, 1943. (Subsequently reissued under authorship of R. P. Coleman and A. M. Feingold as NACA TR 1351, 1958.

2. Deutsch, M. L., "Ground Vibrations of Helicopters," Journal of the Aeronautical Sciences, May 1946.

3. Gabel, R. and V. Capurso, "Exact Mechanical Instability Boundaries as Determined from the Coleman Equation," JAHS, Vol. 7, No. 1, January 1962, pp. 17-21.

4. Donham, R. E., S. V. Cardinale, and I. B. Sachs, "Ground and Air Resonance Characteristics of a Soft Inplane Rigid-Rotor System," JAHS, Vol. 14, No. 4, October 1969, pp. 33-41.

5. Lytwyn, R. T., W. Miao, and W. Woitsch, "Airborne and Ground Resonance of Hingeless Rotors," Preprint No. 414, 26th AHS Forum Washington, D.C., June 1970.

6. Burkan, J. E. and W. L. Miao, "Exploration of Aeroelastic Stability Boundaries with a Soft-in-Plane Hingless-Rotor Model," Preprint No. 610, 28th AHS Forum, Washington, D C , May 1972.

7. Miao, W. L. and H. B. Huber, "Rotor Aeroelastic Stability Coupled with Helicopter Body Motion," Paper No. 14, NASA SP-352, 1974, pp. 137-146.

8. White, R. P. and W. E Nettles, "Examination of the Air Resonance Stability Characteristics of a Bearingless Main Rotor," Preprint No. 78-34-22, 34th AHS Forum, Washington, D.C., May 1975.

9. Staley, J. A., R. Gabel, and H. I. MacDonald, "Full Scale Ground and Air Resonance Testing of the Army- Boeing Vertol Bearingless Main Rotor," Preprint No. 79-23, 35th AHS Forum, Washington, D.C., May 1979.

10. Narmbrodt, W., J. McCloud, M. Scheffler, and J. Staley, "Full-Scale Wind-Tunnel Test of the Aeroelastic Stability of a Bearingless Main Rotor," Preprint No. 81-21, 37th AHS Forum, New Orleans, May 1981.

11. Ormiston, R. A., 'Aeromechanical Stability of Soft Inplane Hingeless Rotor Helicopters," Paper No. 25, 3rd European Rotorcraft Forum, France, 1977.

12. Bousman, W. G., "An Experimental Investigation of Hingeless Helicopter Rotor Body Stability in Hover," NASA TM 78489, June 1978.

13. Bousman, W. G., "An Experimental Investigation of the Effects of Aeroelastic Couplings on Aeromechanical Stability of a Hingeless Rotor Helicopter," Preprint No. 80-25, 36th AHS Forum, Washington, D.C., May 1980.

14. Banerjee, D. B. and J. A. Johnston, "Integrated Technology Rotor Methodology Assessment," Hughes Helicopters, Inc., Report, November 1981.

15. Johnson, W., "Influence of Unsteady Aerodynamics on Hingeless Rotor Ground Resonance," J. Aircraft, Vol. 19, No. 8, August 1982, pp. 668-673.

16. Friedmann, P. P., and C. Venkatesan, "Comparison of Experimental Coupled Helicopter Rotor/Body Stability Results with a Simple Analytical Model," Proceedings of the ITR Methodology Assessment Workshop, NASA Ames Research Center, June 1983.

17. ITR Methodology Assessment Workshop, Proceedings, NASA Ames Research Center, June 1983.

18. Kretz, M., "Relaxation of Rotor Limitations by Feedback Control," Preprint No. 77.33-36, 33rd AHS Forum, Washington, D.C., May 1977.

19. Ham, N. D., ed., "Active Control Systems for Rotorcraft," Vertica, Vol. 4, No. 1, 1980.

20. Ham, N. D., "Helicopter Individual-Blade-Control and its Applications," Proc. 39th AHS Forum, St. Louis, May 1983, pp. 613-623.

21. Johnson, W., "Optimal Control Alleviation of Tilting Proprotor Gust Response," J. Aircraft, Vol. 14., No. 3, March 1977, pp. 301-308.

22. Saito, S., "Application of an Adaptive Blade Control Algorithm to a Gust Alleviation System," Paper No. 64, 9th European Rotorcraft Forum, Italy, September 1983.

23. Wood, E. R., R. W. Powers, J. H. Cline, and C. E. Hammond, "On Developing and Flight Testing a Higher Harmonic Control System," Proc. 39th AHS Forum, St. Louis, Missouri, May 1983, pp. 592-612.

24. Molusis, J. A., C. E. Hammond, and J. H. Cline, "A Unified Approach to the Optimal Design of Adaptive and Gain Scheduled Controllers to Achieve Minimum Helicopter Rotor Vibration," Proc. 37th AHS Forum, New Orleans, May 1981, pp. 188-203.

25. Molusis, J. A., P. Mookerjee, and Y. Bar-Shalom, "Evaluation of the Effect of Vibration Nonlinearity on Convergence Behavior of Adaptive Higher Harmonic Controllers," NASA CR-166424, January 1983.

26. Davis, M. W., "Refinement and Evaluation of Helicopter Real-Time Self-Adaptive Active Vibration Controller Algorithms," November 1983, to be published as NASA CR.

27. Young, M. I., D. J. Bailey, and M. S. Hirschbein, "Open and Closed Loop Stability of Hingeless Rotor Helicopter Air and Ground Resonance," Paper No. 20, NASA SP-352, 1974, pp. 205-219.

28. Ham, N. D., B. L. Behal, and R. M. McKillip, "A Simple System for Helicopter Individual-Blade-Control and its Application to Lag Damping Augmentation Paper No. 10.2, 8th European Rotorcraft Forum, France, 1982.

29. Levin, J., "Formulation of the Helicopter Air Resonance Problem in Hover with Active Controls," M. S. Thesis, University of California, Los Angeles, 1981

30. Peebles, J H., "Optimal Control of a Helicopter Rotor in Hover," M. S. Thesis, George Washington University, Washington, D.C., November 1977.

31. Johnson, W., "A Discussion of Dynamic Stability Measurement Techniques," NASA TM X-73, 081, November 1975.

32. Molusis, J. A., "Rotorcraft Blade Modal Damping Idenfication From Random Responses Using a Recursive Maximum Likelihood Algorithm," NASA CR-3600, September 1982.

33. Molusis, J. A. and Y. Bar-Shalom, "Identification and Stochastic Control of Helicopter Dynamic Modes," NASA CR-166425, January 1983.

34. Venkatesan, C., and P. P. Friedmann, "Aeroelastic Effects in Multirotor Vehicles with Application to Hybrid Heavy Lift System, Part I: Formulation of Equations of Motion," Submitted to NASA for publication as a Contractor Report, December 1982.

35. Friedmann, P., C. E. Hammond, and T. Woo, "Efficient Numerical Treatment of Periodic Systems with Application to Stability Problems," JNME, Vol. 11, 1977, pp 1117-1136.

36. Johnson, W., Helicopter Theory, Princeton University Press, 1980.

37. Hammond, C. E., "An Application of Floquet Theory to Prediction of Mechanical Instability," JAHS, Vol. 19, No. 4, October 1974, pp. 14-23.

38. Brogan, W. L., Modern Control Theory, Quantum Publishers Inc., New York, 1974.

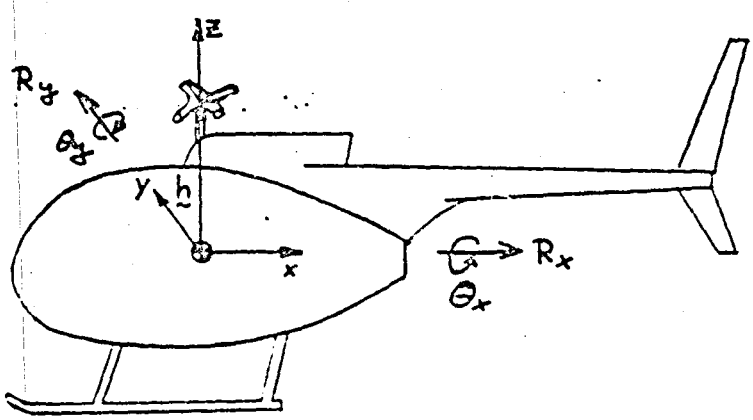

FIGURE 1. Fuselage Model

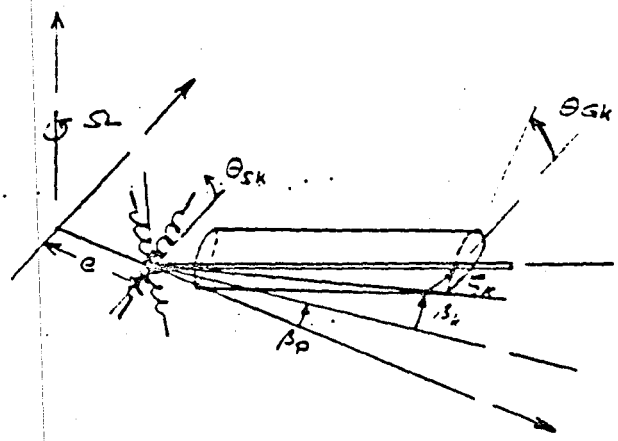

FIGURE 2. Rotor Blade Model

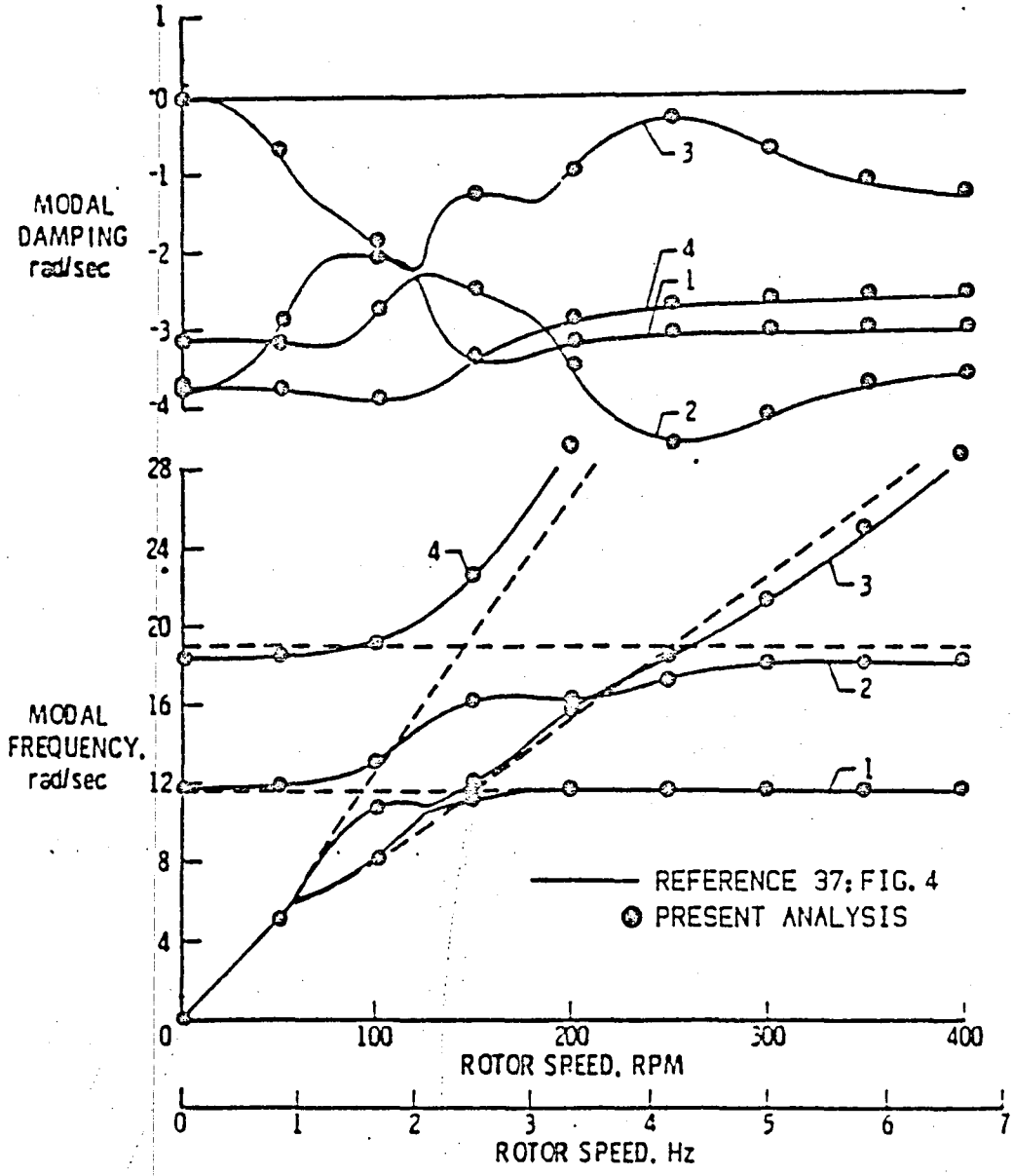

FIGURE 3. Modal Damping and Frequencies Versus Rotor Speed for Classical Ground Resonance Model, Configuration A.

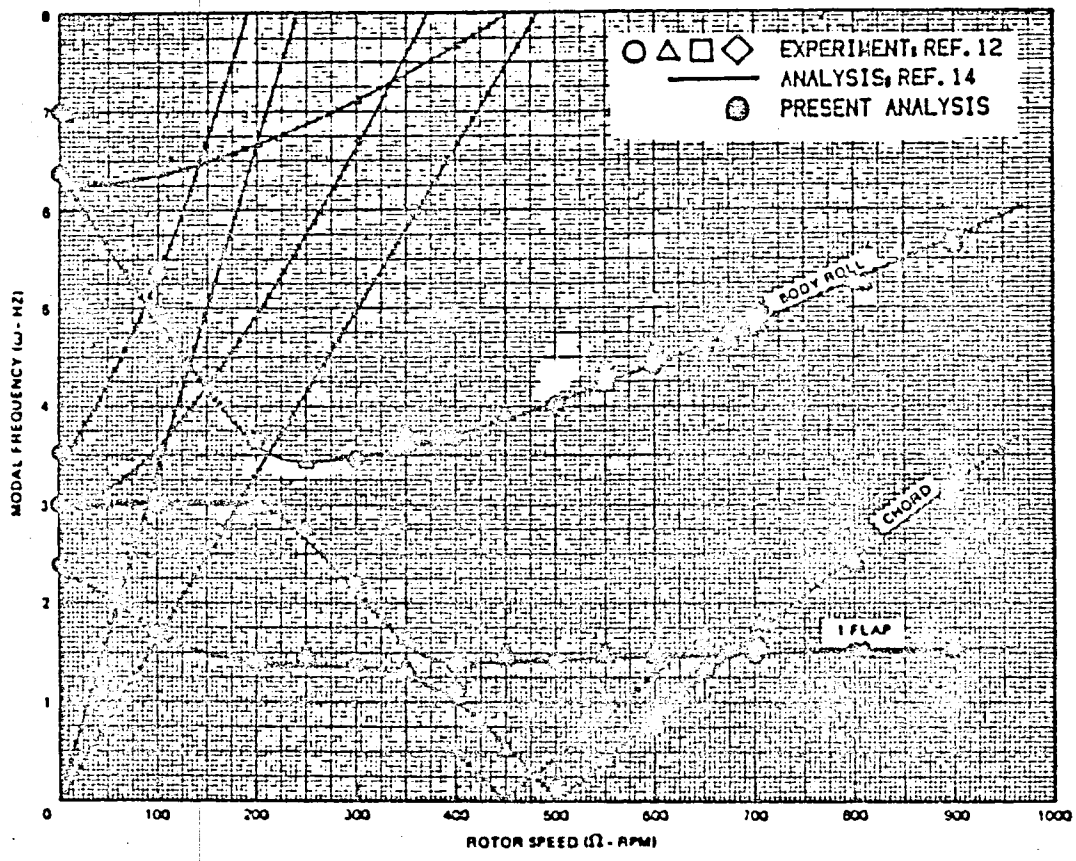

FIGURE 4. Modal Frequencies Versus Rotor Speed, Body Roll Motion Only, Configuration B 1 at Flat Pitch.

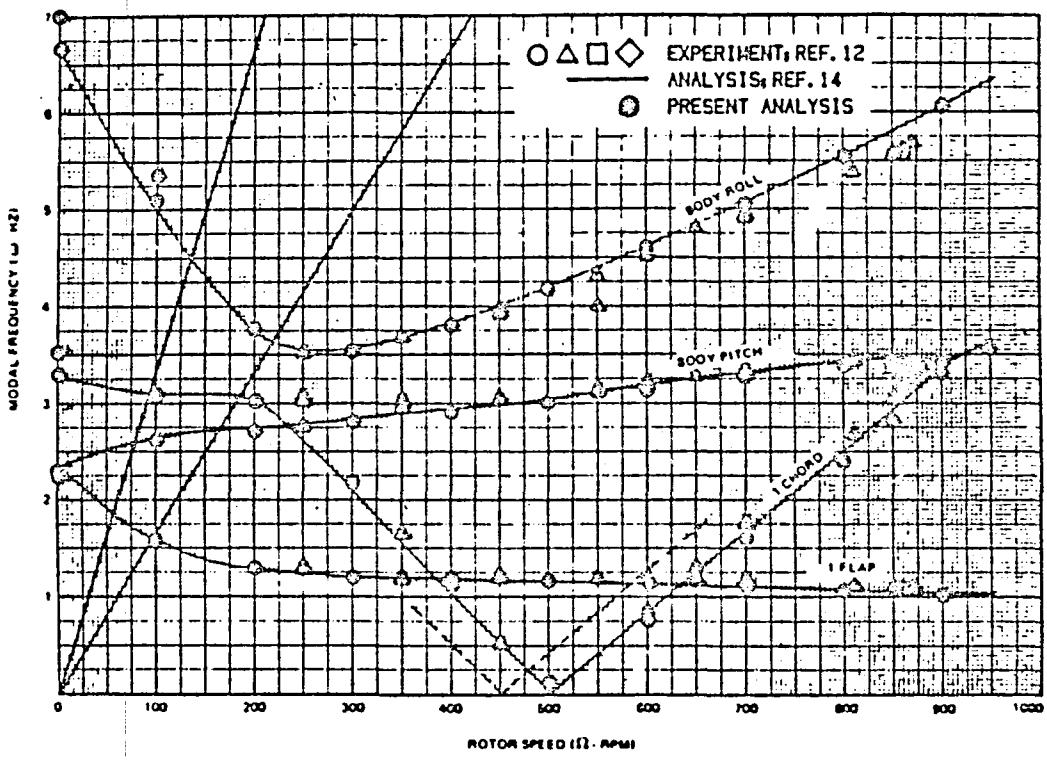

FIGURE 5. Modal Frequencies Versus Rotor Speed, Body Roll and Pitch Motion, Configuration B 2 at Flat Pitch.

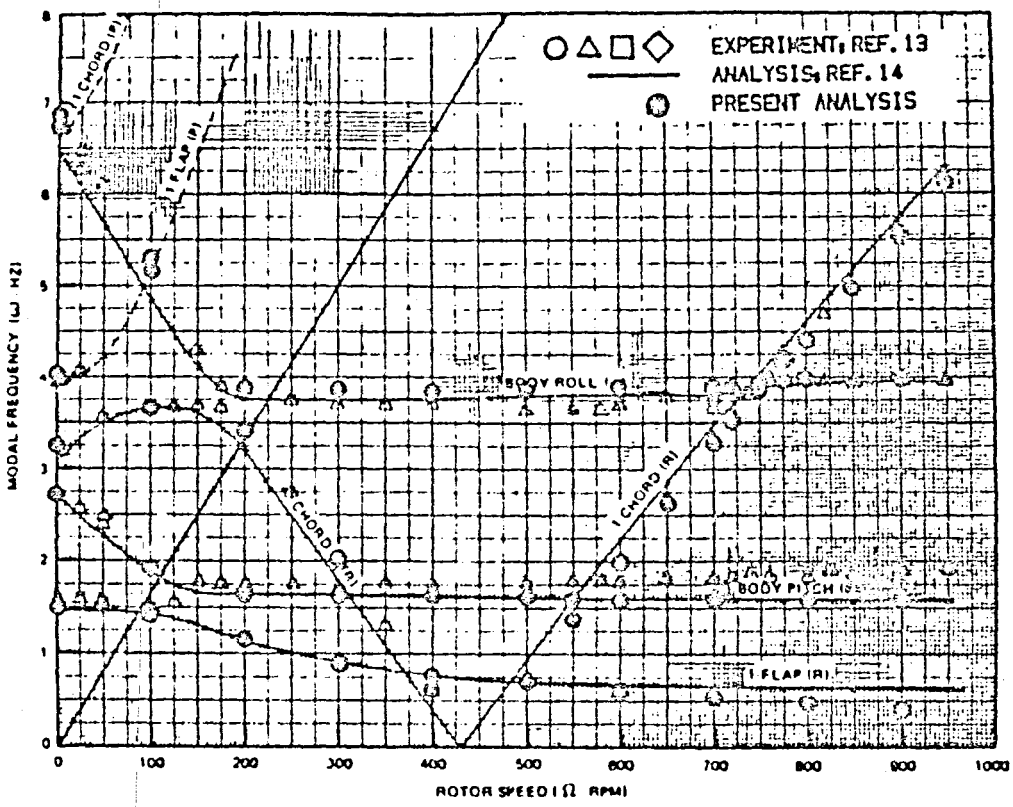

FIGURE 6. Modal Frequencies Versus Rotor Speed, Configuration C at Flat Pitch.

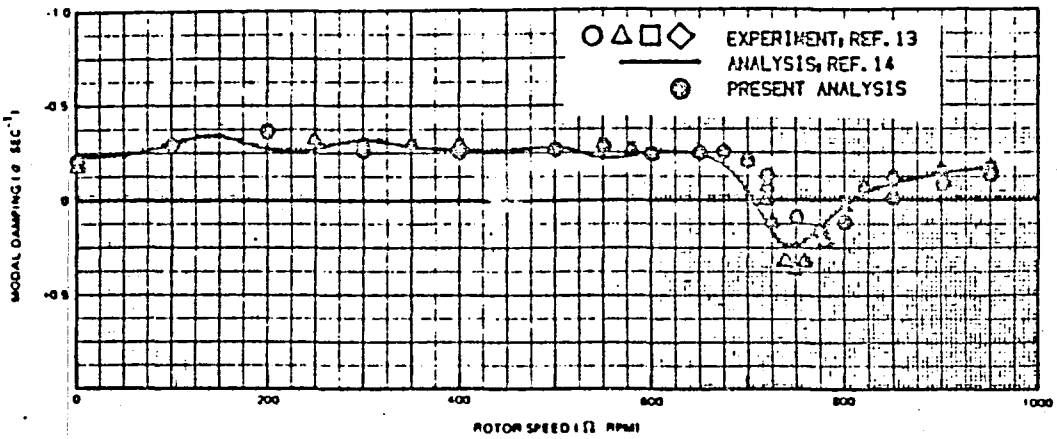

FIGURE 7. Lead-lag Regressing Mode Damping Versus Rotor Speed, Configuration C at Flat Pitch.

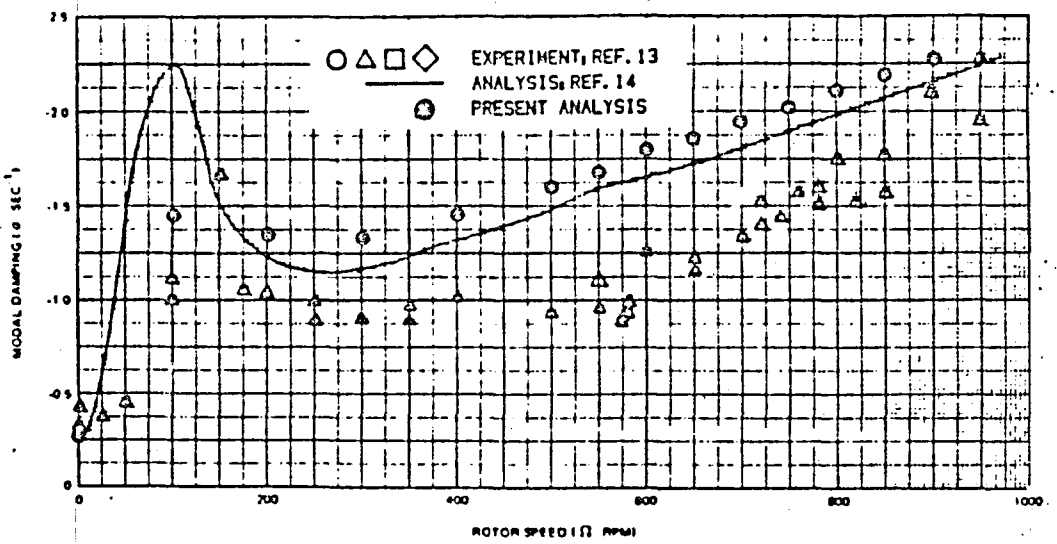

FIGURE 8. Body Pitch Mode Damping Versus Rotor Speed, Configuration C at Flat Pitch.

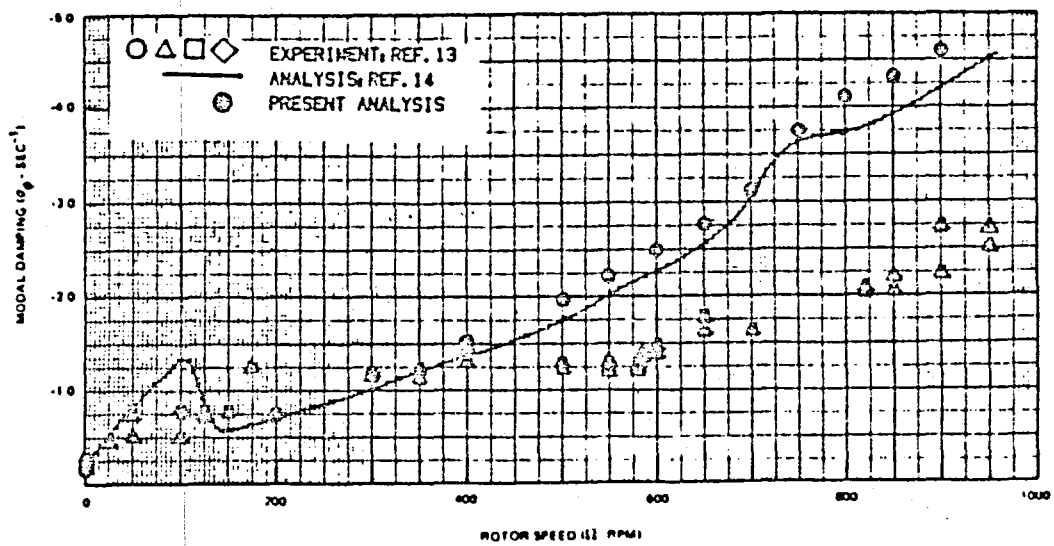

FIGURE 9. Body Roll Mode Damping Versus Rotor Speed, Configuration C at Flat Pitch.

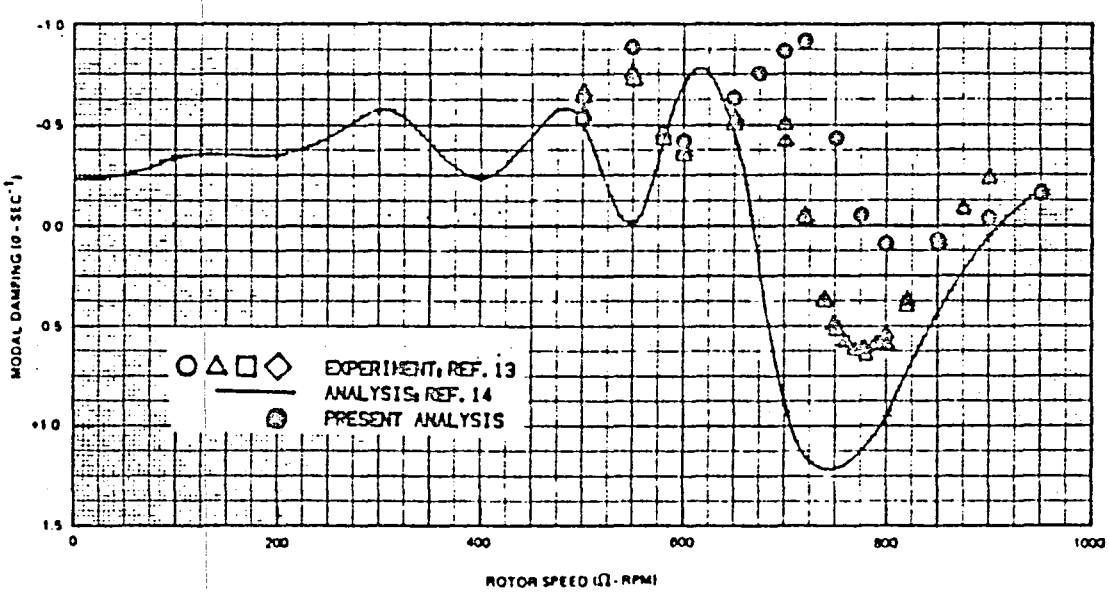

FIGURE 10. Lead-lag Regressing Mode Damping Versus Rotor Speed with Nine Degrees Collective Blade Pitch, Configuration C

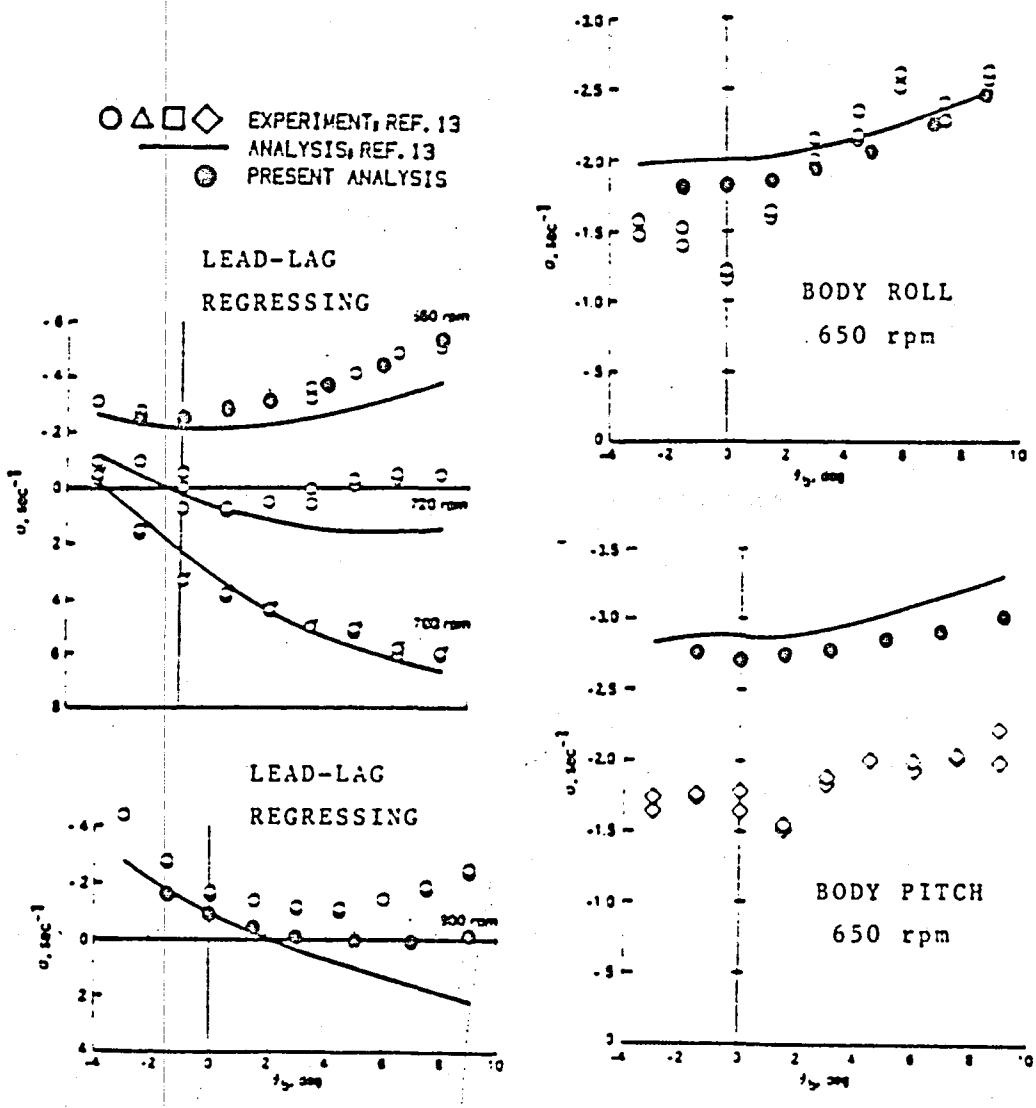

FIGURE 11. Modal Damping as a Function of Blade Pitch Angle, Configuration C.

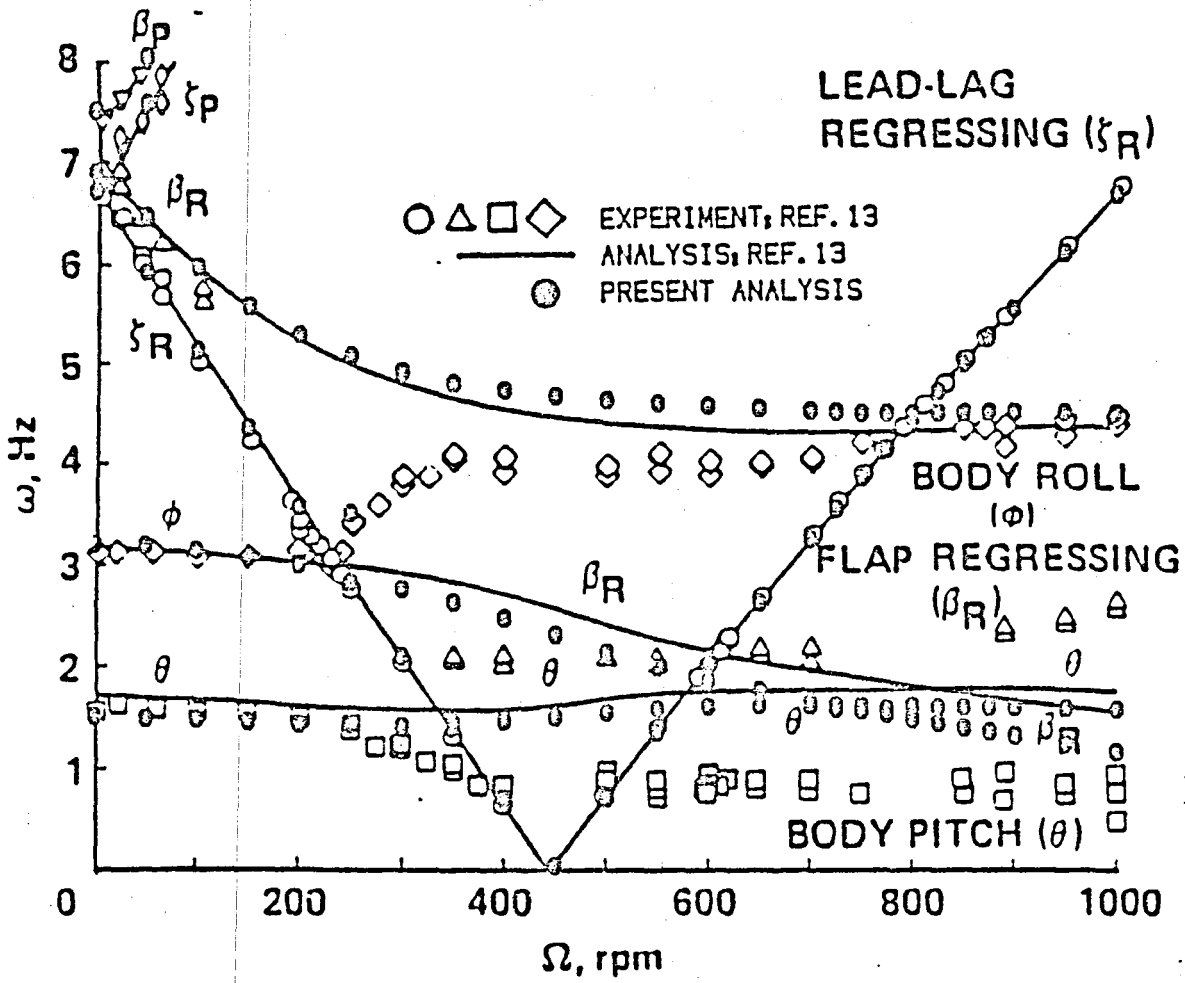

FIGURE 12. Modal Frequencies Versus Rotor Speed, for Matched Stiffness Rotor, Configuration D at Flat Pitch.

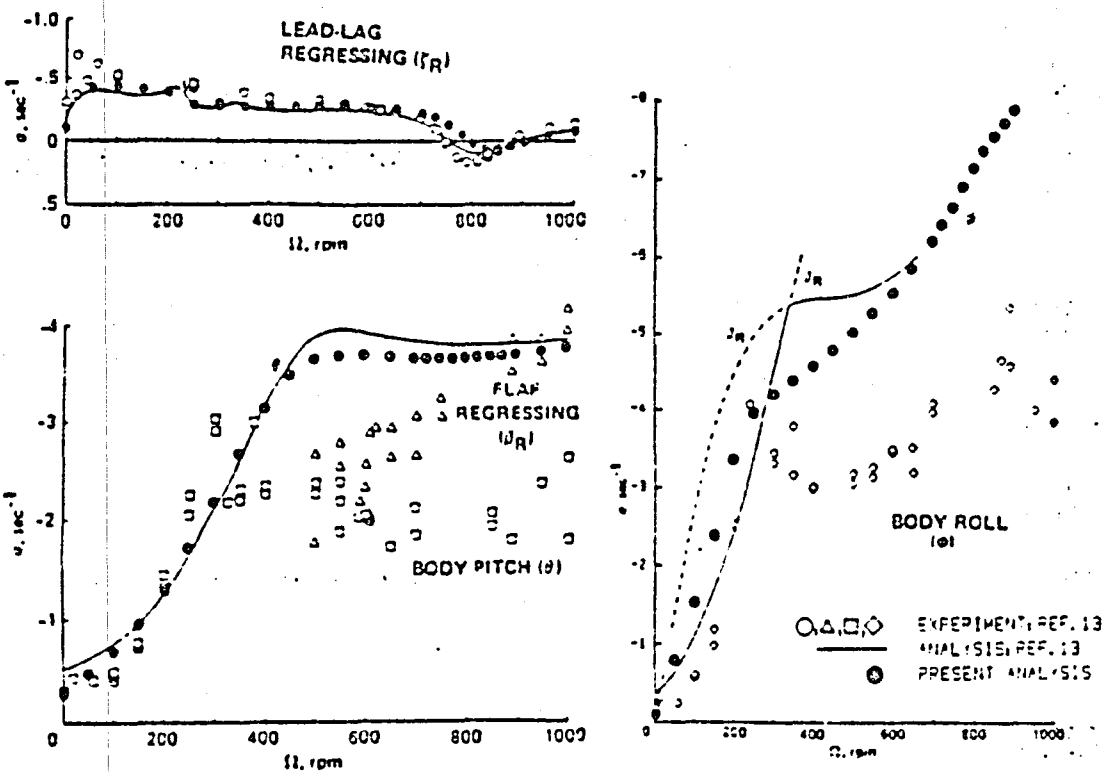

FIGURE 13. Modal Damping Versus Rotor Speed for Matched Stiffness Rotor, Configuration D at Flat Pitch.

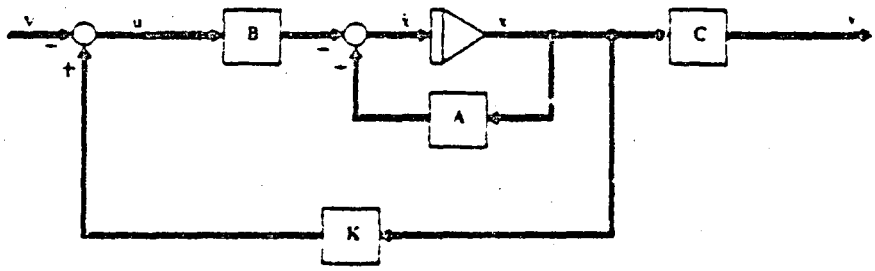

State variable feedback system.

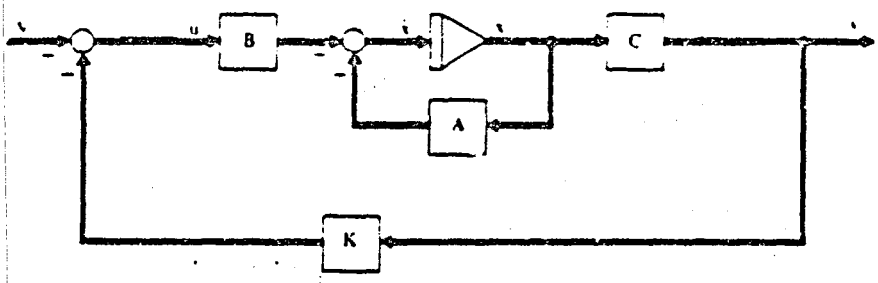

Output feedback system.

FIGURE 14a. State Variable Feedback and Output Feedback Control System.

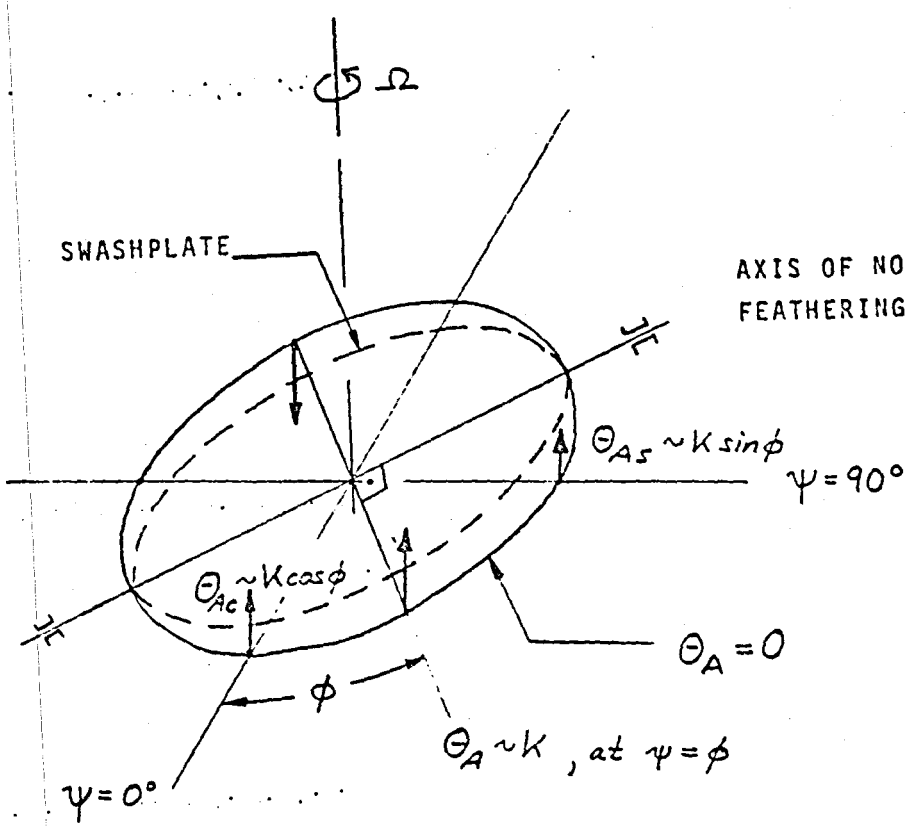

FIGURE 14b. Control Implementation Through Swashplate.

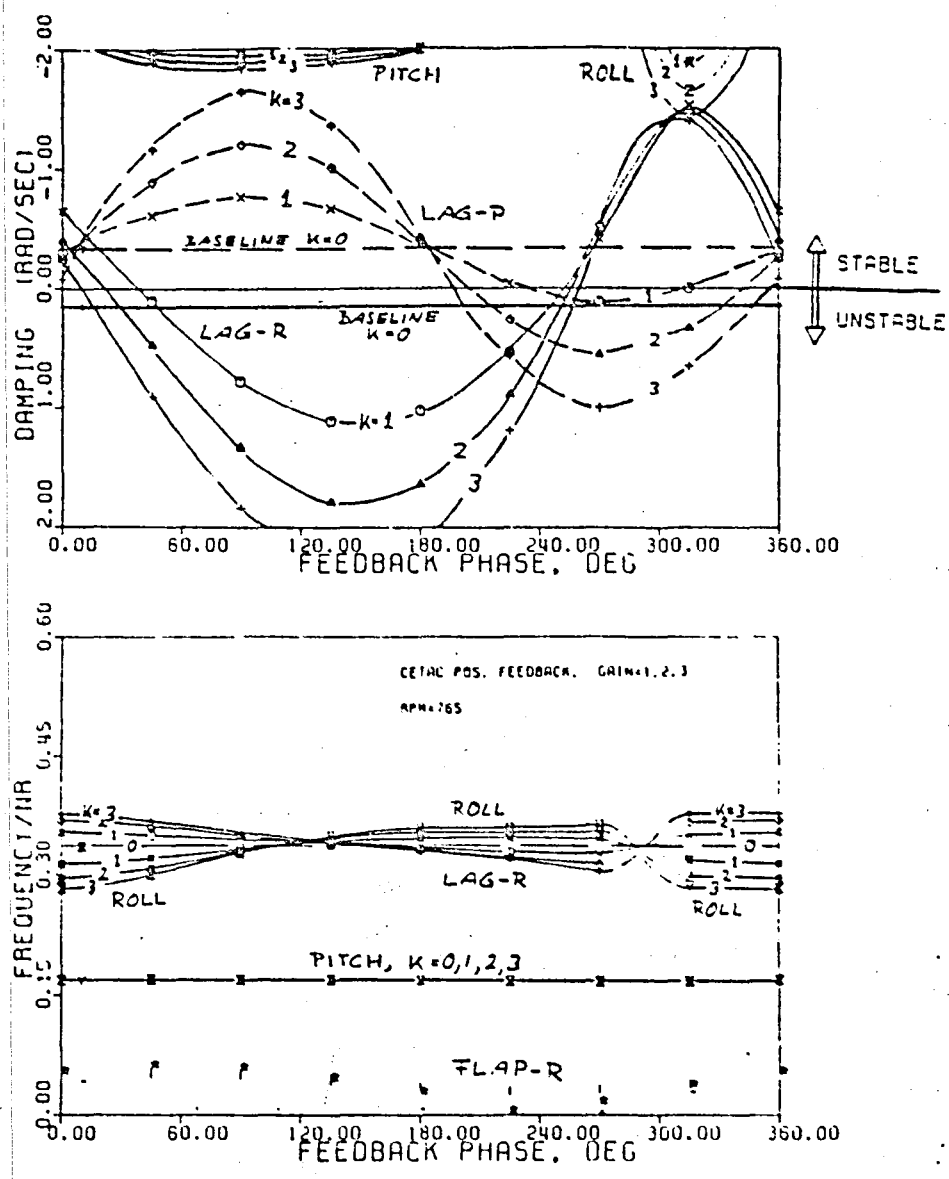

FIGURE 15. Modal Damping and Frequencies Versus Feedback Phase with Cosine Cyclic Lag Feedback, Configuration C.

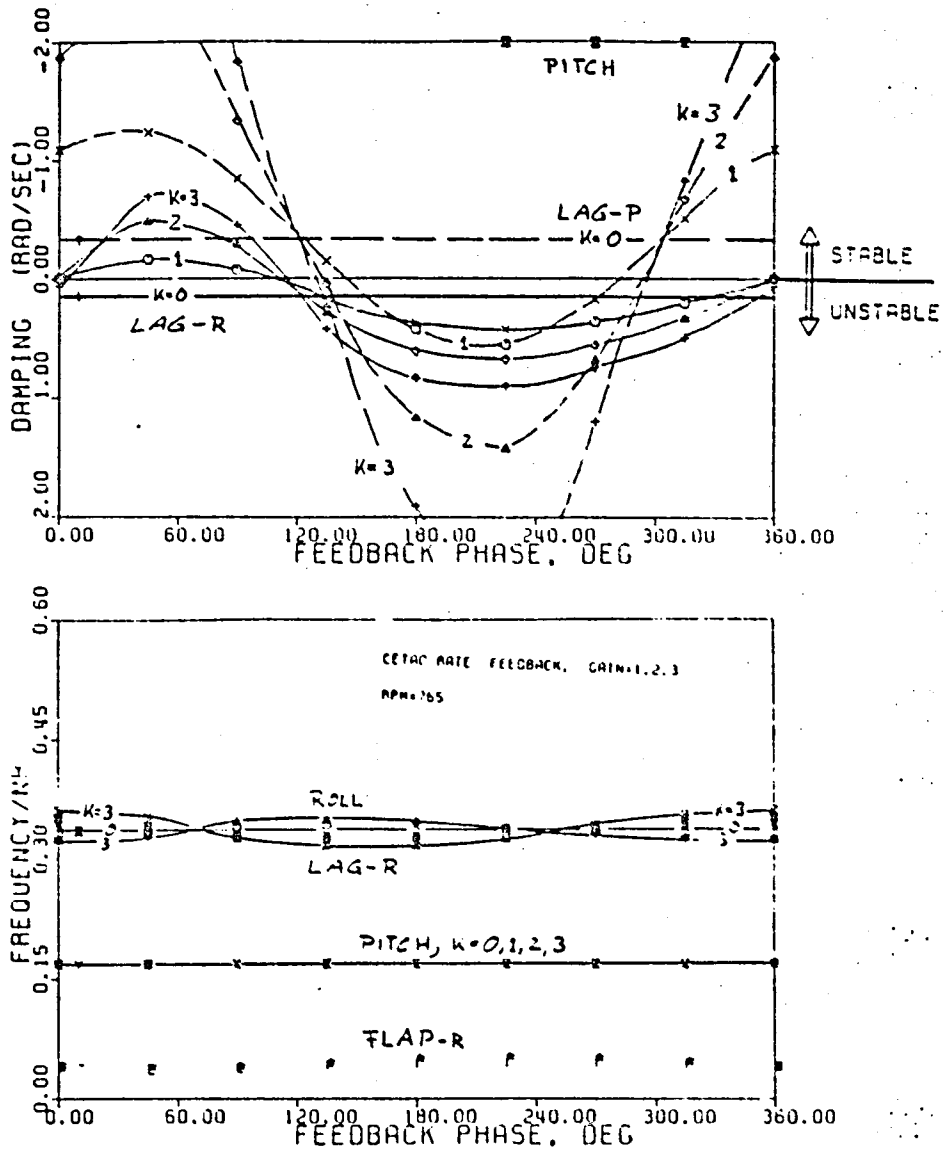

FIGURE 16. Modal Damping and Frequencies Versus Feedback Phase with Cosine Cyclic Lag Rate Feedback, Configuration C.

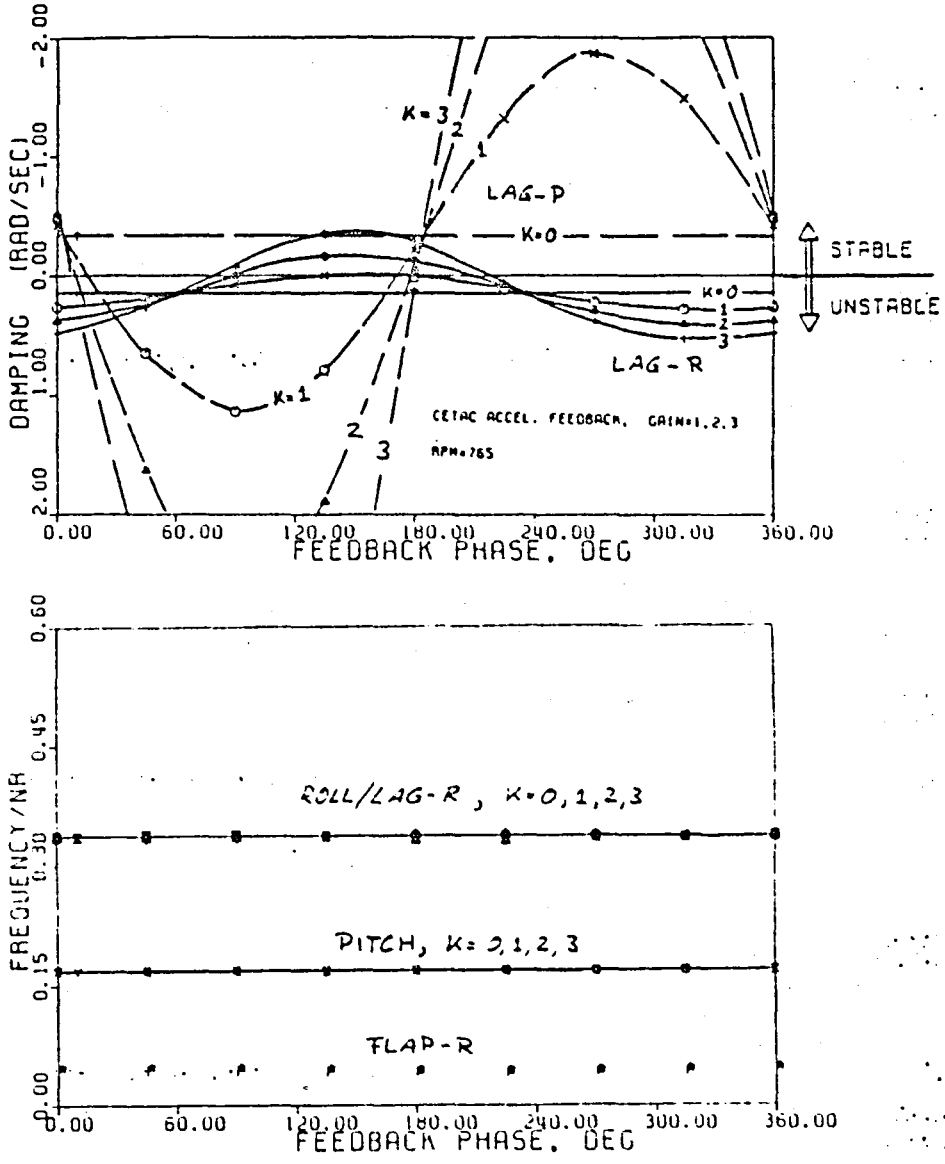

FIGURE 17. Modal Damping and Frequencies Versus Feedback Phase with Cosine Cyclic Lag Acceleration Feedback, Configuration C.

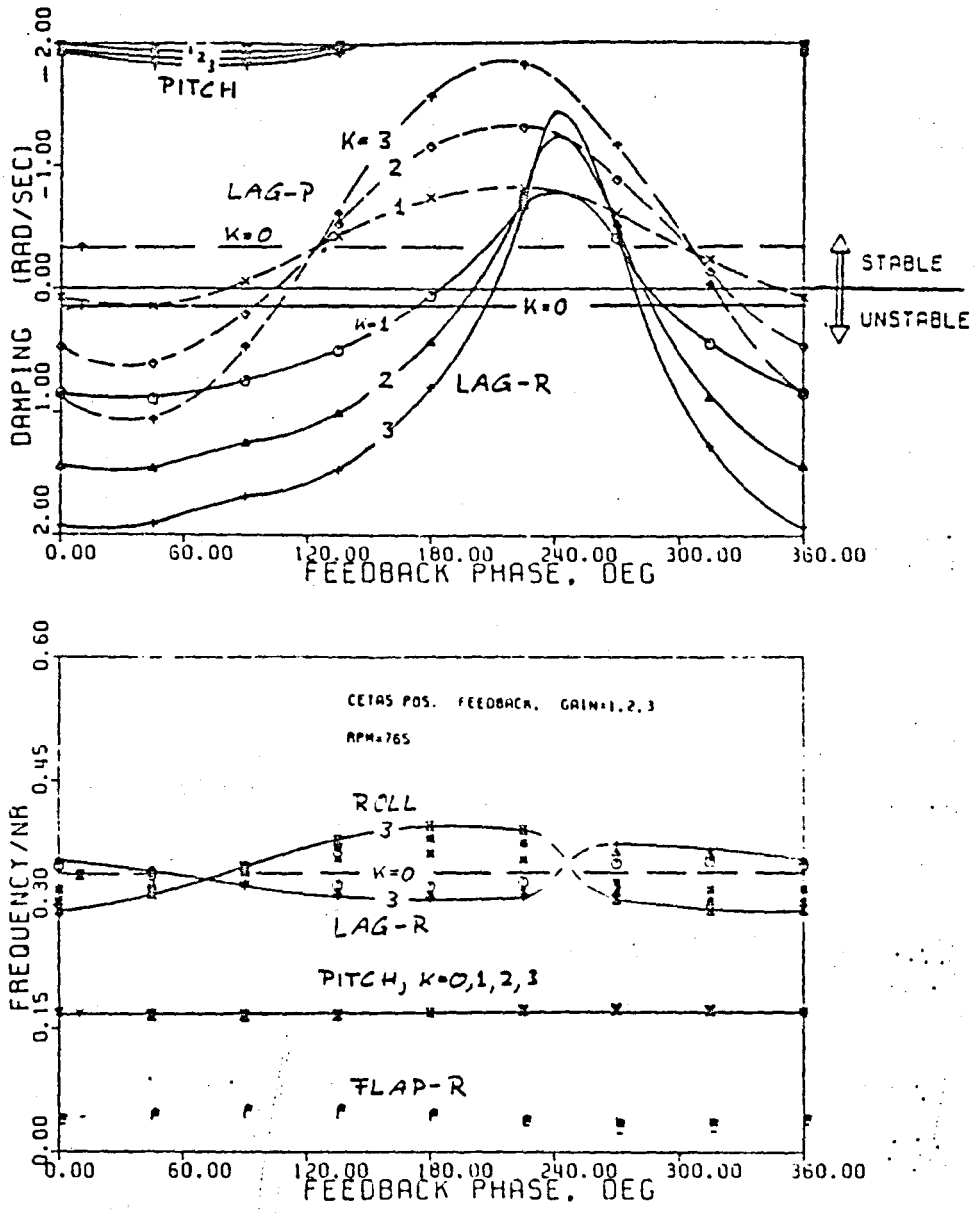

FIGURE 18. Modal Damping and Frequencies Versus Feedback Phase with Sine Cyclic Lag Feedback, Configuration C.

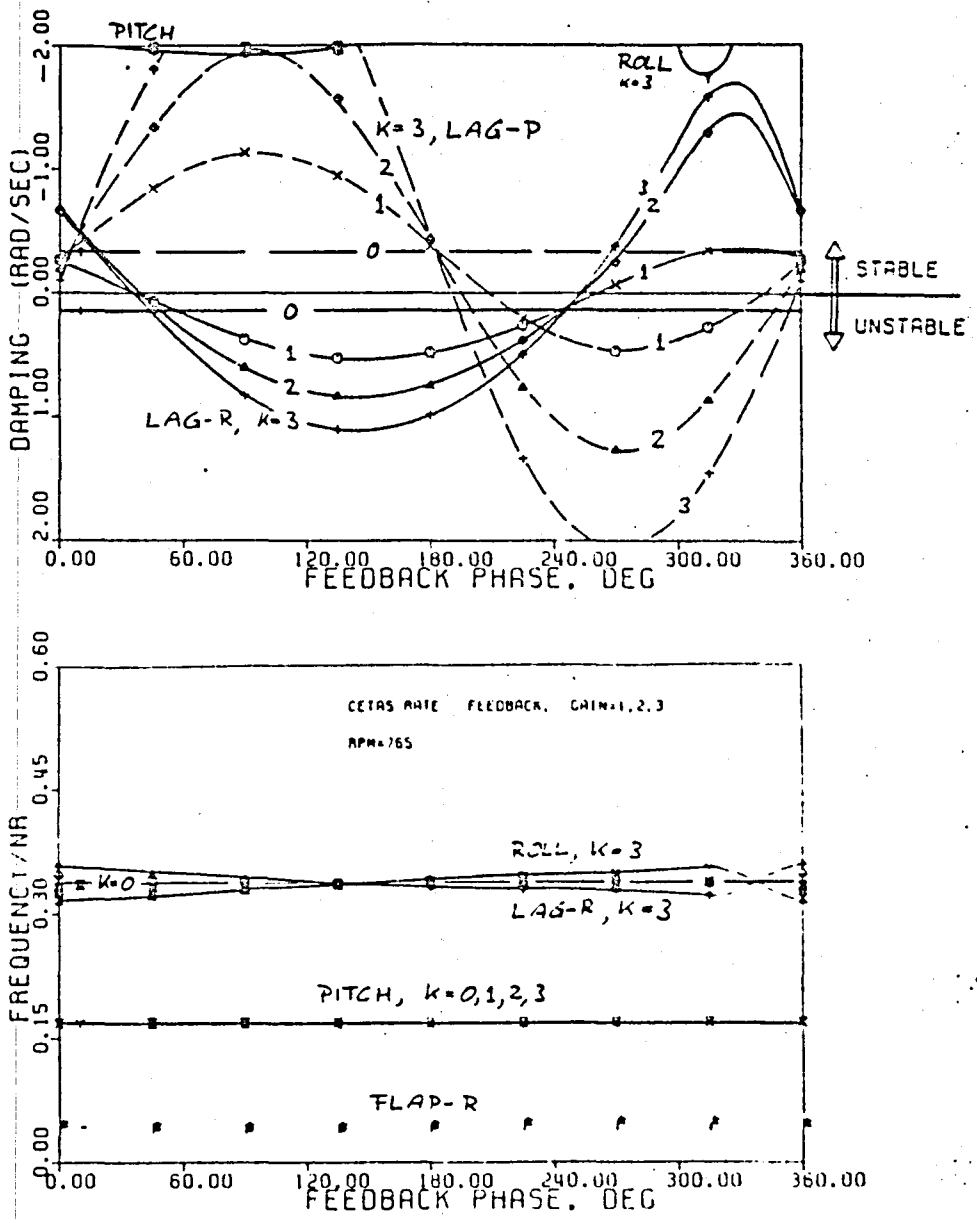

FIGURE 19. Modal Damping and Frequencies Versus Feedback Phase with Sine Cyclic Lag Rate Feedback, Configuration C.

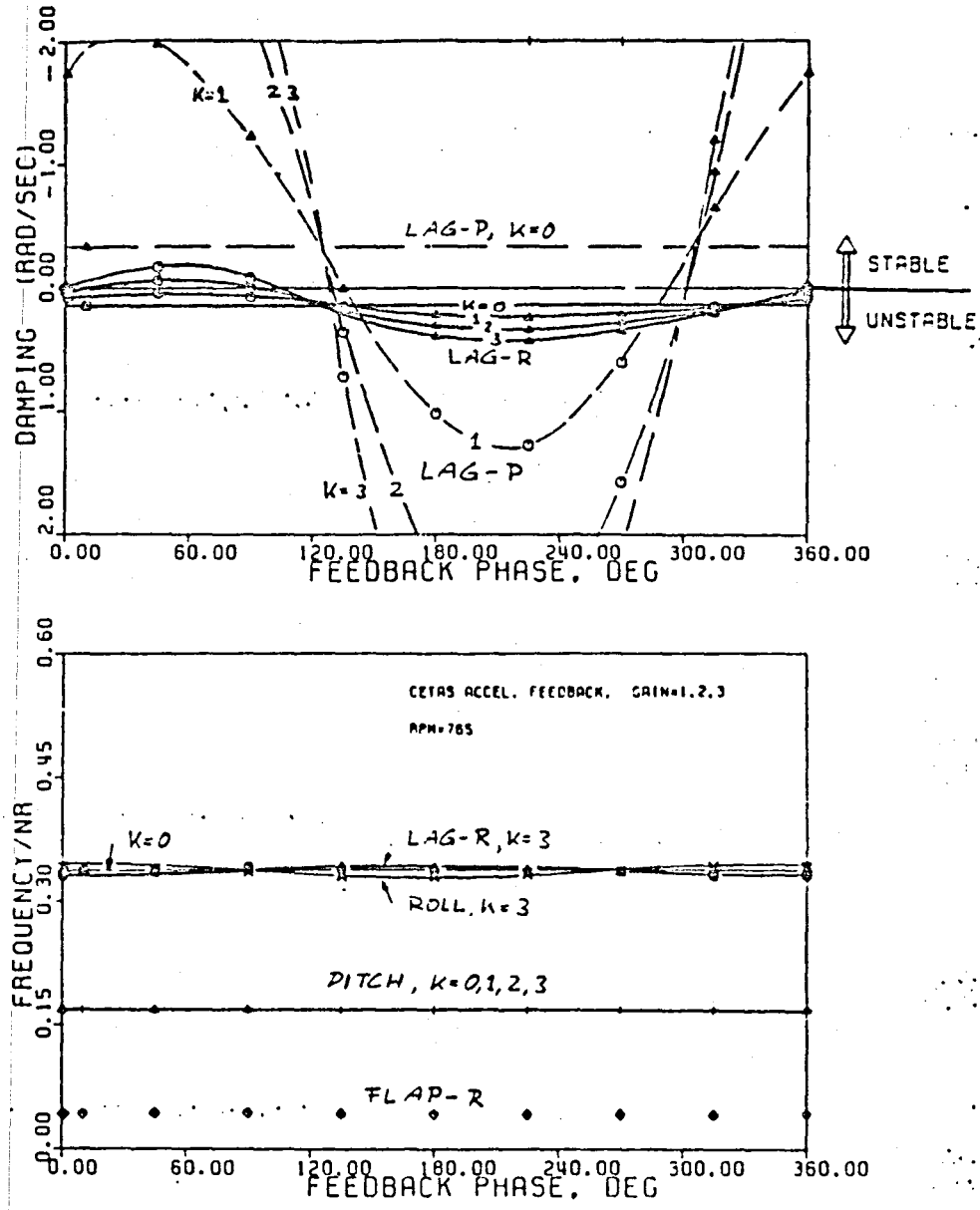

FIGURE 20. Modal Damping and Frequencies Versus Feedback Phase with Sine Cyclic Lag Acceleration Feedback, Configuration C.

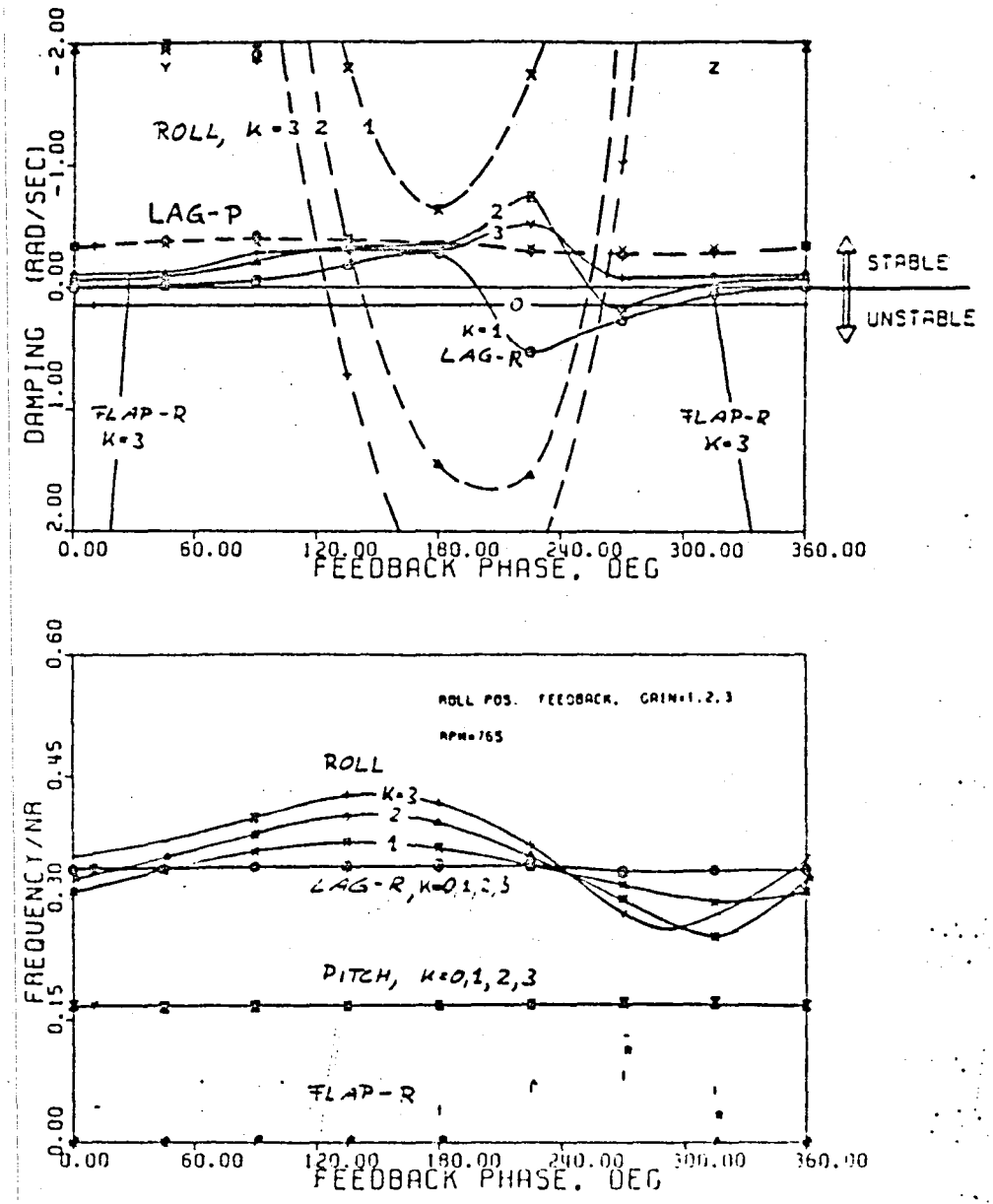

FIGURE 21. Modal Damping and Frequencies Versus Feedback Phase with Roll Feedback, Configuration C.

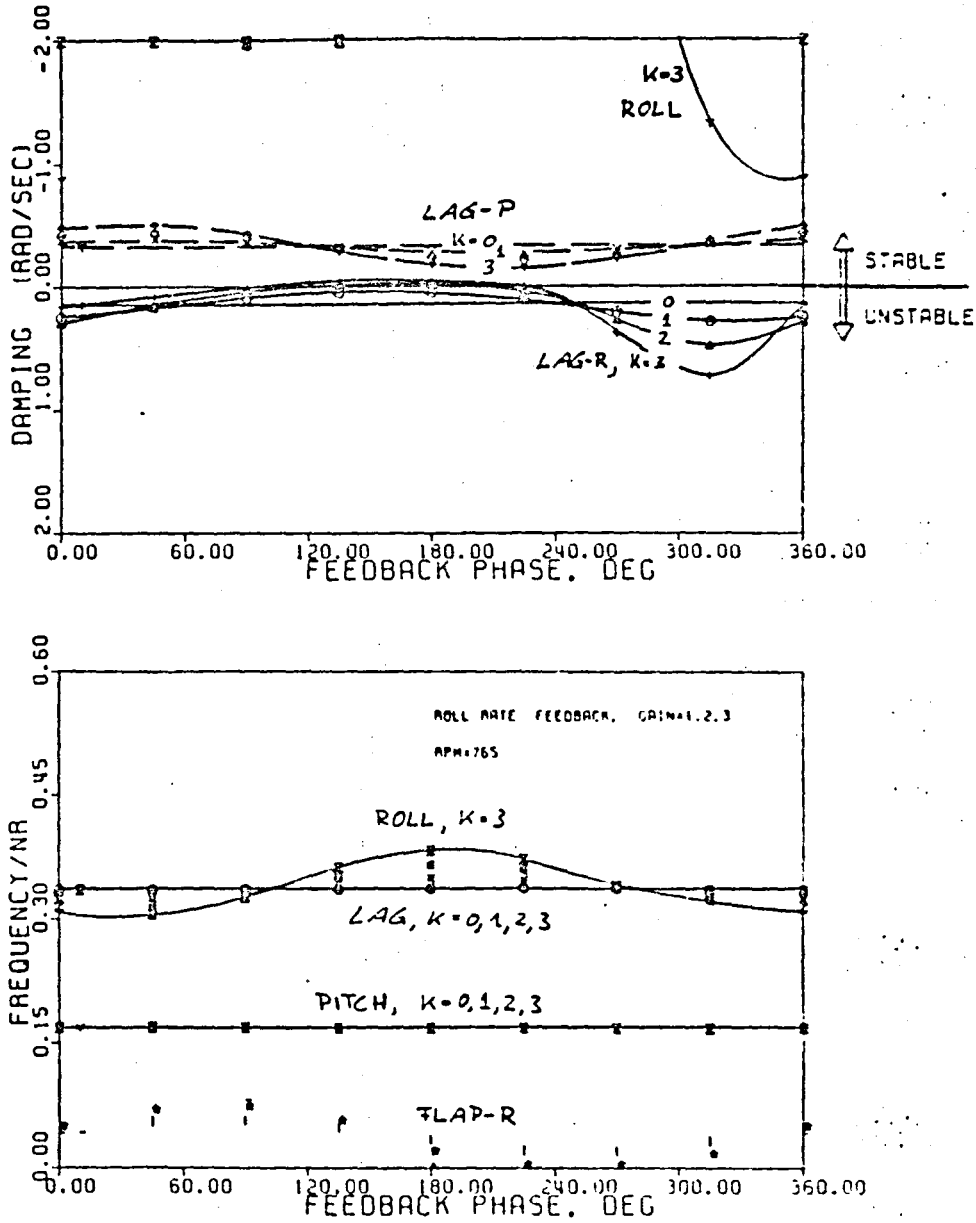

FIGURE 22. Modal Damping and Frequencies Versus Feedback Phase with Roll Rate Feedback, Configuration C.

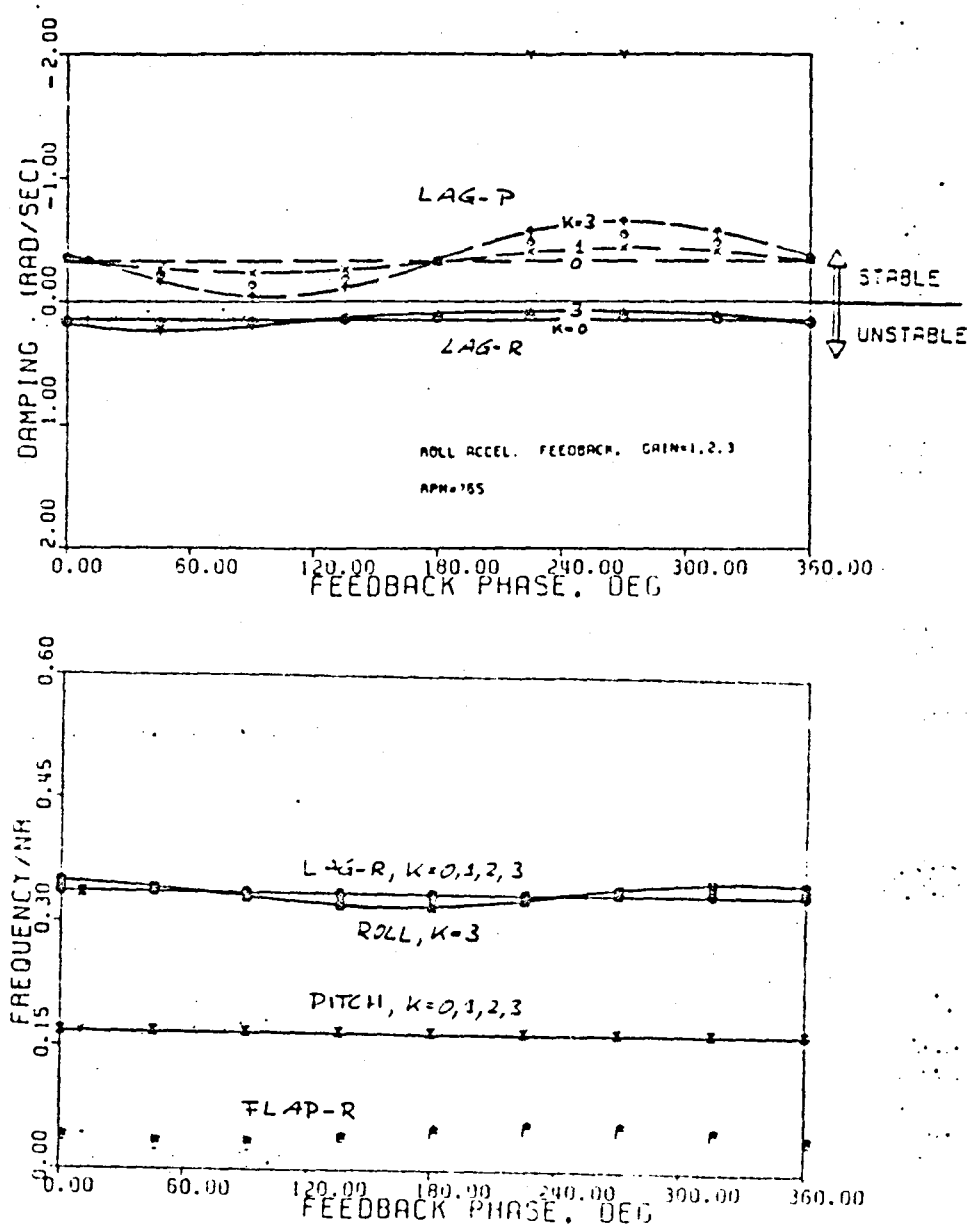

FIGURE 23. Modal Damping and Frequencies Versus Feedback Phase with Roll Acceleration Feedback, Configuration C.

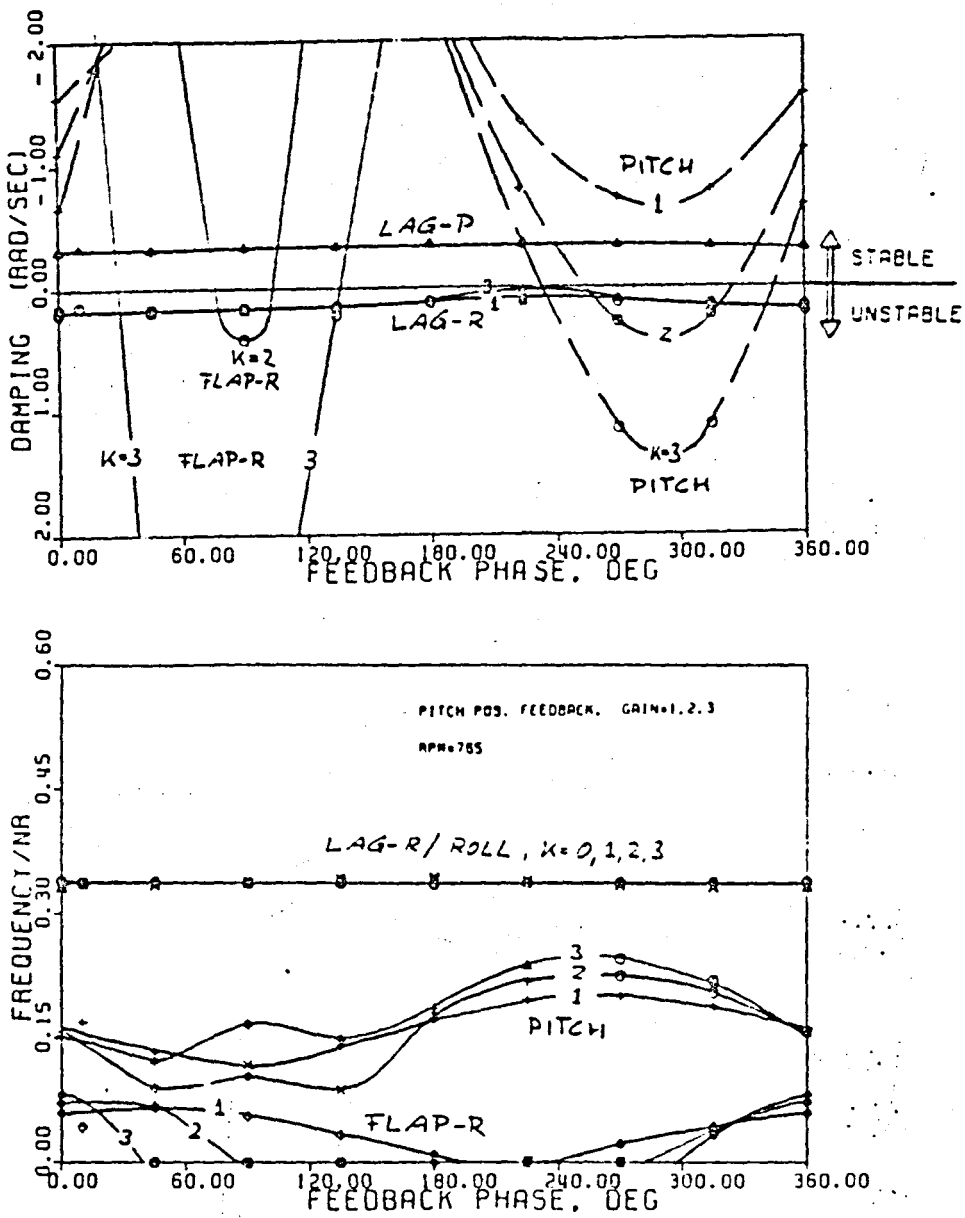

FIGURE 24. Modal Damping and Frequencies Versus Feedback Phase with Pitch Feedback, Configuration C.

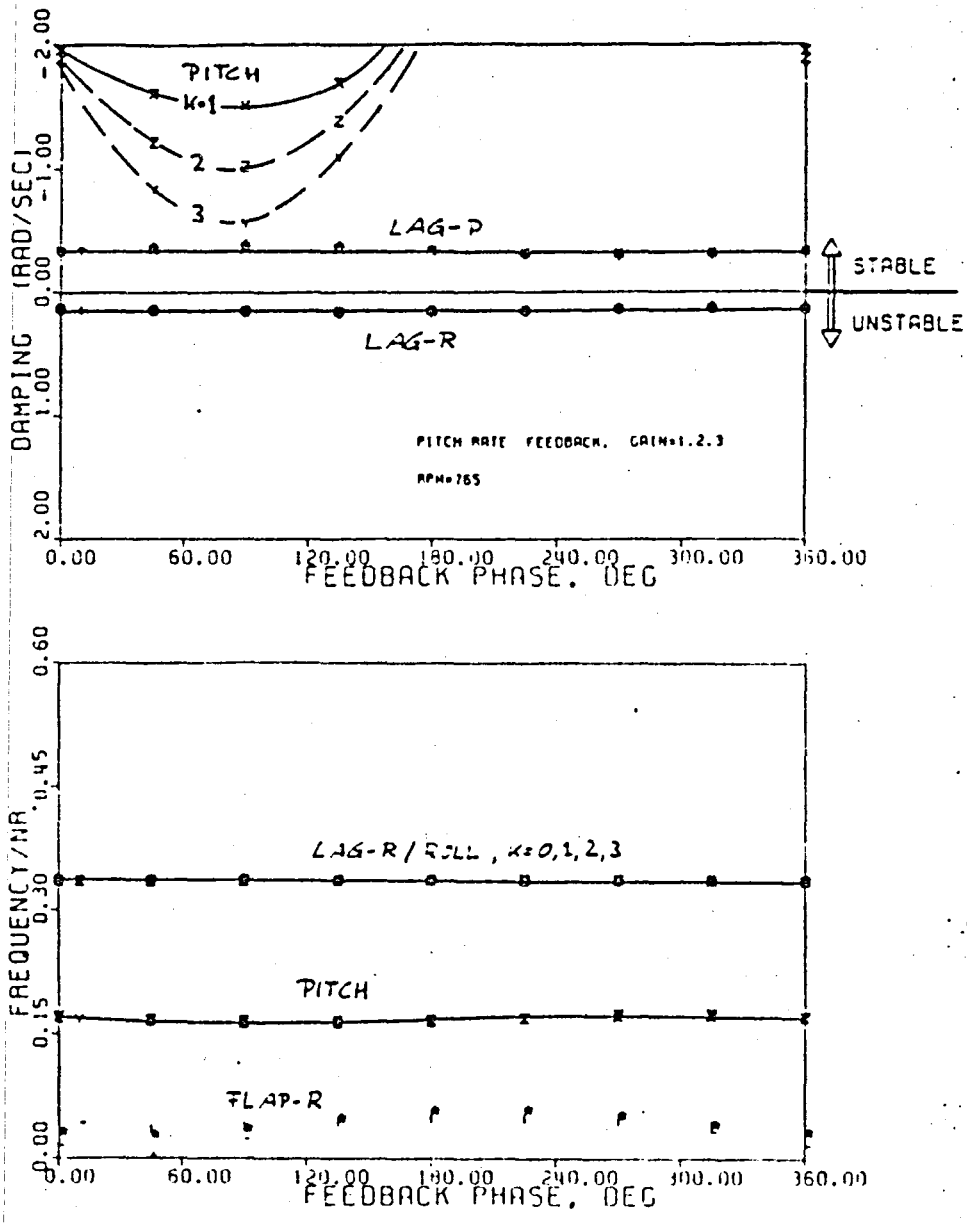

FIGURE 25. Modal Damping and Frequencies Versus Feedback Phase with Pitch Rate Feedback, Configuration C.

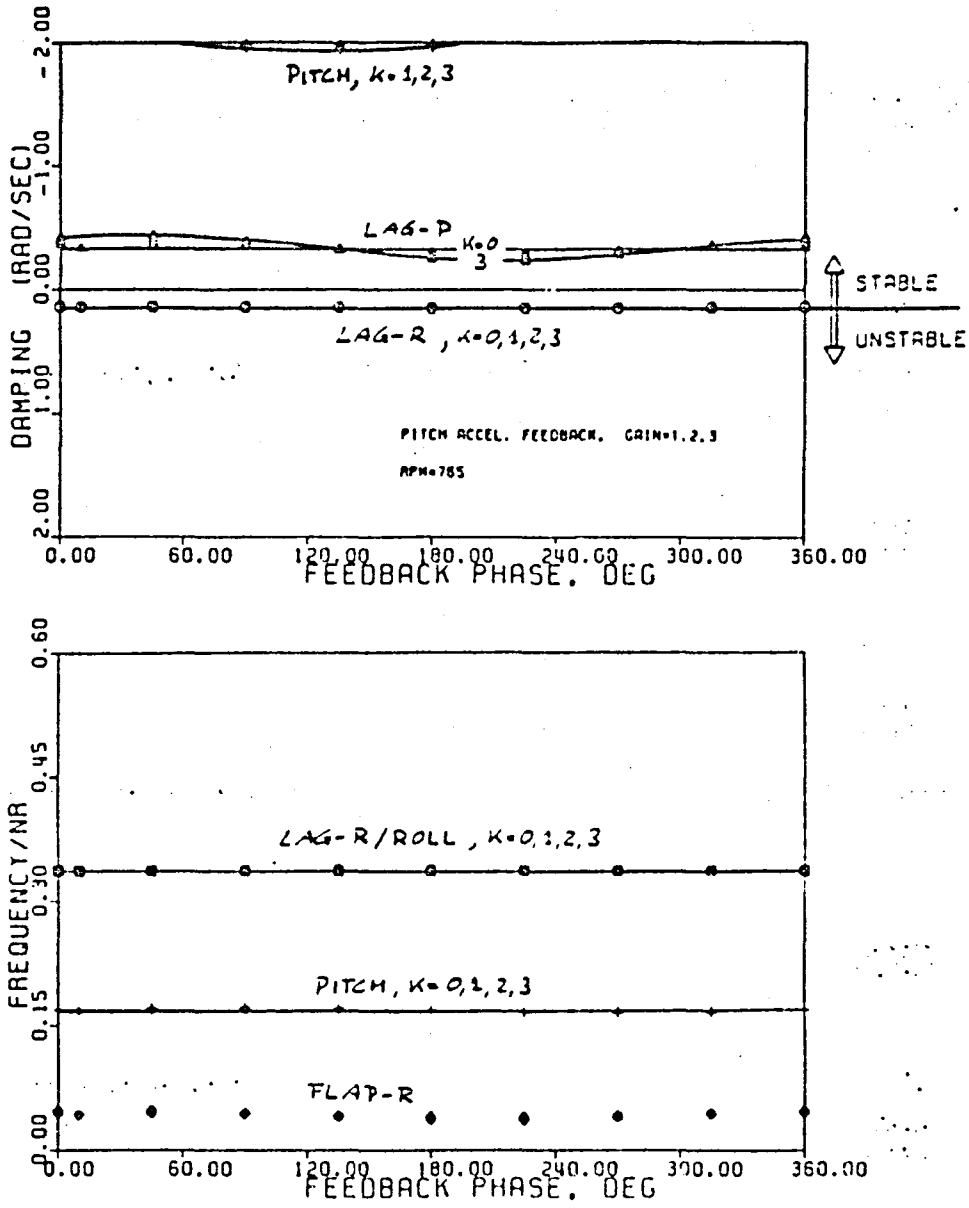

FIGURE 26. Modal Damping and Frequencies Versus Feedback Phase with Pitch Acceleration Feedback, Configuration C.

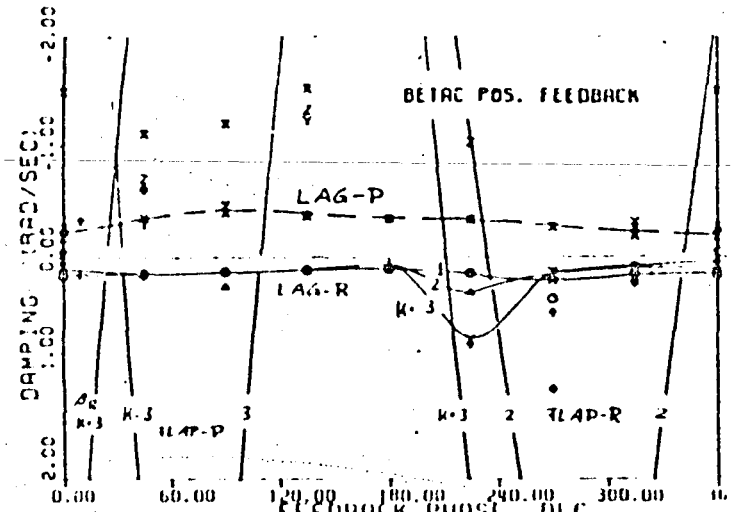

a) β_c Feedback

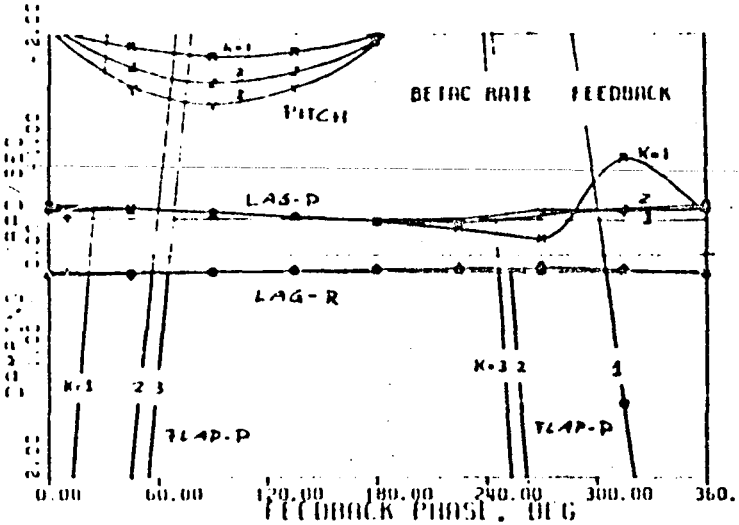

b) $\dot{\beta}_c$ Feedback

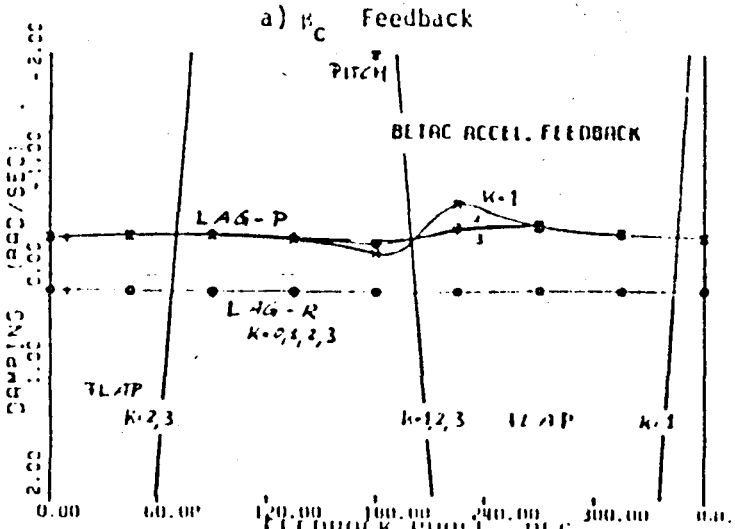

c) $\ddot{\beta}_c$ Feedback

FIGURE 27. Modal Damping Versus Feedback Phase with Cosine Cyclic Flap Feedback, Configuration C.

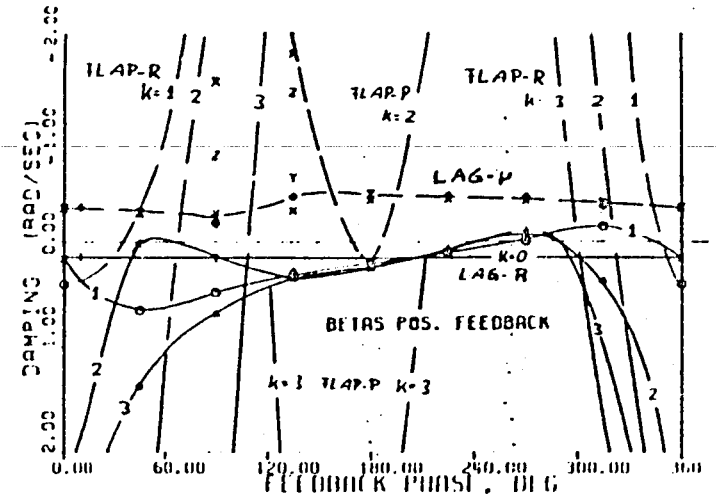

a) β_s Feedback

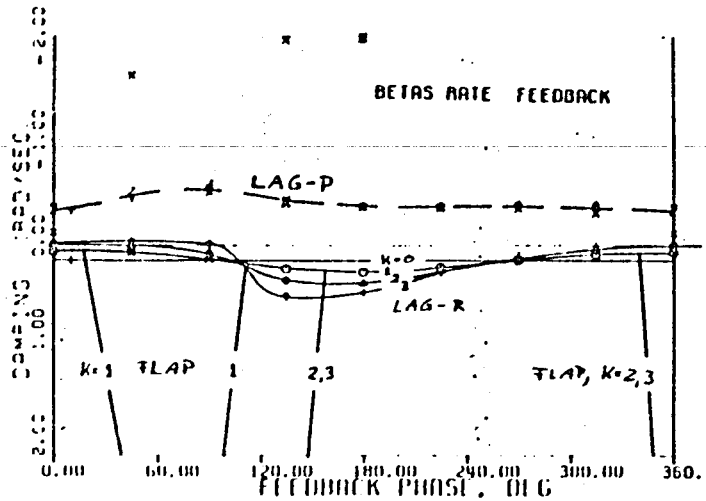

b) $\dot{\beta}_s$ Feedback

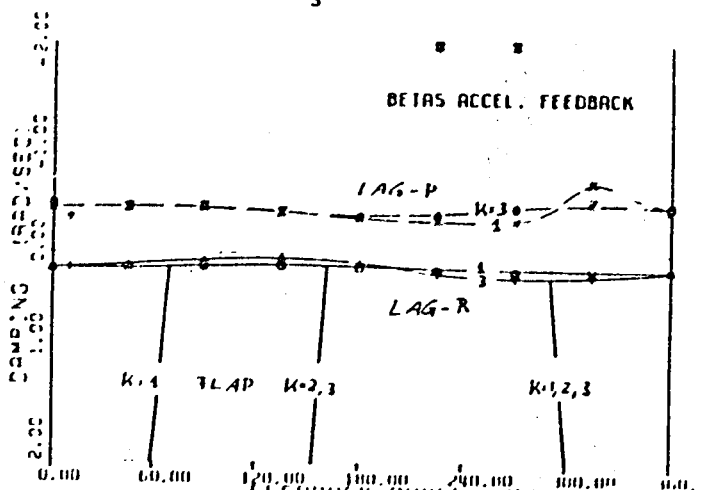

c) $\ddot{\beta}_s$ Feedback

FIGURE 28. Modal Damping Versus Feedback Phase with Sine Cyclic Flap Feedback, Configuration C.

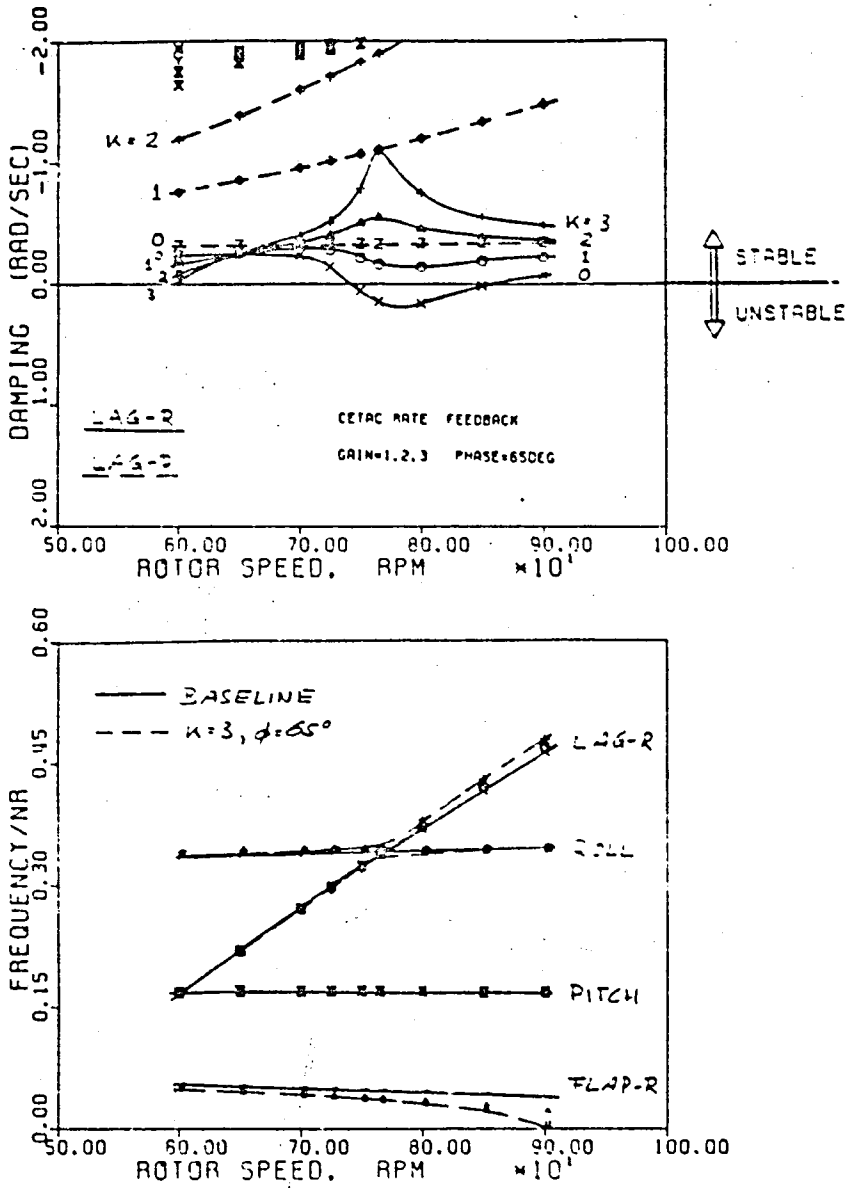

FIGURE 29. Effect of Cosine Cyclic Lag Rate Feedback Gain on Modal Damping and Frequencies, Plotted Versus Rotor Speed, Configuration C.

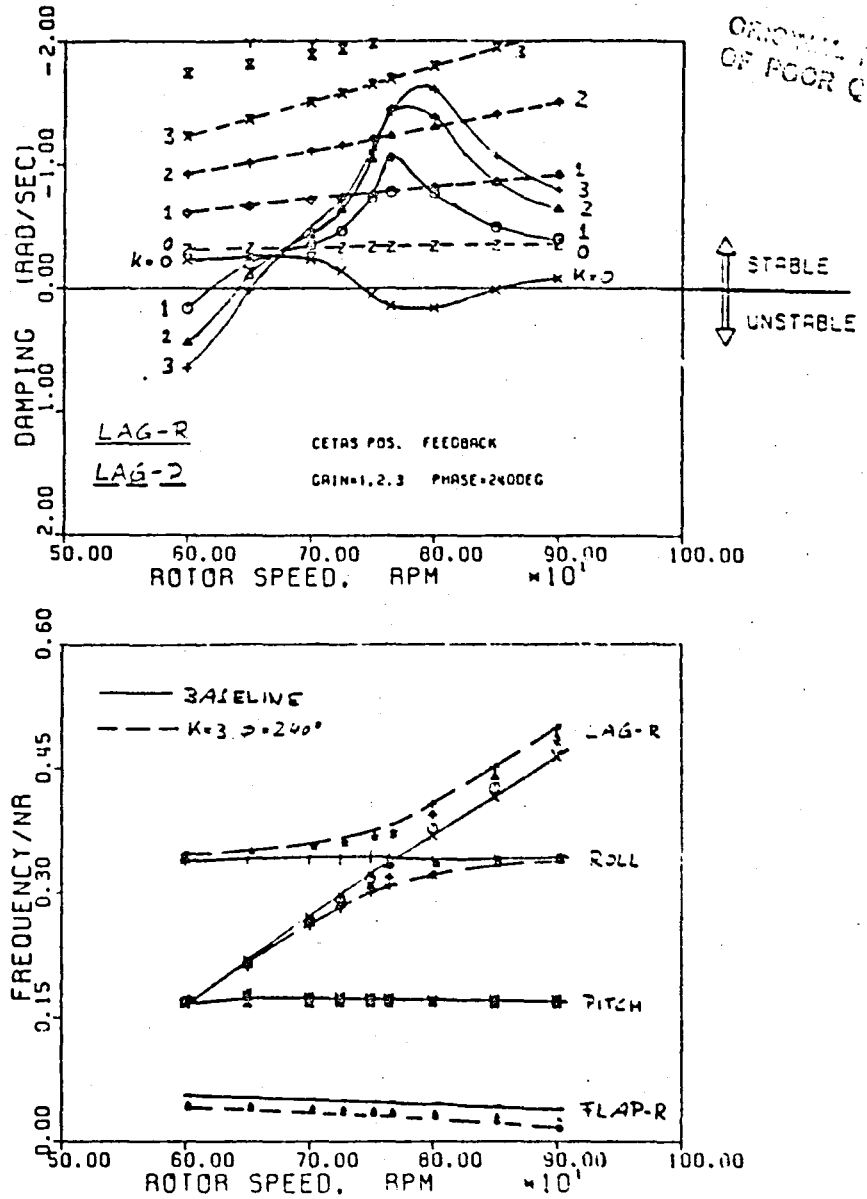

FIGURE 30. Effect of Sine Cyclic Lag Feedback Gain on Modal Damping and Frequencies, Plotted Versus Rotor Speed, Configuration C.

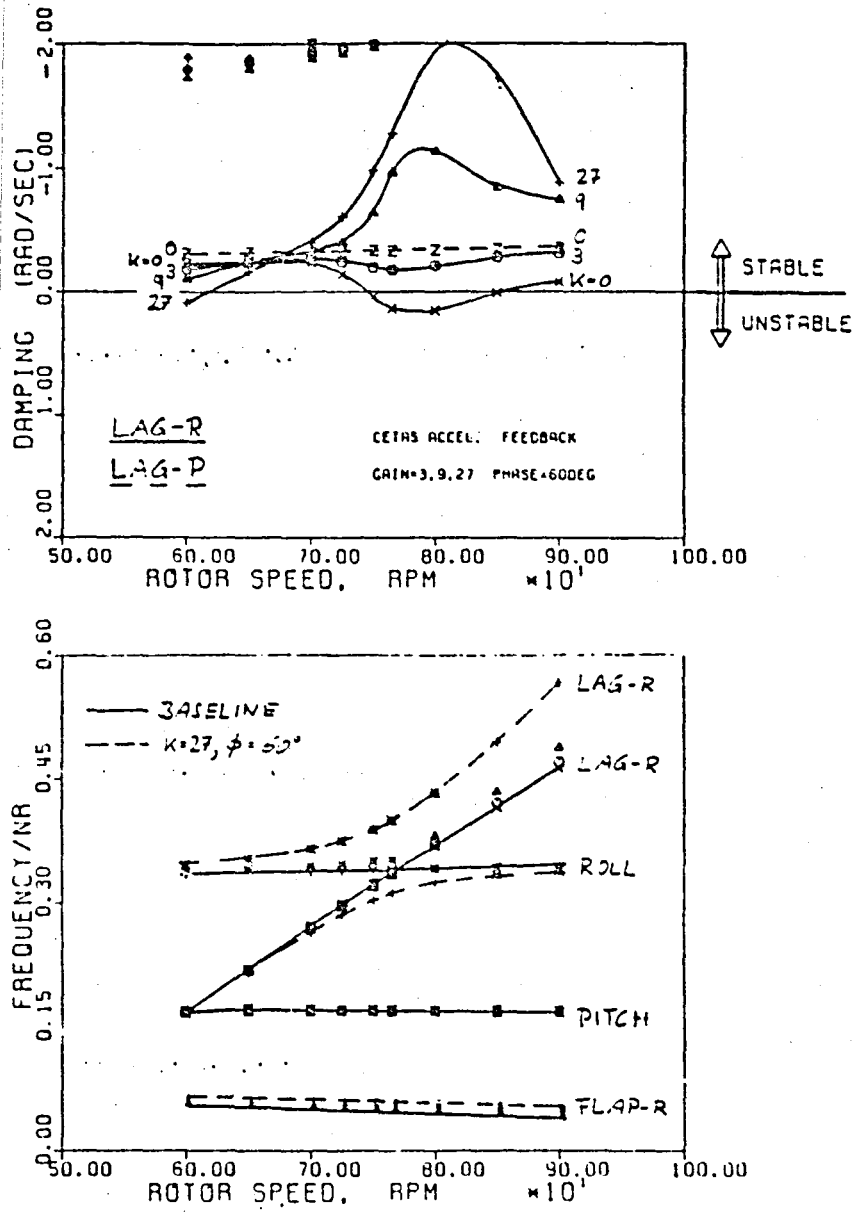

FIGURE 31. Effect of Sine Cyclic Lag Acceleration Feedback Gain on Modal Damping and Frequencies, Plotted Versus Rotor Speed, Configuration C.

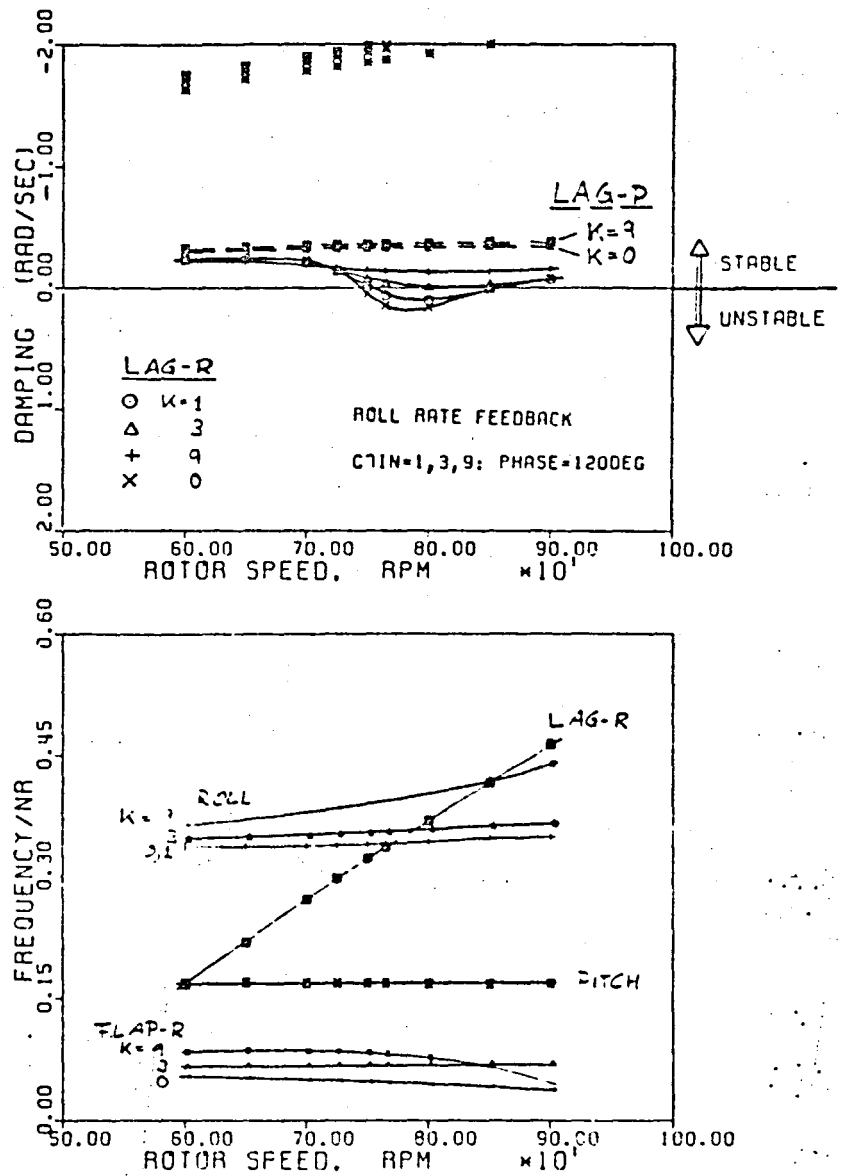

FIGURE 32. Effect of Roll Rate Feedback Gain on Modal Damping and Frequencies, Plotted Versus Rotor Speed, Configuration C.

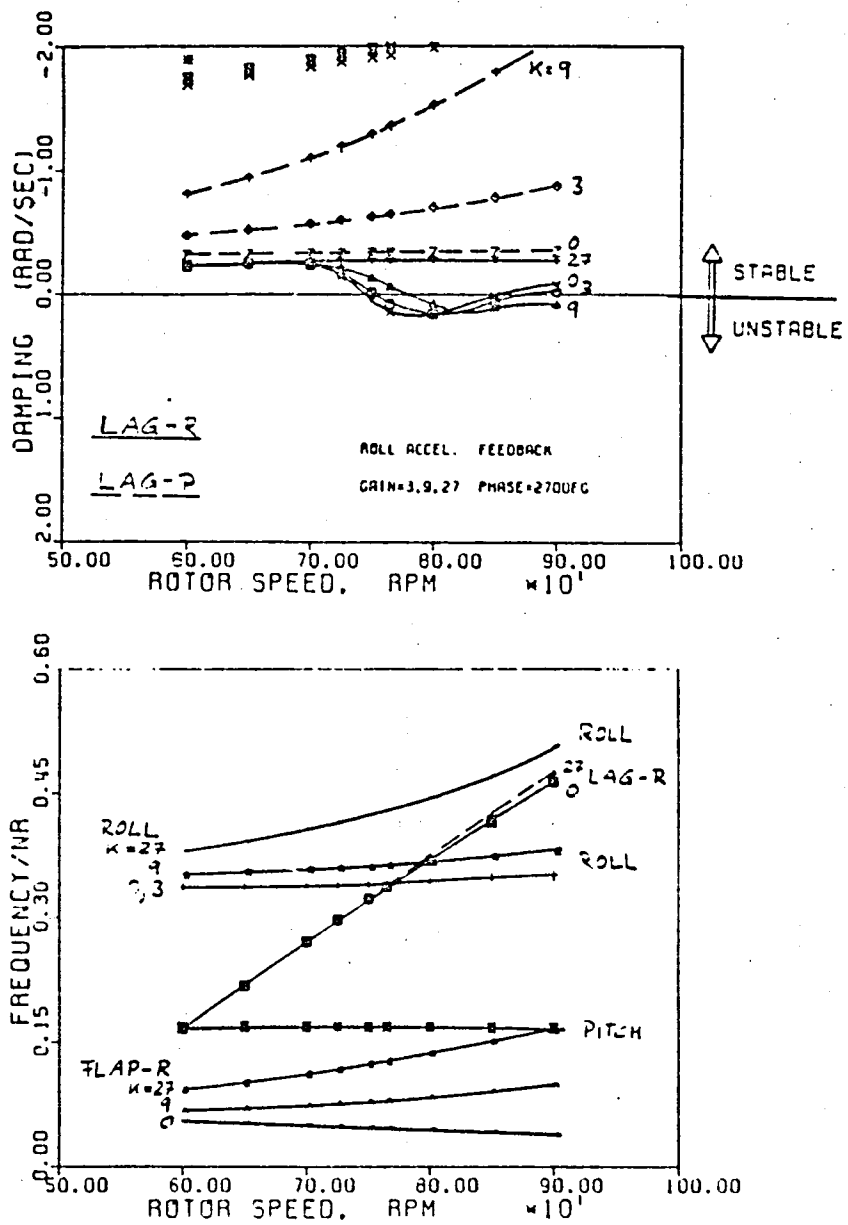

FIGURE 33. Effect of Roll Acceleration Feedback Gain on Modal Damping and Frequencies, Plotted Versus Rotor Speed, Configuration C.

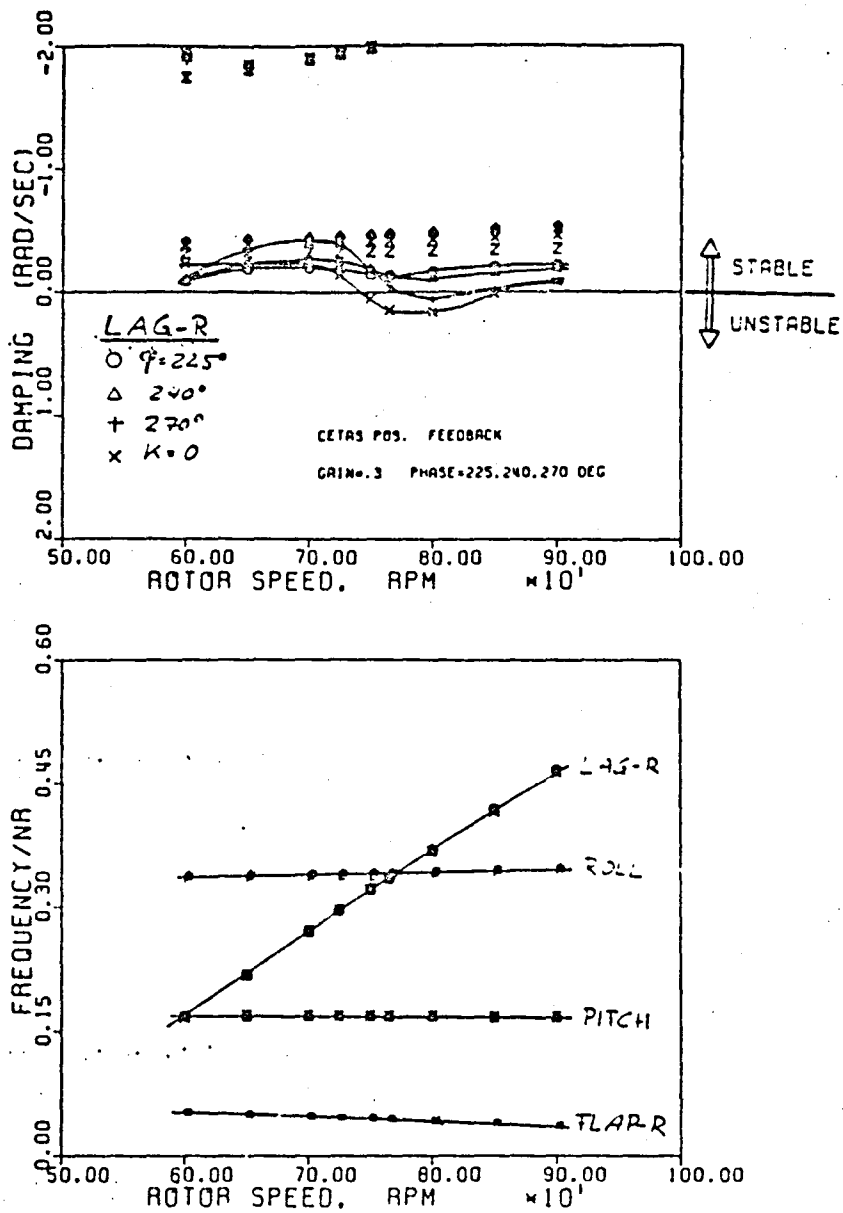

FIGURE 34. Effect of Sine Cyclic Lag Feedback Phase on Modal Damping and Frequencies, Plotted Versus Rotor Speed, Configuration C.

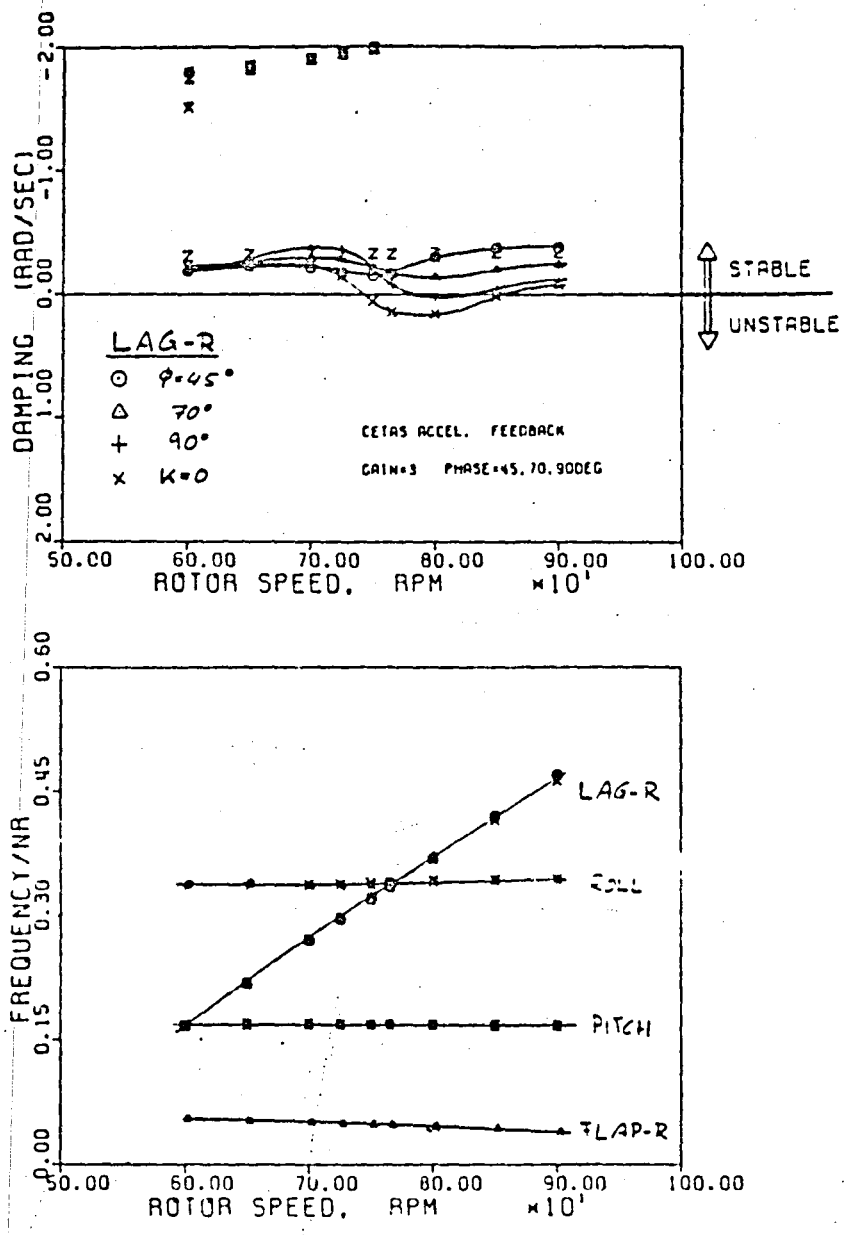

FIGURE 35. Effect of Sine Cyclic Lag Acceleration Feedback Phase on Modal Damping and Frequencies, Plotted Versus Rotor Speed, Configuration C.

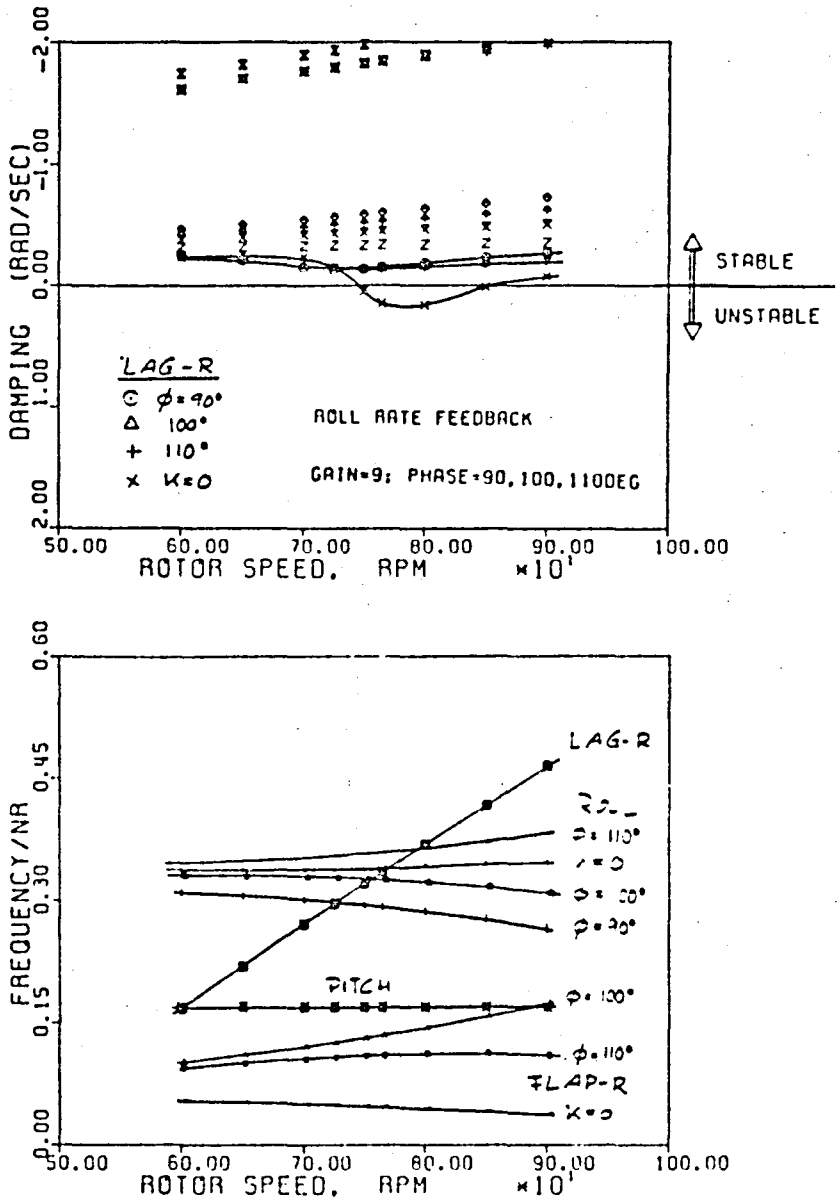

FIGURE 36. Effect of Roll Rate Feedback Phase on Modal Damping and Frequencies, Plotted Versus Rotor Speed, Configuration C.

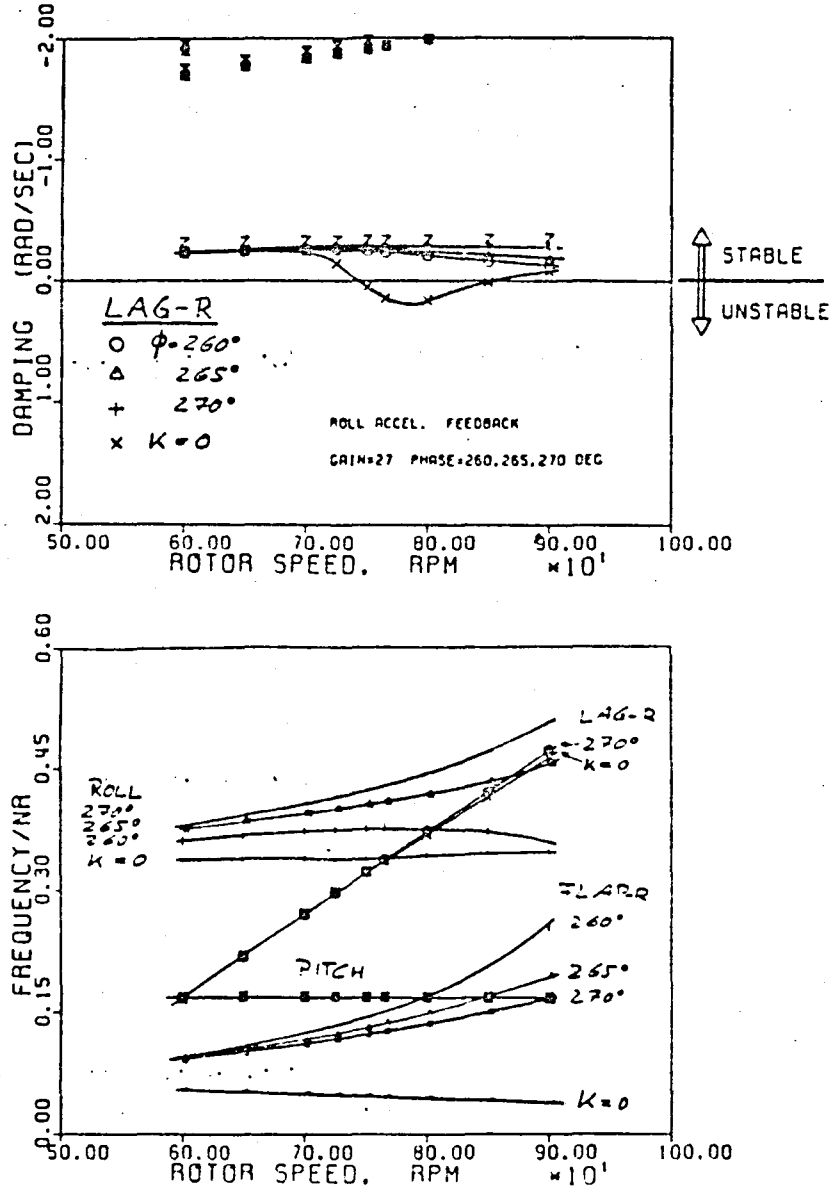

FIGURE 37. Effect of Roll Acceleration Feedback Phase on Modal Damping and Frequencies, Plotted Versus Rotor Speed, Configuration C.

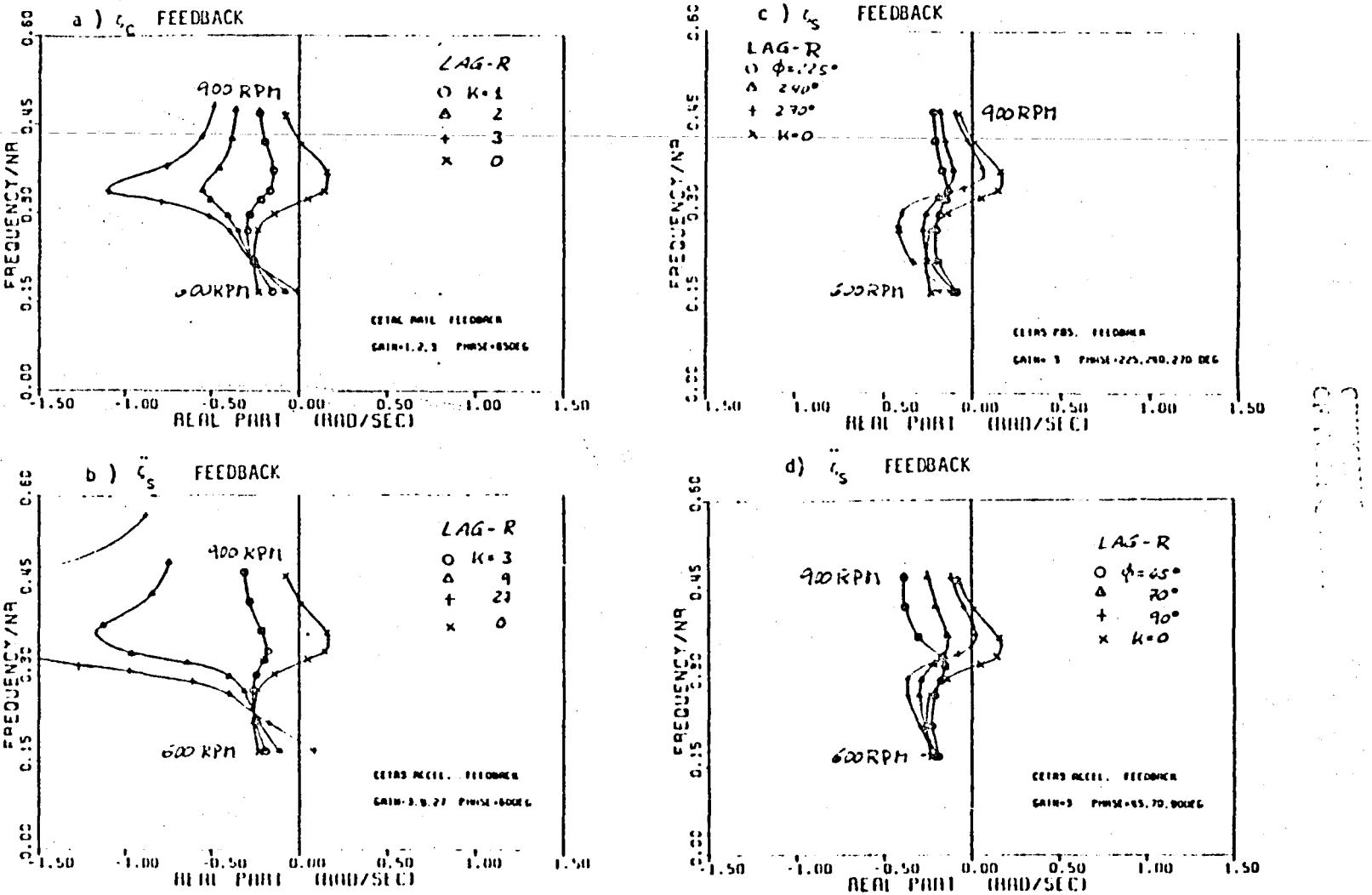

FIGURE 38. Effect of Lead-lag Feedback Gain and Phase on Regressing Lag Mode Dynamics. (root locus parameter - rotor speed).

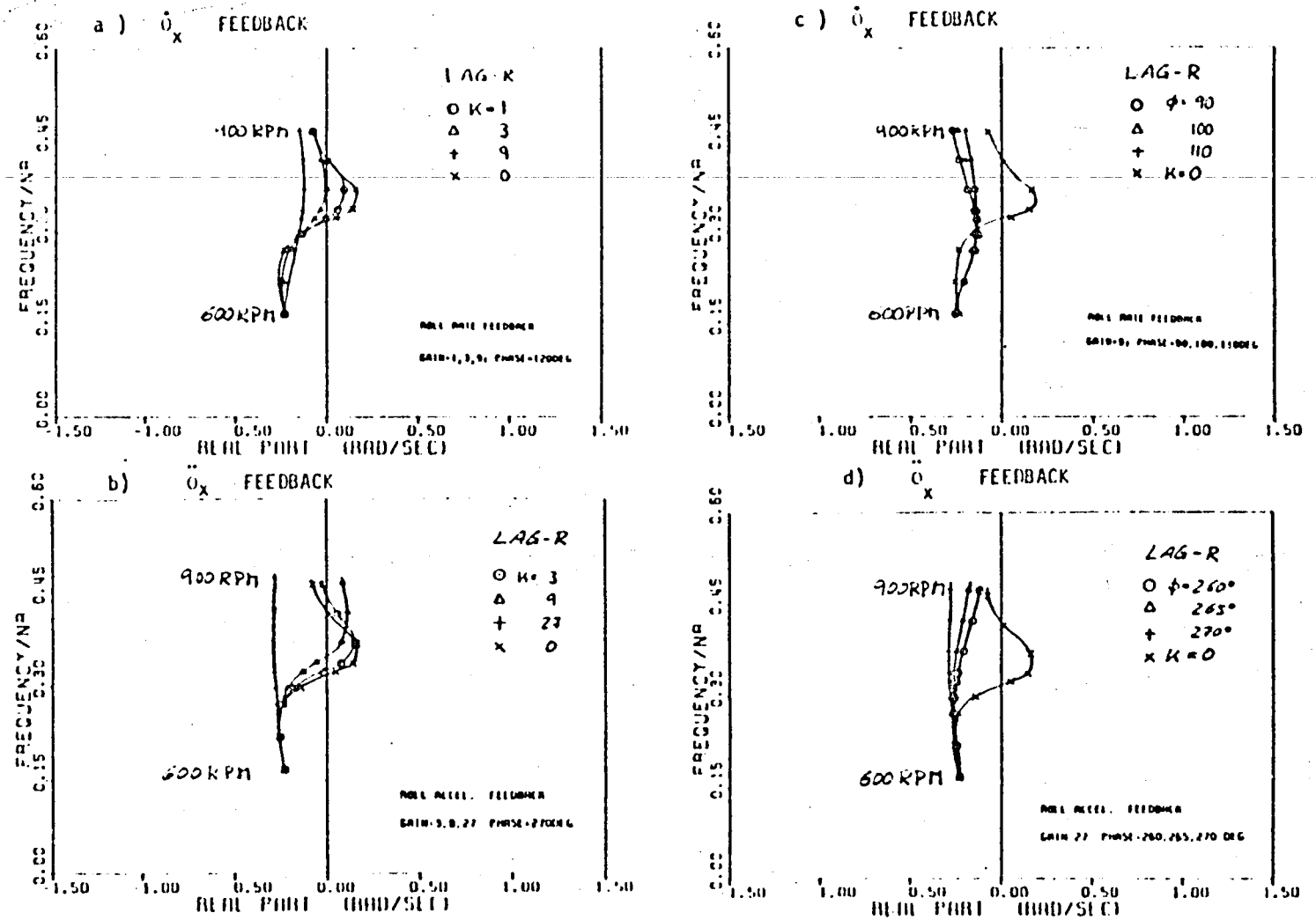

FIGURE 39. Effect of Roll Rate and Acceleration Feedback Gain and Phase on Regressing Lag Mode Dynamics.

(Root locus parameter - rotor speed)

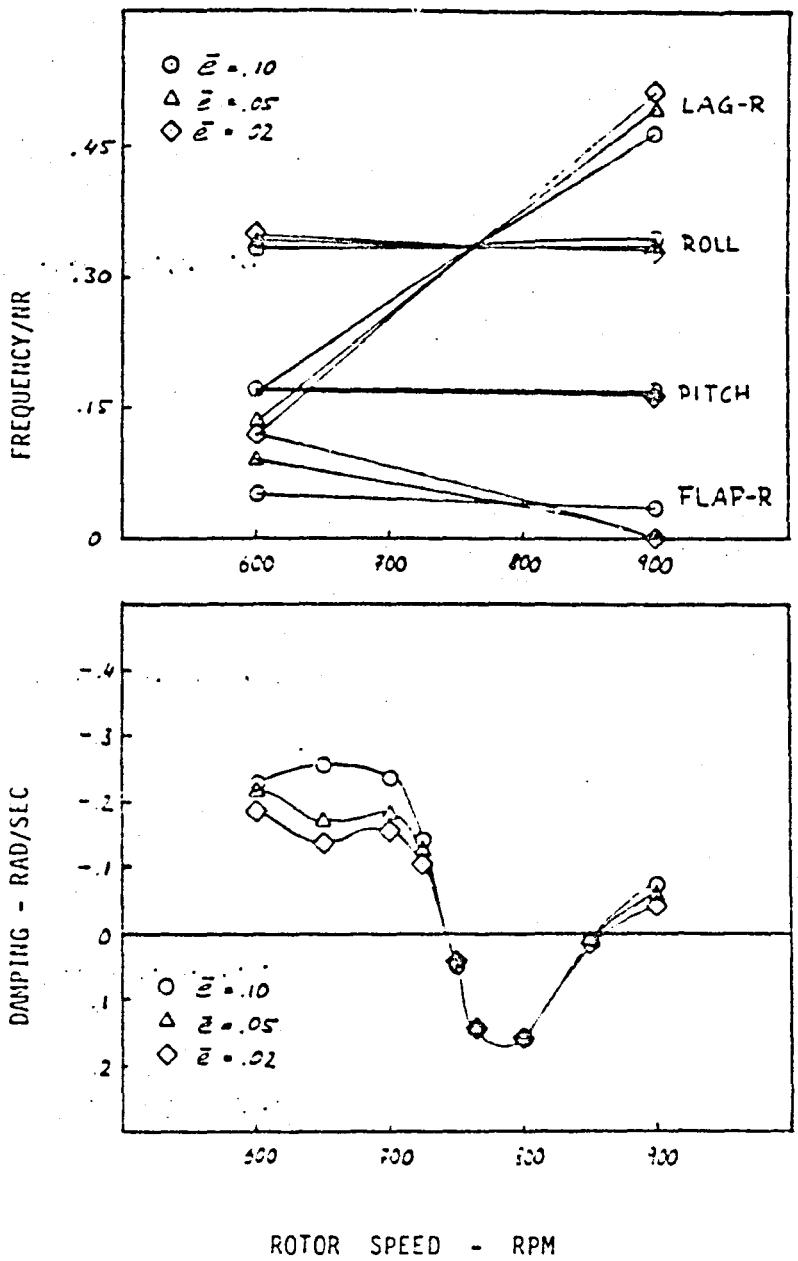

FIGURE 40. Modal Frequencies and Damping for Equivalent Dynamic Systems of Varying Hinge Offset.

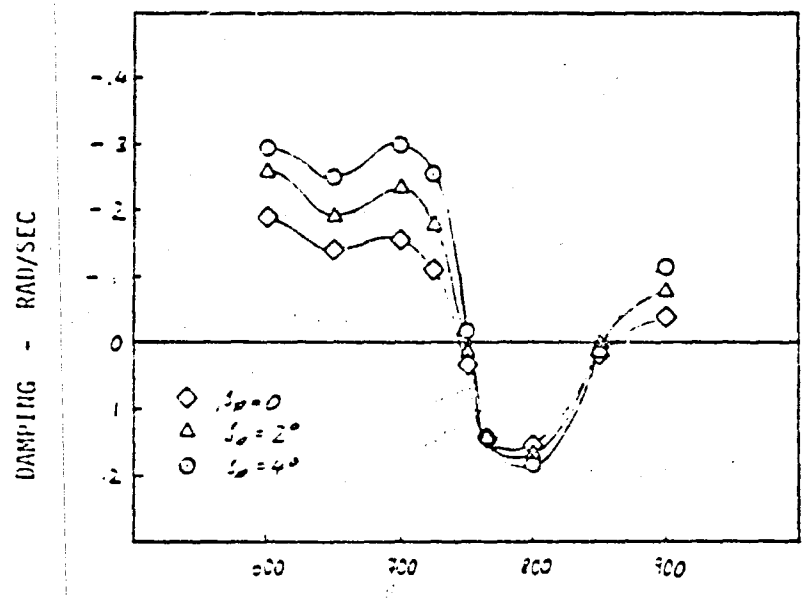

FIGURE 41. Modal Damping for Equivalent Dynamic Systems of Varying Precone. (e=.02R)

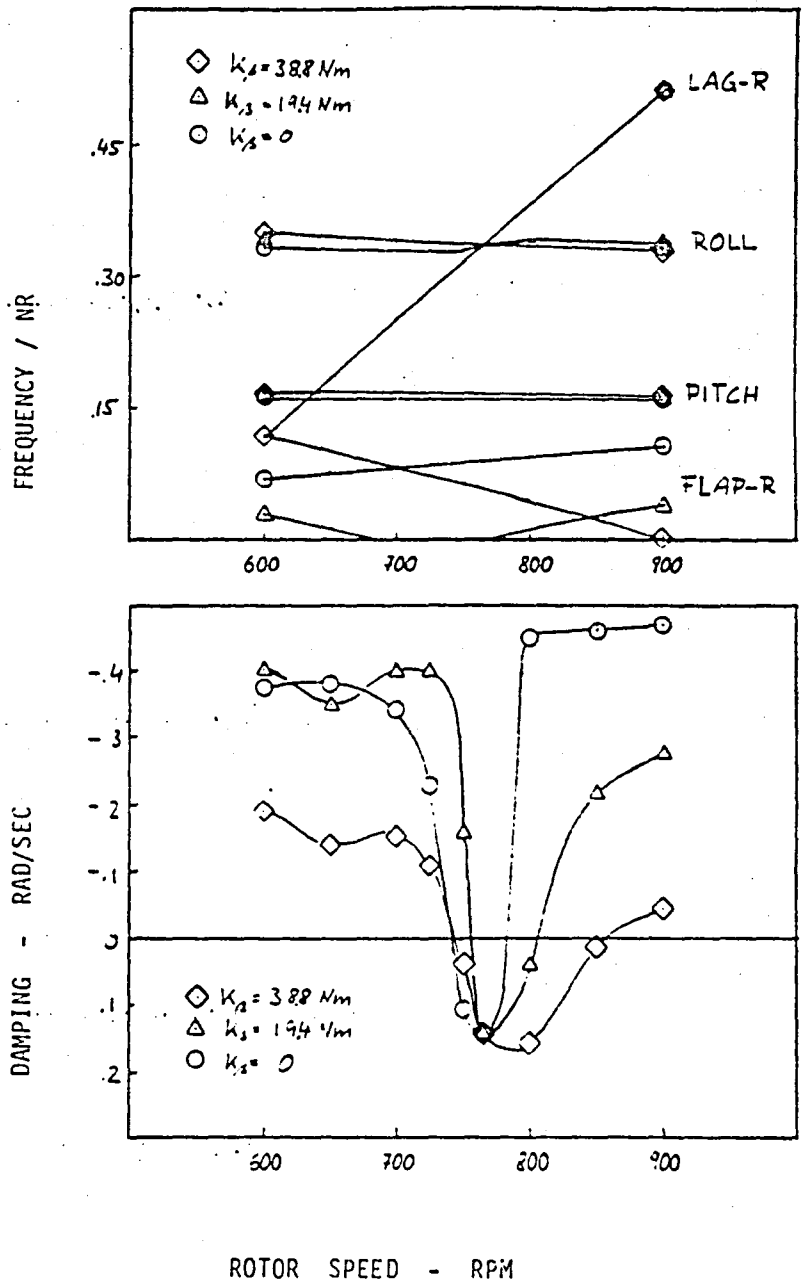

FIGURE 42. Modal Frequencies and Damping for Equivalent Dynamic Systems of Varying Flap Stiffness. (e=.02R)

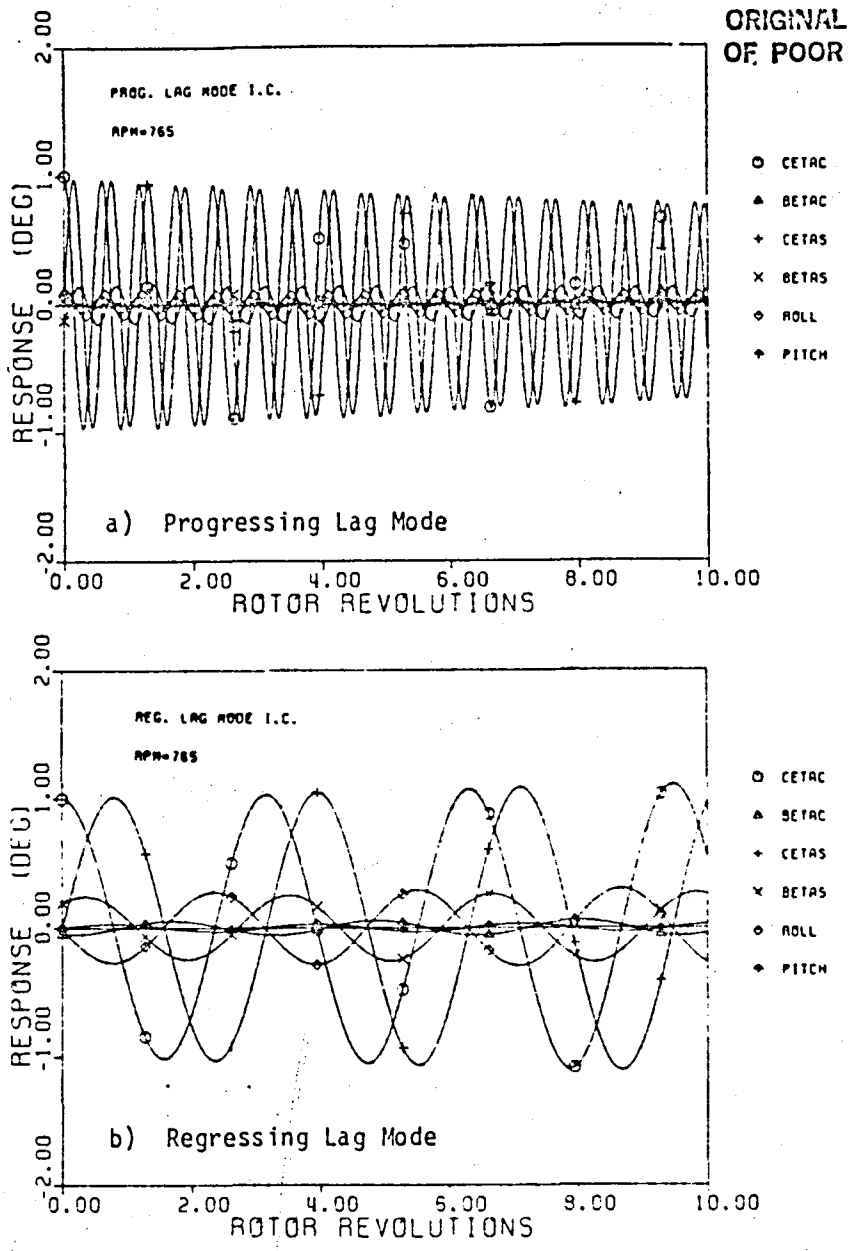

FIGURE 43. System Response Using Progressing and Regressing Lag Eigenvector from Stability Analysis as Initial Condition, Configuration C. (No Feedback Applied)

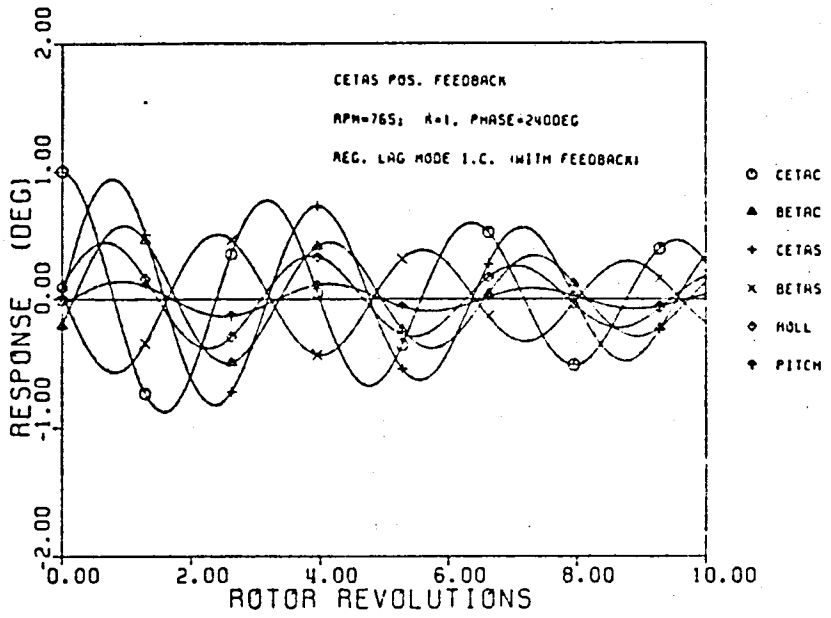

FIGURE 44. System Response with Sine Cyclic Lag Feedback, Using Regressing Lag Eigenvector from Stability Analysis as Initial Condition, Configuration C.

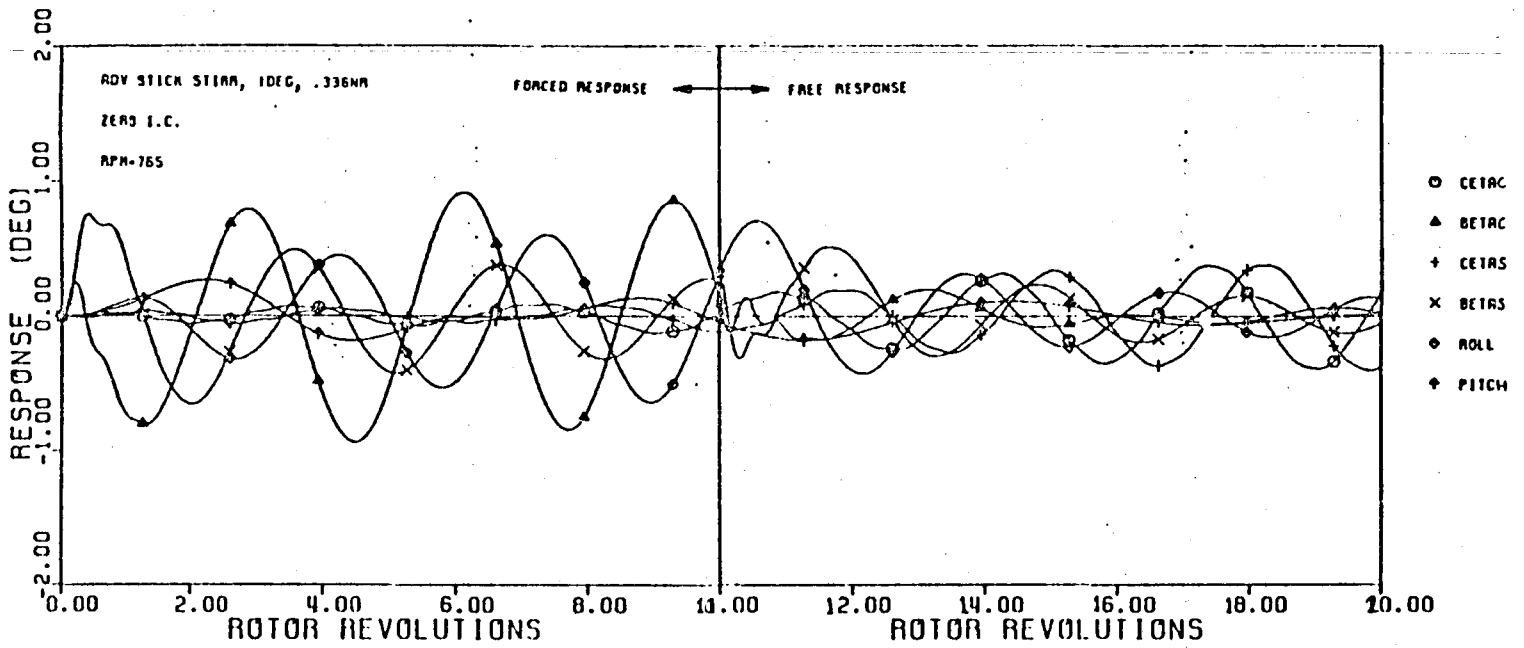

FIGURE 45. System Response to Advancing Stick Stir at Regressing lag Mode Frequency, Zero Initial Conditions, Configuration C. (Excitation Stopped after Ten Rotor Revolutions).

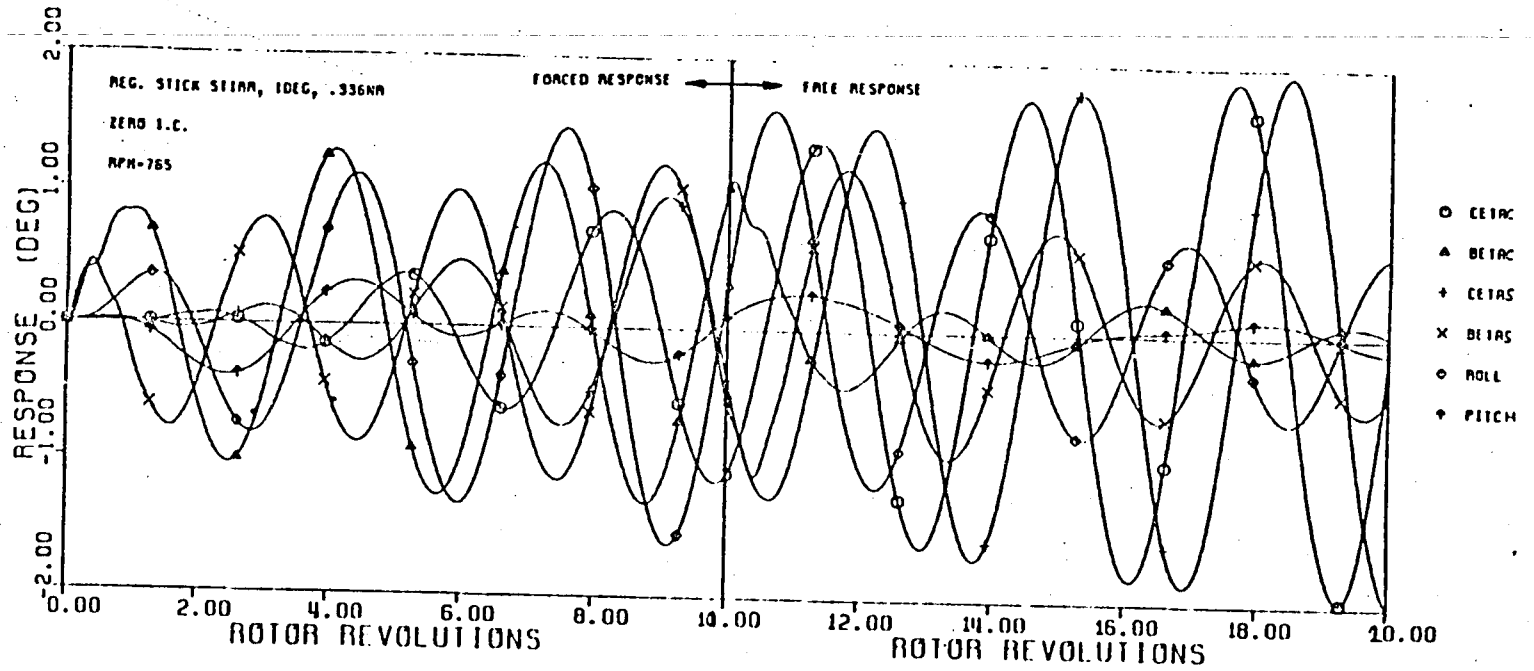

FIGURE 46. System Response to Regressing Stick Stir at Regressing Lag Mode Frequency, Zero Initial Condition, Configuration C. (Excitation Stopped after Ten Rotor Revolutions).

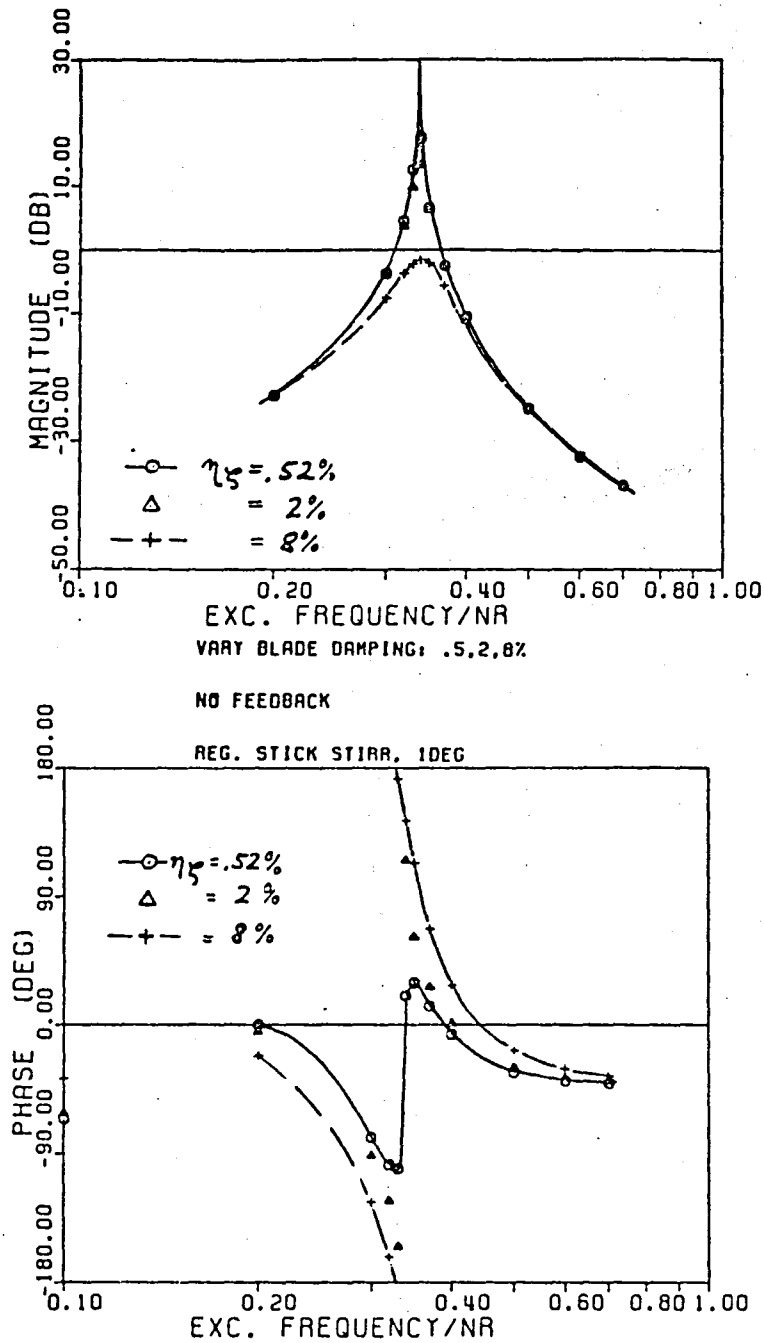

FIGURE 47. Effect of Blade Lead-Lag Damping on Frequency Response of Cosine Cyclic Lag Motion, No Feedback Applied, Configuration C.

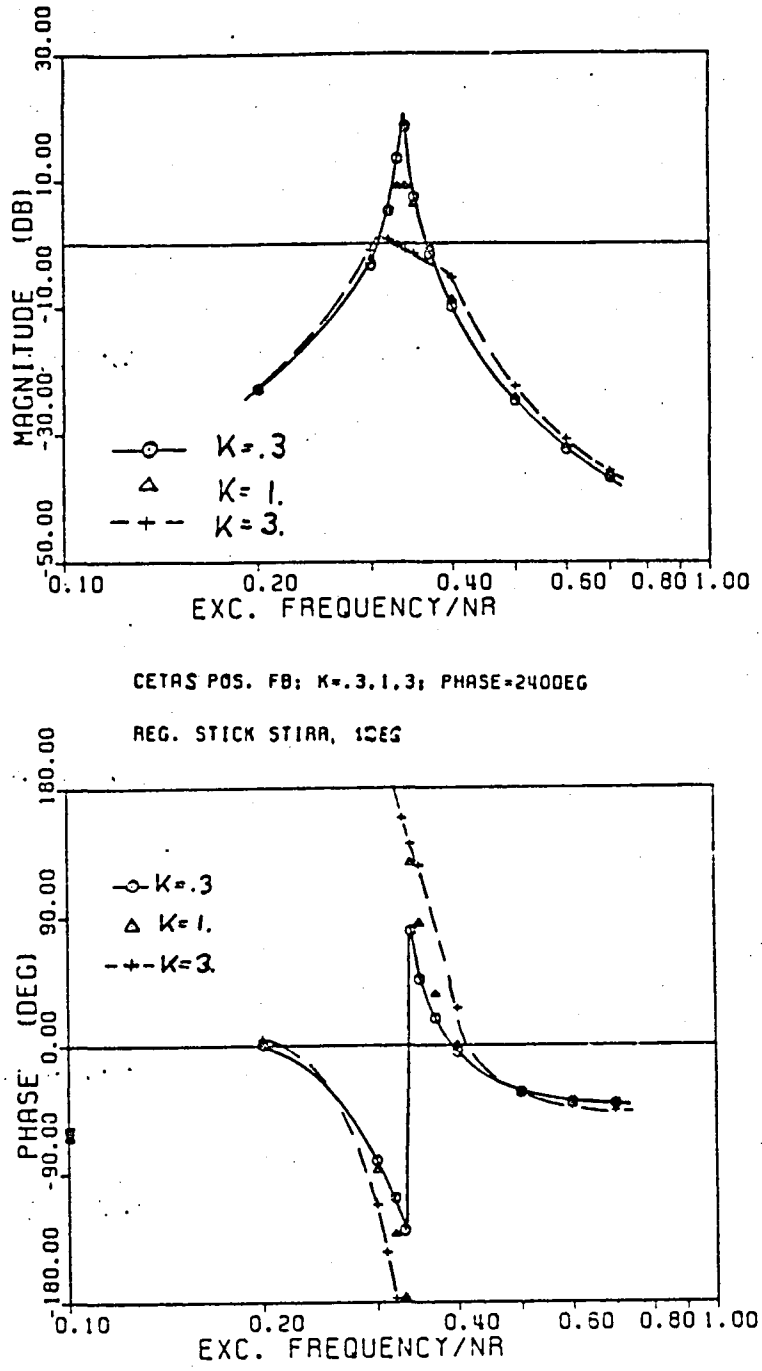

FIGURE 48. Effect of Sine Cyclic Lag Feedback Gain on Frequency Response of Cosine Cyclic Lag Motion, Configuration C.

TABLE 1: Rotor/Body Properties for Configuration A

Number of blades	4	
Hinge offset, ft	1.0	(.3048 m)
Blade mass, slugs	6.5	(94.9 Kg)
Blade first mass moment, slug - ft	65.0	(289.1 Kg - m)
Blade second mass moment, slug - ft^2	800.0	(1084.7 Kg - m^2)
Lag spring, ft - lb	0.0	(0.0 N-m)
Lag damper, ft - lb - sec	3000.0	(4067.5 N-m-s)
Fuselage mass long, slugs	550.0	(8026.6 Kg)
Fuselage mass lat., slugs	225.0	(3283.6 Kg)
Longitudinal Stiffness, lb/ft	85000.0	(1240481.8 N/m)
Lateral Stiffness, lb/ft	85000.0	(1240481.8 N/m)
Longitudinal damping, lb-sec/ft	3500.0	(51078.7 N-S/m)
Lateral damping, lb-sec/ft	1750.0	(25539.3N-s/m)
Rotor radius, ft	24.0	(7.32 m)
Chord, ft	1.75	(.53m)
Nominal rotor speed, rpm	300	
Precone, deg	0	
Height of rotor above body mass, ft	0	

TABLE 2: Rotor/Body Properties, Configuration B

Number of blades	3
Radius, cm	38.01
Chord, cm	1.26
Nominal rotor speed, rpm	1000
Hinge Offset, cm	8.51
Precone, deg	0
Blade airfoil	Circular
Lift curve slope	.0
Profile drag coefficient	1.0
Lock number	.0182 (0.0)
Solidity ratio	0.03179
Blade mass, kg	.699
Blade first mass moment, Kg cm	9.275
Blade second mass moment, Kg cm^2	177
Nonrotating flap frequency, Hz	3.01
Nonrotating lead-lag frequency, Hz	6.39
Damping in lead-lag, % critical	.185
Height of rotor hub above gimbal, cm	24.1
Fuselage mass in pitch, Kg	19.27
Fuselage mass in roll, Kg	19.27
Fuselage inertia in pitch, Kg cm^2	5110
Fuselage inertia in roll, Kg cm^2	1870
Pitch frequency, Hz	B1:27.4; B2: 2.39
Roll frequency, Hz	3.6
Damping in roll, %critical	3.0
Damping in pitch, % critical	3.0

TABLE 3: Rotor/Body Properties, Configuration C and D

Number of blades	3
Radius, cm	81.1
Chord, cm	4.19
Nominal rotor speed, rpm	720
Hinge Offset, cm	8.51
Precone, deg	0.
Blade airfoil	NACA 23012
Lift curve slope	2π
Profile drag coefficient	0.0079
Lock number	7.73
Solidity ratio	0.0494
Blade mass, Kg	.209
Blade first mass moment, Kg cm	3.887
Blade second mass moment, Kg cm^2	173
Nonrotating flap frequency, Hz	C: 3.13 ; D: 6.63
Nonrotating lead-lag frequency, Hz	6.70 6.73
Damping in lead-lag, % critical	0.52 0.53
Height of rotor hub above gimbal, cm	24.1
Fuselage mass in pitch, Kg	22.60
Fuselage mass in roll, Kg	19.06
Fuselage inertia in pitch, Kg cm^2	6330
Fuselage inertia in roll, Kg cm^2	1830
Pitch frequency, Hz	1.59; 2*
Roll frequency, Hz	3.9; 4*
Damping in pitch, % critical	3.20
Damping in roll, % critical	0.929

*Body Frequencies used in study of active control.

FEEDBACK STATE	K	ϕ deg	σ rad/sec	η % c_c	Θ_{Amax} deg
BASELINE	0	-	.145	-.58	-
$\dot{\zeta}_c$	1	60	-.164	.65	.32
ζ_s	.3	240	-.137	.54	.29
$\ddot{\zeta}_s$	3	60	-.178	.71	.34
$\dot{\Theta}_x$	9	90	-.149	.59	.33
$\ddot{\Theta}_x$	27	270	-.284	1.13	.39

TABLE 4. Summary of State Feedback Results for Configuration C.

(Ω = 765 rpm)

Hinge Offset % R	σ rad/sec	η + $\%c_c$	θ_{Amax} deg	Feedback State	K	ϕ deg	c_{lag} N-m-sec	k_{lag} N-m	k_{flap} N-m
10	-.137	.54	.29	ζ_s	.3	240	.0076	30.66	6.69
5	-.097	.38	.29	ζ_s	.3	240	.0049	41.8	26.0
2	-.077	.31	.29	ζ_s	.3	240	.0036	47.8	38.8
10	-.284	1.13	.39	$\ddot{\theta}_x$	27	270	.0076	30.66	6.69
5	-.158	.63	.45	$\ddot{\theta}_x$	27	270	.0049	41.8	26.0
2	-.119	.47	.37	$\ddot{\theta}_x$	27	270	.0036	47.8	38.8

TABLE 5: Effect of Hinge Offset on Feedback Results for Configuration C., Equivalent Dynamic Systems. (Ω = 765 rpm)

+ Without active control (K=0) system damping is η = -.58% critical for all three values of hinge offset.

Precone deg	σ rad/sec	η^+ $\%c_c$	θ_{Amax} deg	Feedback State	K	ϕ deg	c_{lag} N-m-sec	k_{lag} N-m	k_{flap} N-m
0	-.077	.31	.29	ζ_s	.3	240	.0036	47.8	38.8
2	-.116	.46	.29	ζ_s	.3	240	.0063	47.8	38.8
4	-.157	.62	.29	ζ_s	.3	240	.0089	47.8	38.8
0	-.119	.47	.37	$\ddot{\theta}_x$	27	270	.0036	47.8	38.8
2	-.288	1.14	.43	$\ddot{\theta}_x$	27	270	.0063	47.8	38.8
4	-.507	2.01	.50	$\ddot{\theta}_x$	27	270	.0089	47.8	38.8

TABLE 6: Effect of Precone on Feedback Results for Configuration C., Equivalent Dynamic Systems.

(Ω = 765 rpm, e = .02R)

+ Without active control (K=0) system damping is η = -.58% critical for all three values of precone.

Flap Stiffness N-m	σ rad/sec	η^+ $\%c_c$	θ_{Amax} deg	Feedback State	K	ϕ deg	c_{lag} N-m-sec	k_{lag} N-m	k_{roll} N-m
38.8	-.077	.31	.29	ζ_s	.3	240	.0036	47.8	115.6
19.4	-.181	.71	1.00	ζ_s	1.	240	.0110	48.1	132.0
0	-.132	.52	1.83	ζ_s	2.	225	.0595	47.5	138.0
38.8	-.119	.47	.37	$\ddot{\theta}_x$	27	270	.0036	47.8	115.6
19.4	-.232	.91	1.17	$\ddot{\theta}_x$	27	270	.0110	48.1	132.0
0	-.334	.36	2.41	$\ddot{\theta}_x$	27	225	.0595	47.5	138.0

TABLE 7: Effect of Flap Stiffness on Feedback Results for Configuration C., Equivalent Dynamic Systems.

(Ω =765 rpm, e=.02R)

+ Without active control (K=0) system damping is η = -.58% critical for all three values of flap stiffness.

APPENDIX A: LIST OF SYMBOLS

a	Lift Curve Slope
[A]	State Space System Matrix
[B]	State Space Control Input Matrix
c	Blade Chord
c_{do}	Profile Drag Coefficient
c_x	Fuselage Longitudinal Damping
c_y	Fuselage Lateral Damping
$c_{\theta x}$	Fuselage Roll Damping
$c_{\theta y}$	Fuselage Pitch Damping
c_ζ	Blade Lead-Lag Damping
[C]	Damping Matrix, State Space Output Matrix
e	Blade Root Hinge Offset
f	Forcing Vector
[F]	Control Input Matrix
g_{SL}, g_{SF}	Blade Structural Lag and Flap Damping
h	Offset of Rotor Hub from Fuselage C.G.
I_b	Blade Second Mass Moment of Inertia
I_x	Fuselage Roll Inertia
I_{xy}	Fuselage Product of Inertia
I_y	Fuselage Pitch Inertia
k	Blade Index, k=1 . N
K	Feedback Gain Constant
k_β	Blade Flapping Spring
k_ζ	Blade Lead-Lag Spring
k_x	Fuselage Longitudinal Stiffness

k_y	Fuselage Lateral Stiffness
$k_{\theta x}$	Fuselage Roll Stiffness
$k_{\theta y}$	Fuselage Pitch Stiffness
$[K]$	Stiffness Matrix, Matrix of Feedback Gains
ℓ	Length of Blade, from Root Hinge to Tip
M_b	Blade Mass
M_x	Fuselage Longitudinal Mass
M_y	Fuselage Lateral Mass
$[M]$	Mass Matrix
N	Number of Blades
NR	Nominal Rotor Speed
q	Vector of Generalized Coordinates
R	Rotor Radius
R_x	Fuselage Longitudinal Motion
R_y	Fuselage Lateral Motion
S_b	Blade First Mass Moment of Inertia
u	Vector of Control Inputs
v	Open Loop Forcing Signal
x	Vector of State Space Variables
y	Vector of Output Measurements
β_k	Flapping Motion of the k'th Blade
β_c, β_s	Rotor Cosine, Sine Cyclic Flap Degrees of Freedom
β_p	Precone
γ	Lock Number
ϵ	Order of Magnitude
ζ_k	Lead-Lag Motion of k'th Blade
ζ_c, ζ_s	Rotor Cosine, Sine Cyclic Lead-Lag Degrees of Freedom

η	Modal Damping Coefficient, % Critical
η_ζ	Blade Lead-Lag Damping, % Critical
θ_o	Rotor Collective Pitch Angle
θ_{Ak}	Active Control Blade Feathering Angle
θ_{Ac}, θ_{As}	Active Control Feathering Inputs to Nonrotating Swash Plate
θ_{Amax}	Maximum Active Control Blade Feathering Angle Per Degree of Lead-Lag Motion
θ_G	Blade Aerodynamic Pitch Angle
θ_S	Orientation of Blade Root Springs at Flat Pitch
θ_x	Fuselage Roll Motion
θ_y	Fuselage Pitch Motion
λ	Inflow Ratio
σ	Real Part of Eigenvalue, i.e., Modal Damping, rad/sec; Rotor Solidity
ϕ	Feedback Phase, i.e., Weighting Between Cyclic Controls
ϕ_c, ϕ_s	Phase of Open Loop Cyclic Control Inputs
ψ	Nondimensional Time Parameter, Rotor Azimuth
ψ_k	Azimuth Angle of k'th Blade
ω	Imaginary Part of Eigenvalue, i.e., Modal Frequency, rad/sec
ω_A	Open Loop Forcing Frequency
Ω	Rotor Speed
Ω_o	Nominal Rotor Speed
$\bar{(\ )}$	Nondimensional Quantity
$(\ )_o$	Steady-State Equilibrium Value
$(\ )'$	$d(\ )/d\psi$

APPENDIX B: EQUATIONS OF MOTION

The nonlinear steady-state blade equilibrium equations and the linearized periodic coefficient perturbation equations for the blade and fuselage degrees of freedom are given in this Appendix.

STEADY-STATE EQUILIBRIUM

Lag:

$$\zeta_0 \left\{ \bar{K}_\beta \sin^2\theta_s + \bar{K}_\zeta \cos^2\theta_s + \bar{\Omega}^2 \bar{e}\, \bar{S}_6 + \bar{\Omega}^2 \Gamma \bar{\ell}_4 \theta_0 \beta_p \right\}$$
$$+ \beta_0 (\bar{K}_\zeta - \bar{K}_\beta) \sin\theta_s \cos\theta_s$$
$$+ \beta_0 \zeta_0 \Gamma \bar{\Omega}^2 \theta_0 (\bar{\ell}_4 - \bar{\ell}_5)$$
$$+ \bar{\Omega}^2 \Gamma \left(\theta_0 \bar{\ell}_2 \lambda_0 + \frac{c_{d0}}{a} \bar{\ell}_5 - \frac{\bar{\ell}^2}{2} \lambda_0^2 \right) = 0$$

Flap:

$$\zeta_0 \left\{ (\bar{K}_\zeta - \bar{K}_\beta) \sin\theta_s \cos\theta_s + \bar{\Omega}^2 \Gamma \bar{\ell}_4 \beta_p \right\}$$
$$+ \beta_0 \left\{ \bar{K}_\beta \cos^2\theta_s + \bar{K}_\zeta \sin^2\theta_s + \bar{\Omega}^2 (\bar{e}\, \bar{S}_6 + \bar{I}_6) + \bar{\Omega}^2 \Gamma \bar{\ell}_4 \theta_0 \beta_p \right\}$$
$$+ \bar{\Omega}^2 \Gamma \left\{ \bar{\ell}_4 \beta_0 \zeta_0 + \left(\theta_0 \tfrac{1}{2} \bar{\ell}_5 - \theta_0 \bar{\ell}_4\right)(\zeta_0^2 - \beta_0^2) \right\}$$
$$+ \bar{\Omega}^2 \Gamma (-\theta_0 \bar{\ell}_5 + \bar{\ell}_2 \lambda_0) + \bar{\Omega}^2 \beta_p (\bar{e}\, \bar{S}_6 + \bar{I}_6) = 0$$

Lag:

$$\bar{\Omega}^2 \bar{I}_6 \ddot{\zeta}_{0k} + \zeta_{0k}\{-\bar{\Omega}(\bar{g}_{SL} + \bar{C}_\zeta \cos^2\theta_S) + \bar{\Omega}^2\Gamma(\theta_0 \tfrac{\bar{\ell}^3}{3}\lambda + \tfrac{C_{d_0}}{a} 2\bar{\ell}_4)\}$$

$$+ \beta_k\{-\bar{\Omega}^2 2\bar{I}_6(\beta_p+\beta_0) + \bar{\Omega}\bar{C}_\zeta \sin\theta_S\cos\theta_S + \bar{\Omega}^2\Gamma(\theta_0\bar{\ell}_4 - 2\tfrac{\bar{\ell}^3}{3}\lambda)\}$$

$$+ \zeta_k\{\bar{K}_S \sin^2\theta_S + \bar{K}_\zeta \cos^2\theta_S + \bar{\Omega}^2 \bar{e}\,\bar{S}_6 + \bar{\Omega}^2\Gamma\theta_0(\bar{\ell}_4(\beta_p+\beta_0) - \bar{\ell}_5\beta_0)\}$$

$$+ \beta_k\{(\bar{K}_\zeta - \bar{K}_S)\sin\theta_S\cos\theta_S + \bar{\Omega}^2\Gamma\theta_0(\bar{\ell}_4 - \bar{\ell}_5)\zeta_0\}$$

$$+ \bar{\Omega}^2\cos\psi_k\{\ddot{\theta}_x(-\bar{h}\bar{S}_6 - (\beta_p+\beta_0)\bar{I}_6) - \ddot{\theta}_y\bar{h}\bar{S}_6\zeta_0$$

$$- \ddot{\ddot{R}}_x\bar{S}_6\zeta_0 + \ddot{\ddot{R}}_y\bar{S}_6 + \dot{\theta}_z 2\Gamma(\bar{\ell}_2\lambda - \theta_0\bar{\ell}_5)\}$$

$$+ \bar{\Omega}^2\sin\psi_k\{\ddot{\theta}_x\bar{h}\bar{S}_6\zeta_0 - \ddot{\theta}_z(\bar{h}\bar{S}_6 - \bar{I}_6(\beta_p+\beta_0))$$

$$- \ddot{\ddot{R}}_x\bar{S}_6 - \ddot{\ddot{R}}_y\bar{S}_6\zeta_0 + \dot{\theta}_x 2\Gamma(\theta_0\bar{\ell}_5 - \bar{\ell}_2\lambda)\}$$

$$+ \theta_{Ak}\bar{\Omega}^2\Gamma\bar{\ell}_2\lambda = 0$$

Flap:

$$\bar{\Omega}^2 \bar{I}_b \ddot{\beta}_K$$

$$+ \dot{\zeta}_K \{ \bar{\Omega} \bar{C}_\zeta \sin\theta_s \cos\theta_s + \bar{\Omega}^2 \bar{I}_b 2(\beta_p+\beta_0) + \bar{\Omega}^2 \Gamma (\frac{\bar{l}^3}{3}\lambda - 2\theta_0 \bar{l}_4) \}$$

$$+ \dot{\beta}_K \{ \bar{\Omega} (\bar{g}_{SF} + \bar{C}_\zeta \sin^2\theta_s) + \bar{\Omega}^2 \Gamma \bar{l}_4 \}$$

$$+ \zeta_K \{ (\bar{K}_\zeta - \bar{K}_\beta) \sin\theta_s \cos\theta_s + \bar{\Omega}^2 \Gamma (\bar{l}_4(\beta_p+\beta_0) - \theta_0(2\bar{l}_4 - \bar{l}_5)\zeta_0) \}$$

$$+ \beta_K \{ \bar{K}_\beta \cos^2\theta_s + \bar{K}_\zeta \sin^2\theta_s + \bar{\Omega}^2 (\bar{e}\bar{S}_b + \bar{I}_b)$$

$$+ \bar{\Omega}^2 \Gamma (\bar{l}_4 \zeta_0 + 2\theta_0 \bar{l}_4 (\beta_p+\beta_0) - \theta_0 \bar{l}_5 \beta_0) \}$$

$$+ \bar{\Omega}^2 \cos\psi_K \{ \ddot{\theta}_x \bar{I}_b \zeta_0 + \ddot{\theta}_y (-\bar{h}\bar{S}_b(\beta_p+\beta_0) - (\bar{e}\bar{S}_b + \bar{I}_b))$$

$$+ \ddot{\bar{R}}_x (-\bar{S}_b(\beta_p+\beta_0))$$

$$+ \dot{\theta}_x (2(\bar{e}\bar{S}_b + \bar{I}_b) + 2\Gamma(\bar{h}\bar{l}_2\theta_0 + \bar{l}_4\zeta_0 - \bar{h}\frac{\bar{l}^2}{2}\lambda))$$

$$+ \dot{\theta}_y (2\bar{I}_b\zeta_0 + 2\Gamma(-\bar{l}_5 - \bar{h}\bar{l}_2(\beta_p+\beta_0)))$$

$$+ \dot{\bar{R}}_x (-2\Gamma\bar{l}_2(\beta_p+\beta_0)) + \dot{\bar{R}}_y 2\Gamma(-\theta_0\bar{l}_2 + \frac{\bar{l}_2^2}{2}\lambda) \}$$

$$+ \bar{\Omega}^2 \sin\psi_K \{ \ddot{\theta}_x (\bar{h}\bar{S}_b(\beta_p+\beta_0) + \bar{e}\bar{S}_b + \bar{I}_b) + \ddot{\theta}_y \bar{I}_b \zeta_0$$

$$+ \ddot{\bar{R}}_y (-\bar{S}_b(\beta_p+\beta_0))$$

$$+ \dot{\theta}_x (-2\bar{I}_b\zeta_0 + 2\Gamma(\bar{l}_5 + \bar{h}\bar{l}_2(\beta_p+\beta_0)))$$

$$+ \dot{\theta}_y (2(\bar{e}\bar{S}_b + I_b) + 2\Gamma(\bar{h}\bar{l}_2\theta_0 + \bar{l}_4\zeta_0 - \bar{h}\frac{\bar{l}^2}{2}\lambda))$$

$$+ \dot{\bar{R}}_x 2\Gamma(\bar{l}_2\theta_0 - \frac{\bar{l}^2}{2}\lambda) - \bar{R}_y 2\Gamma\bar{l}_2(\beta_p+\beta_0) \}$$

$$+ \theta_{AK}(-\bar{\Omega}^2\Gamma\bar{l}_5) = 0$$

Longitudinal:

$$\bar{\Omega}^2 \ddot{\bar{R}}_x + \bar{\Omega}\,\bar{C}_x\,\dot{\bar{R}}_x + \bar{K}_x\,\bar{R}_x - P_x = 0$$

$$\begin{aligned}
P_x = {} & \gamma_x \bar{\Omega}^2 \frac{2}{N} \sum_k \cos\psi_k \Big\{ \ddot{\zeta}_k \bar{S}_6 \zeta_0 + \ddot{\beta}_k \bar{S}_6 (\beta_p + \beta_0) \\
& + \dot{\zeta}_k \left(2\bar{S}_6 + \Gamma(-2\theta_0 \bar{l}_2 (\beta_p + \beta_0)) \right) \\
& + \dot{\beta}_k \Gamma(\bar{l}_2 (\beta_p + \beta_0) + \zeta_0 \theta_0 \bar{l}_2) \\
& + \zeta_k \left(-\bar{S}_6 \zeta_0 + \Gamma(\theta_0 \bar{l}_1 \lambda + \frac{c_{d_0}}{a} \bar{l}_3) \right) \\
& + \beta_k \left(-\bar{S}_6 (\beta_p + \beta_0) - \Gamma(\theta_0 \bar{l}_3 - \bar{l}_1 \lambda) \right) \Big\} \\
& + \gamma_x \bar{\Omega}^2 \frac{2}{N} \sum_k \sin\psi_k \Big\{ \ddot{\zeta}_k \bar{S}_6 \\
& + \dot{\zeta}_k \left(-2\bar{S}_6 \zeta_0 + \Gamma(\theta_0 \frac{\bar{l}^2}{2} \lambda + 2\bar{l}_2 \frac{c_{d_0}}{a}) \right) \\
& + \dot{\beta}_k \left(-2\bar{S}_6 (\beta_p + \beta_0) + \Gamma(\theta_0 \bar{l}_2 - 2\frac{\bar{l}^2}{2} \lambda) \right) \\
& + \zeta_k \left(-\bar{S}_6 + \Gamma \theta_0 \bar{l}_2 (\beta_p + \beta_0) \right) + \beta_k \Gamma \theta_0 \bar{l}_2 \zeta_0 \Big\} \\
& + 2\gamma_x \bar{\Omega}^2 \Big\{ -\bar{M}_b \ddot{\bar{R}}_x - (\bar{M}_b \bar{h} + \bar{S}_6 (\beta_p + \beta_0)) \ddot{\theta}_0 \\
& + \dot{\theta}_x \Gamma(\theta_0 \bar{l}_2 - \bar{l}_1 \lambda) - \dot{\theta}_0 \Gamma(\beta_0 + \beta_0) \bar{l}_3 \\
& + \theta_0 \Gamma(\theta_0 \bar{l}_3 - \bar{l}_1 \lambda) \Big\} \\
& + \gamma_x \bar{\Omega}^2 \frac{2}{N} \sum_k \theta_{Ak} \Gamma \left\{ \sin\psi_k (\bar{l}_1 \lambda) - \cos\psi_k (\beta_p + \beta_0) \bar{l}_3 \right\}
\end{aligned}$$

Lateral:

$$\bar{\Omega}^2 \ddot{\bar{R}}_y + \bar{\Omega} \bar{C}_y \dot{\bar{R}}_y + \bar{K}_y \bar{R}_y - P_y = 0$$

$$\begin{aligned}
P_y = {} & \nu_y \bar{\Omega}^2 \frac{2}{N} \sum_k \cos\psi_k \Big\{ -\ddot{\zeta}^{\circ}_k \bar{S}_6 \\
& + \dot{\zeta}_k \left(2\zeta_0 \bar{S}_6 - \Gamma\left(\theta_0 \frac{\bar{l}^2}{2}\lambda + 2\bar{l}_2 \frac{c_{d0}}{a} \right) \right) \\
& + \dot{\beta}_k \left(2(\beta_p+\beta_0)\bar{S}_6 + \Gamma\left(2\frac{\bar{l}^2}{2}\lambda - \theta_0 \bar{l}_2\right)\right) \\
& + \zeta_k \left(\bar{S}_6 - \Gamma\theta_0 \bar{l}_2 (\beta_p+\beta_0)\right) + \beta_k \left(-\Gamma\theta_0 \bar{l}_2 \zeta_0\right) \Big\} \\
& + \nu_y \bar{\Omega}^2 \frac{2}{N} \sum_k \sin\psi_k \Big\{ \ddot{\zeta}_k \bar{S}_6 \zeta_0 + \ddot{\beta}_k \bar{S}_6 (\beta_p+\beta_0) \\
& + \dot{\zeta}^{\circ}_k \left(2\bar{S}_6 - \Gamma 2\theta_0 \bar{l}_2 (\beta_p+\beta_0)\right) \\
& + \dot{\beta}_k \Gamma \left((\beta_p+\beta_0)\bar{l}_2 + \theta_0 \bar{l}_2 \zeta_0 \right) \\
& + \zeta_k \left(-\zeta_0 \bar{S}_6 + \Gamma\left(\theta_0 \bar{l}_1 \lambda + \frac{c_{d0}}{a}\bar{l}_3\right)\right) \\
& + \beta_k \left(-\bar{S}_6(\beta_p+\beta_0) + \Gamma(\bar{l}_1\lambda - \theta_0 \bar{l}_3)\right) \Big\} \\
& + 2\nu_y \bar{\Omega}^2 \Big\{ -\bar{m}_6 \ddot{\bar{R}}_y + \left(\bar{m}_6 \bar{h} + \bar{S}_6 (\beta_p+\beta_0)\right) \ddot{\theta}^{\circ}_x \\
& + \dot{\theta}_x \Gamma \bar{l}_3 (\beta_p+\beta_0) + \dot{\theta}_z \Gamma (\theta_0 \bar{l}_3 - \bar{l}_1 \lambda) \\
& + \theta_x \Gamma (\bar{l}_1 \lambda - \theta_0 \bar{l}_3) \Big\} \\
& + \nu_y \bar{\Omega}^2 \frac{2}{N} \sum_k \theta_{Ak} \Gamma \left\{ -\cos\psi_k (\bar{l}_1 \lambda) - \sin\psi_k (\beta_p+\beta_0)\bar{l}_3 \right\}
\end{aligned}$$

Roll:

$$\bar{\Omega}^2 \ddot{\theta}_x + \bar{\Omega}^2 I_{xy}/I_y \ddot{\theta}_y + \bar{\epsilon} \bar{C}_{\theta_y} \dot{\theta}_x + \bar{K}_{\theta_x} \theta_x - Q_x = 0$$

$$\begin{aligned}
Q_x = {} & \gamma_{\theta_x} \bar{\Omega}^2 \frac{2}{N} \sum_k \cos\psi_k \Big\{ \ddot{\xi}_k \left(\bar{I}_6 (\lambda_{1p}+\lambda_{1o}) + \bar{h}\bar{S}_6 \right) + \ddot{\beta}_k (-\xi_0 \bar{I}_6) \\
& + \dot{\xi}_k \Big\langle -\bar{h}\bar{S}_6 2\xi_0 + \Gamma[2\theta_0 \xi_0 \bar{l}_4 + \bar{h}\frac{\bar{e}^2}{2}\dot{\theta}_0 \lambda - \frac{C_{x\theta}}{a} 2\bar{h}\bar{l}_2] \Big\rangle \\
& + \dot{\beta}_k \Big\langle -2\bar{h}\bar{S}_6 (\lambda_{1p}+\lambda_{1o}) + \Gamma[-\bar{l}_4 \xi_0 + (\lambda_{1p}+\lambda_{1o})\xi_0 \bar{l}_4 + \bar{h}(\bar{l}_2\theta_0 - 2\frac{\bar{l}_2^2}{2}\lambda)] \Big\rangle \\
& + \xi_k \Big\langle -\bar{I}_6 (\lambda_{1p}+\lambda_{1o}) - \bar{h}\bar{S}_6 + \Gamma[\theta_0 \bar{l}_5 - \bar{l}_2 \lambda + \bar{h}\bar{l}_2 \theta_0 (\lambda_{1p}+\lambda_{1o})] \Big\rangle \\
& + \beta_k \Big\langle -\bar{I}_6 \xi_0 + \Gamma[\theta_0 \bar{l}_2 \lambda + \frac{C_{x\theta}}{a}\bar{l}_5 + \bar{h}\theta_0 \bar{l}_2 \xi_0] \Big\rangle \Big\} \\
& + \gamma_{\theta_y} \bar{\Omega}^2 \frac{2}{N} \sum_k \sin\psi_k \Big\{ \ddot{\xi}_k (-\bar{h}\bar{S}_6 \xi_0) + \ddot{\beta}_k (-\bar{I}_6 - \bar{e}\bar{S}_6 - \bar{h}\bar{S}_6 (\lambda_{1p}+\lambda_{1o})) \\
& + \dot{\xi}_k \Big\langle -2\bar{I}_6 (\lambda_{1p}+\lambda_{1o}) - \bar{h}2\bar{S}_6 + \Gamma[2\theta_0 \bar{l}_4 - \frac{\bar{l}^3}{3}\lambda + 2\theta_0 \bar{l}_2 (\bar{e} + \bar{h}(\lambda_{1p}+\lambda_{1o}))] \Big\rangle \\
& + \dot{\beta}_k \Gamma \Big\langle -\bar{l}_4 - \bar{e}\bar{l}_2 - \bar{h}\bar{l}_2 (\lambda_{1p}+\lambda_{1o}) - \bar{h}\theta_0 \bar{l}_2 \xi_0 \Big\rangle \\
& + \xi_k \Big\langle \bar{h}\bar{S}_6 \xi_0 - \Gamma[-\bar{l}_4 (\lambda_{1p}+\lambda_{1o}) - \xi_0 \theta_0 (2\bar{l}_4 - \bar{l}_5) - \bar{h}(\theta_0 \bar{l}_1 \lambda + \frac{C_{x\theta}}{a}\bar{l}_3)] \Big\rangle \\
& + \beta_k \Big\langle -\bar{e}\bar{S}_6 - \bar{I}_6 + \bar{h}\bar{S}_6 (\lambda_{1p}+\lambda_{1o}) - \Gamma[-\bar{l}_4 \xi_0 - 2\bar{l}_4 \xi_0 (\lambda_{1p}+\lambda_{1o}) + \bar{l}_5 \theta_0 \lambda_{1o} \\
& \qquad + \bar{h}(\bar{l}_3 \theta_0 - \bar{l}_1 \lambda)] \Big\rangle \Big\} \\
& + 2\gamma_{\theta_x} \bar{\Omega}^2 \Big\{ \ddot{\theta}_x [-2\bar{h}_1 (\lambda_{1p}+\lambda_{1o})\bar{S}_6 - \bar{h}^2 \bar{M}_6 - \frac{1}{2}(\bar{e}^2 \bar{M}_6 + 2\bar{e}\bar{S}_6 + \bar{I}_6)] \\
& + \ddot{\theta}_y \frac{1}{2}\bar{e}\bar{S}_6 \xi_0 + \ddot{R}_y \left(\bar{S}_6 (\lambda_{1p}+\lambda_{1o}) + \bar{h}\bar{M}_6 \right) \\
& + \dot{\theta}_x \Big\langle -\bar{e}\bar{S}_6 \xi_0 - \Gamma[\bar{l}_5 + \bar{h}(\bar{l}_2 + \bar{l}_3)(\lambda_{1p}+\lambda_{1o}) + \bar{e}\bar{l}_2] \Big\rangle \\
& + \dot{\theta}_y \Big\langle -\frac{1}{2}(\bar{e}^2 \bar{M}_5 + 2\bar{e}\bar{S}_6 + \bar{I}_5) + \Gamma[\xi_0 (\bar{l}_5 - \bar{l}_6) - \bar{h}(\theta_0 (\bar{l}_3 + \bar{l}_2) - \lambda(\bar{l}_1 + \frac{\bar{l}^2}{2}))] \Big\rangle \\
& + \dot{\bar{R}}_x \Gamma (\frac{\bar{l}^2}{2}\lambda - \bar{l}_1 \theta_0) + \dot{\bar{R}}_y \Gamma \bar{l}_2 (\lambda_{1p}+\lambda_{1o}) + \theta_y (-\bar{e}\bar{S}_6 \xi_0) \Big\} \\
& + \gamma_{\theta_x} \bar{\Omega}^2 \frac{2}{N} \sum_k \theta_{0k} \Gamma \Big\{ \cos\psi_k (\xi_0 \bar{l}_5 + \bar{h}\bar{l}_1 \lambda) + \\
& \qquad + \sin\psi_k (\bar{l}_5 + \bar{e}\bar{l}_3 + \bar{h}(\lambda_{1p}+\lambda_{1o})\bar{l}_3) \Big\}
\end{aligned}$$

Pitch:

$$\bar{\Omega}^2 \ddot{\theta}_y + \bar{\Omega}^2 I_{xy}/I_y \ddot{\theta}_x + \bar{\Omega}^2 \bar{c}_{\theta_y} \dot{\theta}_y - \bar{K}_{\theta_x} \theta_y - Q_y = 0$$

$$Q_y = \gamma_{\theta_y} \bar{\Omega}^2 \frac{2}{N} \sum_k \cos\psi_k \Big\{ \ddot{\zeta}_{0_k} \bar{h}\bar{S}_6 \zeta_0 + \ddot{\beta}_k (\bar{e}\bar{S}_6 + \bar{I}_6 + \bar{h}\bar{S}_6(\beta_p/\beta_0))$$

$$+ \dot{\zeta}_{0_k} \Big\langle 2\bar{I}_0(\beta_p/\beta_0) + 2\bar{h}\bar{S}_6 + \Gamma\Big[\frac{\bar{\ell}^3}{3}\lambda - 2\theta_0\bar{\ell}_4 - 2\theta_0\bar{\ell}_2(\bar{e} + \bar{h}(\beta_p/\beta_0))\Big]\Big\rangle$$

$$+ \dot{\beta}_k \Gamma \Big\langle \bar{\ell}_4 + \bar{e}\bar{\ell}_2 + \bar{h}\bar{\ell}_2(\beta_p/\beta_0) + \bar{h}\bar{\ell}_2\theta_0\zeta_0 \Big\rangle$$

$$+ \zeta_{0_k} \Big\langle -\bar{h}\bar{S}_6\zeta_0 + \Gamma\Big[\bar{\ell}_4(\beta_p/\beta_0) + \theta_0\zeta_0(\bar{\ell}_5 - 2\bar{\ell}_4) + \bar{h}\Big(\theta_0\bar{\ell}_1\lambda + \frac{c_{a_0}}{a}\bar{\ell}_2\Big)\Big]\Big\rangle$$

$$+ \beta_k \Big\langle \bar{e}\bar{I}_6 - \bar{I}_6 - \bar{h}\bar{I}_6(\beta_p/\beta_0) + \Gamma\Big[\bar{\ell}_4\zeta_0 + \theta_0 2\bar{\ell}_4(\beta_p/\beta_0) - \bar{\ell}_5\theta_0\beta_0 + \bar{h}(\bar{\ell}_1\lambda - \theta_0\bar{\ell}_2)\Big]\Big\rangle \Big\}$$

$$+ \gamma_{\theta_y} \bar{\Omega}^2 \frac{2}{N} \sum_k \sin\psi_k \Big\{ \ddot{\zeta}_{0_k}\Big(\bar{I}_6(\beta_p/\beta_0) + \bar{h}\bar{S}_6\Big) + \ddot{\beta}_k(-\bar{I}_6\zeta_0)$$

$$+ \dot{\zeta}_{0_k}\Big\langle -2\bar{h}\bar{S}_6\zeta_0 + \Gamma\Big[2\theta_0\bar{\ell}_4\zeta_0 + \bar{h}\Big(\theta_0\frac{\bar{\ell}^2}{2}\lambda + 2\frac{c_{a_0}}{a}\bar{\ell}_2\Big)\Big]\Big\rangle$$

$$+ \dot{\beta}_k\Big\langle -2\bar{h}\bar{S}_6(\beta_p/\beta_0) + \Gamma\Big[\bar{\ell}_4(\theta_0(\beta_p/\beta_0) - \zeta_0) + \bar{h}\Big(\theta_0\bar{\ell}_2 - 2\frac{\bar{\ell}}{2}\dot{\lambda}\Big)\Big]\Big\rangle$$

$$+ \zeta_{0_k}\Big\langle -\bar{S}_6(\beta_p/\beta_0) - \bar{h}\bar{S}_6 + \Gamma\Big[\theta_0\bar{\ell}_5 - \bar{\ell}_2\lambda + \bar{h}\theta_0\bar{\ell}_2(\beta_p/\beta_0)\Big]\Big\rangle$$

$$+ \beta_k\Big\langle -\bar{I}_6\zeta_0 + \Gamma\Big[\theta_0\bar{\ell}_2\lambda + \frac{c_{a_0}}{a}\bar{\ell}_5 + \bar{h}\bar{\ell}_2\theta_0\zeta_0\Big]\Big\rangle \Big\}$$

$$+ 2\gamma_{\theta_z}\bar{\Omega}^2\Big\{ \ddot{\theta}_x\Big(-\frac{1}{2}\bar{e}\bar{S}_6\zeta_0\Big) + \ddot{\theta}_z\Big[-2\bar{h}(\beta_p/\beta_0)\bar{S}_6 - \bar{h}^2\bar{M}_6$$

$$- \frac{1}{2}(\bar{e}^2\bar{M}_6 + 2\bar{e}\bar{S}_6 + \bar{I}_6)\Big] + \ddot{\bar{R}}_x(-\bar{S}_6(\beta_p/\beta_0) - \bar{h}\bar{M}_6)$$

$$+ \dot{\theta}_x\Big\langle \bar{e}^2\bar{M}_6 + 2\bar{e}\bar{S}_6 + \bar{I}_6 + \Gamma\Big[\bar{h}\Big(\theta_0\bar{\ell}_2 - \frac{\bar{\ell}^2}{2}\lambda\Big) + (\bar{\ell}_4 - \bar{\ell}_5)\zeta_0 + \bar{h}(\theta_0\bar{\ell}_2 - \bar{\ell}_1\lambda)\Big]\Big\rangle$$

$$+ \dot{\theta}_y\Big\langle -\zeta_0\bar{e}\bar{S}_6 + \Gamma\Big[-\bar{\ell}_5 - \bar{h}(\bar{\ell}_2 + \bar{\ell}_3)(\beta_0/\beta_0) - \bar{e}\bar{\ell}_3\Big]\Big\rangle$$

$$+ \ddot{\bar{R}}_x\Gamma(-\bar{\ell}_2(\beta_p/\beta_0)) + \ddot{\bar{R}}_y\Gamma\Big(\frac{\bar{\ell}^2}{2}\lambda - \theta_0\bar{\ell}_2\Big) + \theta_x\bar{e}\bar{S}_6\zeta_0\Big\}$$

$$+ \gamma_{\theta_y}\bar{\Omega}^2\frac{2}{N}\sum_k \theta_{A_k}\Gamma\Big\{\cos\psi_k(-\bar{\ell}_5 - \bar{e}\bar{\ell}_3 - \bar{h}\bar{\ell}_3(\beta_p/\beta_0)) + \sin\psi_k(\zeta_0\bar{\ell}_5 + \bar{h}\bar{\ell}_1\lambda)\Big\}$$

where:

$\bar{\ell} = \ell/R$ $\quad \bar{e} = e/R$ $\quad \bar{h} = h/R$

$\mathcal{L}_1 = e\ell + \frac{\ell^2}{2}$ $\quad \mathcal{L}_4 = e\frac{\ell^3}{3} + \frac{\ell^4}{4}$

$\mathcal{L}_2 = e\frac{\ell^2}{2} + \frac{\ell^3}{3}$ $\quad \mathcal{L}_5 = e^2\frac{\ell^2}{2} + 2e\frac{\ell^3}{3} + \frac{\ell^4}{4}$

$\mathcal{L}_3 = e^2\ell + 2e\frac{\ell^2}{2} + \frac{\ell^3}{3}$

$\bar{\Omega} = \Omega/\Omega_0$ $\quad \Gamma = \frac{\rho_a a \, C_2 R}{M_b/\ell}$

$m_0 = M_b/\ell$

$\bar{M}_b = M_b/m_0 R$ $\quad \bar{S}_b = \frac{S_b}{m_0 R^2}$ $\quad \bar{I}_b = \frac{I_b}{m_0 R^3}$

$\bar{C}_\xi = C_\xi/(m_0\Omega_0 R^3)$ $\quad \bar{g}_{SL} = g_{SL}/(m_0\Omega_0 R^3)$ $\quad \bar{g}_{SF} = g_{SF}/(m_0\Omega_0 R^3)$

$\bar{K}_z = K_z/(m_0\Omega_0^2 R^3)$ $\quad \bar{K}_\xi = K_\xi/(m_0\Omega_0^2 R^3)$

$\bar{C}_x = C_x/(M_x\Omega_0)$ $\quad \bar{K}_x = K_x/(M_x\Omega_0^2)$

$\bar{C}_y = C_y/(M_y\Omega_0)$ $\quad \bar{K}_y = K_y/(M_y\Omega_0^2)$

$\bar{C}_{\theta_x} = C_{\theta x}/(I_x\Omega_0)$ $\quad \bar{K}_{\theta x} = (K_{\theta x} - N\cdot M_b\cdot h)/(I_x\Omega_0^2)$

$\bar{C}_{\theta_y} = C_{\theta y}/(I_y\Omega_0)$ $\quad \bar{K}_{\theta_y} = (K_{\theta y} - N\cdot M_b\cdot h)/(I_y\Omega_0^2)$

$\sigma_x = \frac{1}{2} N m_0 R/M_x$ $\quad \sigma_y = \frac{1}{2} N m_0 R/M_y$

$\sigma_{\theta x} = \frac{1}{2} N m_0 R^3/I_x$ $\quad \sigma_{\theta y} = \frac{1}{2} N m_0 R^3/I_y$

$\bar{R}_x = R_x/R$ $\quad \bar{R}_y = R_y/R$

End of Document